Effectiveness of Unmanned Aerial Vehicle-Based Remote Sensing for Assessing the Impact of Catastrophic Windstorm Events on Timberland

by

Dipika Badal

A thesis submitted to the Graduate Faculty of
Auburn University
in partial fulfillment of the
requirements for the Degree of
Master of Science

Auburn, Alabama
May 4, 2024

Keywords: UAVs, lidar, downed timber, CHM, windstorms

Approved by

Richard Cristan, Chair, Extension Specialist & Assistant Professor, College of Forestry, Wildlife and Environment
Lana Narine, Assistant Professor, College of Forestry, Wildlife and Environment
Sanjiv Kumar, Associate Professor, College of Forestry, Wildlife and Environment

Abstract

The forests in the southeastern United States are of great importance for their economic, ecological, and cultural values. However, these forests are increasingly threatened by climate-induced windstorms, such as hurricanes and tornadoes, which can cause significant damage to the forest structure and increase the likelihood of secondary ecological disturbances such as wildfires and insect attacks. To assess the impact of these windstorms, advanced remote sensing technology, specifically unmanned aerial vehicles (UAVs) equipped with Light Detection and Ranging (lidar) and RGB camera was used. The study conducted a comparative analysis of three classification techniques, Maximum Likelihood (ML), Decision Tree (DT), and Random Forest (RF), on two datasets, one integrated with lidar-derived Canopy Height Models (CHM) and one without. The results showed that Random Forest (RF) consistently outperformed the others, achieving an overall accuracy of 94.52% with CHM and 77.56% without. These findings emphasize the effectiveness of UAV-lidar and RGB imagery as rapid and efficient tools for rapid windstorm damage assessment. These findings have significant implications for landowners, policymakers, and further research in environmental monitoring and disaster management across diverse forested landscapes.

Keywords: UAVs, lidar, hurricane, tornado CHM, random forest

Acknowledgments

Reflecting on this journey, I am very grateful to everyone who has contributed to making this accomplishment possible. First and foremost, I want to express my heartfelt thanks to my advisor, Dr. Richard Cristan, for providing me with this amazing opportunity and for his unwavering support and guidance throughout this process. I also extend my sincere appreciation to my committee members, Dr. Lana Narine and Dr. Sanjiv Kumar. Their invaluable suggestions and guidance have been instrumental in shaping and implementing my research, greatly enhancing my learning and research capabilities.

I am also grateful to the College of Forestry, Wildlife, and Environment for their unwavering support and for providing me with the resources and environment conducive to my research. The opportunities and experiences afforded to me by the College have been crucial in completing this thesis. I would then like to thank the US Endowment for Forestry & Communities for funding the project. I would also like to thank Caroline Whiting and Trent Philips from the Department of Biosystems Engineering for providing the required equipment during the fieldwork. I am thankful to Nisham Thapa and Abubakar Tahiru for their support during the research study,

I extend my deepest gratitude to Arjun Rijal and Manisha Parajuli for their invaluable contributions to this project. Their dedication and enthusiasm made the field data collection process truly enriching. Despite long hours and demanding schedules, their commitment to our project was exceptional. Their presence transformed difficult days into memorable adventures, and I am deeply thankful for that.

Finally, I want to express my heartfelt appreciation to my family, including my parents, Dilip Badal and Kalpana Badal, my brother, Sulav Badal, and my close friends, Anusha Maharjan, Bikram Kharel, Sanchita Budhathoki, and Aparana Pant. Your consistent support, love, and encouragement have been my rock during this journey. Your unwavering faith in me has been a constant source of inspiration, and I am deeply thankful for all the support and understanding you have given me.

Table of Contents

List of Tables

List of Figures

Chapter 1. Literature Review on Climate-Induced Windstorms on Southeastern US Forests: Assessing Vulnerabilities and Advancements in Lidar Technology

1.1. Abstract

Forests in the southeastern United States are widely recognized for their economic, ecological, and cultural significance. These forests constitute a significant source of timber production for the entire nation and globally. However, changes in climatic and environmental conditions are increasing the likelihood of high-intensity windstorm events such as hurricanes and tornadoes, posing a serious threat to the structure and adaptive capacity of these forests. Increasing windstorms cause a substantial impact on forestland by damaging, snapping, and uprooting trees. In addition to the direct impact of timber damage, these hazards also increase the likelihood of secondary ecological disturbances such as wildfires and insect attacks. Understanding the effects of windstorm events on forests is critical for both landowners and policymakers, as it will help reduce potential economic and ecological losses by timely extracting downed timber and reducing fuel loads. Forestry applications have become more cost-effective, time-efficient, and precise with the latest advancements in remote sensing technology, particularly Light Detection and Ranging (lidar). Lidar technology enables the collection of spatially precise, accurate, and high-resolution three-dimensional (3D) information on forest attributes across large inventory areas, easing the process of forest management and damage assessment. Lidar-derived products such as Canopy Height Models (CHMs) have enhanced vegetation mapping and classification accuracy, especially when paired with advanced classification algorithms.

Keywords: Unmanned aerial vehicles, UAVs, lidar, hurricane, tornado, downed timber

1.2. Introduction

Forests occupy an overall 31% of the earth's land area (Global Forest Resources Assessment, 2020) and are a crucial source of renewable resources and energy. Forests also play an important role in preserving and protecting biodiversity, soil erosion, and global climate (Canadell & Raupach, 2008). Southern United States (US) forestlands are economically, ecologically, and culturally significant (Sharma et al., 2021). The humid, temperate, and subtropical climate promotes quick growth rates of tree species. While accounting for only 2% of the global forest area, these forests are considered among the most productive in the world, providing approximately 18% of the world's pulpwood and 7% of the world's industrial wood supply, and are also renowned as the nation's "wood basket" (Sharma et al., 2021; Wear & Greis, 2012).

Forest ecosystems are affected by numerous factors which positively and negatively influence growth and development. Climate-induced storm events, wildfires, excessive rainfall, landslides, illicit logging, invasive species, diseases, and pests are some major factors influencing forests. Changes in climatic conditions are increasing the likelihood of climate-induced disasters, such as severe drought and storm events, which pose a serious threat to the adaptability of forests in the southeastern US (Mitchell et al., 2014). High-intensity storm events such as tornadoes and hurricanes alter species composition, structure, and habitat of forests, making them more vulnerable to subsequent disturbances (Bigelow et al., 2021). The main visible effect of such occurrences on forest resources is timber loss (Merrens & Peart, 1992), which can exceed $1 billion annually (Miranda, 1996). A striking example is Hurricane Ivan's aftermath in 2004, which led to the destruction of timber worth more than $610 million on

almost 1.1 million hectares of land in Alabama alone, as highlighted by Sharma et al. (2021). In addition to its primary impacts of storms, secondary disturbances such as erosion, insect attacks, invasive species threats, landfall events, and wildfires are potential problems that can occur (Cannon et al., 2017; Shinoda & Akasaka, 2020). If downed trees are not removed from impacted forest stands, downed trees, debris, and litter can increase fuel loads, cause more intense wildfires, and increase susceptibility to secondary disturbances, posing a major threat to adjacent forest stands and the public (Miranda, 1996; McNulty, 2001).

Understanding the implications of weather-induced storm disasters is critical for both landowners and policymakers. For an effective and economical harvest of the downed timber, reliable information on the location, tree characteristics and volume of trees in the damaged forest stands is crucial (Hamdi et al., 2019). Wind-related damage assessment is an important component of forest monitoring and management, as well as forest economics (Duan et al., 2017). Field surveys have traditionally been used to examine storm-damaged timber but present some challenges (Ståhl et al., 2001). While field measurements are regarded as the most precise strategy for forest management, they are time-consuming and labor-intensive (Klauberg et al., 2016). Fallen timber can be found close to (snapped and leaning) or on the ground, where they can stay covered by understory vegetation, compromising data integrity (Rondeux & Sanchez, 2010). In addition, trees that are snapped and leaning can present safety concerns. Remote sensing technologies can provide a solution to such challenges.

Remote sensing techniques used in Forestry have received considerable attention in recent decades due to their ability to provide detailed information without being on the site

(Banu et al., 2016). When combined with automatic processing techniques, this technology enables rapid and precise details of large-scale areas (Dalponte et al., 2008). Changes in forest canopy structure caused by natural disturbances can be studied with high precision by employing active remote sensing sensors such as Light Detection and Ranging (lidar), which are viewed as an alternative to overcome the difficulty of field techniques (Lefsky et al., 2002). Lidar has demonstrated potential to improve accuracy and lower the time and labor cost of recurrent forest survey activities (Akay et al., 2009; Guo et al., 2023; Rijal et al., 2023). Many platforms, including airborne, spaceborne, terrestrial, mobile, and unmanned aerial vehicles (UAV), are used to collect lidar data. Among these, UAV-lidar holds the most promise in effectiveness, precision, and data quality, all of which are crucial for real-time forest inventory data (Guo et al., 2017). Over the last decade, increased attention, research interests, dataset accessibility, and technological advancements have drastically improved and increased the usage of lidar technology in forestry (Silva et al., 2014). Lidar-derived CHMs have been used to detect individual trees, delineate tree crowns, and estimate biophysical parameters such as biomass and stem volume (Hudak et al., 2016; Popescu, 2007; Popescu et al., 2003; Silva et al., 2014). Similarly, several studies have demonstrated that integrating lidar data and remotely sensed imagery provides significant advantages in ecological and forestry applications such as wetland monitoring and management, urban tree species mapping, and vegetation mapping (Kim et al., 2020; Amani et al., 2020; Liang et al., 2020).

Drones and lidar technologies are still in the experimental stage in Forestry applications but have significant future potential due to their increasing accessibility in cost, lower time, and coverage areas (Banu et al., 2016). Lidar has been evaluated for storm damage (Duan et al.,

2017; Honkavaara et al., 2013; Selvarajan, 2011), but further research is needed, particularly for the southeastern US. Although some studies have used UAVs to analyze forest attributes (Jaud et al., 2016; Mancini et al., 2013), research on their effectiveness on storm-damaged stands is needed.

1.3. Literature Review

1.3.1. Forest Ecosystem in Southeast US and its Influencing Factors

Forests play an essential role in supporting and regulating global climate and ecosystems. They support a wide range of species, such as managed loblolly pine (*Pinus taeda*) plantations, shortleaf pine (*Pinus echinata*) forests, oak-hickory (*Quercus spp.-Carya spp.)* forests, as well as coastal mangrove and live oak (*Quercus spp.)* forests. This rich tapestry of woodland allows a diverse biota comprising of 1,027 native terrestrial vertebrates, 178 amphibians, 504 birds, 158 mammals, and 187 reptiles (Wear & Greis, 2012).

Disturbances are important phenomena in maintaining the dynamics of forest ecosystems (Page & Jenkins, 2007). They strongly influence the structure, composition, and functionality of forests (Seidl et al., 2011). Southeastern forests have been exposed to various factors that have altered their structure and composition over time, including changing climate and wind patterns (Sharma et al., 2021). Climate change plays a crucial role in intensifying disturbances, including wildfires, storm-induced disasters, insect attacks, and drought, which have severely impacted the livelihoods of people and the environment (Mitchell et al., 2014). Every year, extreme windstorm events kill and injure hundreds of people in the US (Greenough et al., 2001). The impact of climate-related storm events on forests is determined primarily by storm intensity, soil,

and other landscape characteristics (Rutledge et al., 2021). They significantly impact forest structure by damaging forest resources and modifying forest structure and species distribution (Xi et al., 2008). There has been an observable increase in the intensity and frequency of windstorm events in the Atlantic and the Gulf of Mexico regions since 1995. The 2020 hurricane season has been declared the most intense season recorded, with 30 named storms, indicating a concerning trend in the region's weather patterns (NOAA, 2020; Reed et al., 2022; Sharma et al., 2021). Such increased and unprecedented frequency of windstorm events raises concerns for the long-term sustainability of forests.

1.3.2. Storm Events on Forests

Intense windstorms such as hurricanes and tornadoes impact the US annually, causing loss of life, damage to property, and generating a massive amount of downed timber (Fortuin et al., 2021). Windthrow hazards not only result in timber damage and economic loss but also have a tremendous impact on forest ecosystems (Gardiner et al., 2010). Factors such as aspect, windspeed, topography, and exposure highly influence forest vulnerability and resilience to windstorm damage (Taylor et al., 2019). In 2023, the US experienced 25 individual weather and climate disasters (including hurricanes and tornadoes), each incurring losses of over $1 billion, accumulating to a staggering total of $81 billion in damages (NOAA, 2023). The most visible effect caused by these hazards in forests is the snapping of trees along with uprooting. Rainfall combined with wind damage weakens the soil, causing significant defoliation, snapping, and blowdown of trees, which can lead to flooding, erosion, and runoff (Tanner et al., 1991).

Major storm disasters strike at least twice a year in the southeast. Between 1900 and 1996, 60 significant hurricanes made landfall along the southern coast (NOAA, 1997), with majority of the impact (greater than 55%) on forestland (McNulty, 2001). The southeastern US is a major hub for timber markets, and the growing frequency of climate-induced disasters can have a massive impact on these markets and forest industry (McNulty, 2001). The impact of Hurricane Michael in 2018 resulted in over 5.30 million acres of forestland damage, which totaled 3.19 billion cubic feet of timber and impacted 91,000 individual landowners (Brandeis et al., 2022). The frequency and intensity of windstorm hazards are getting stronger each year, with the Intergovernmental Panel on Climate Change (IPCC) predicting an increase in the magnitude and severity of climate-related disasters (Knutti et al., 2013). Increased storms will result in increased timber destruction and the accumulation of downed timber, leading to substantial economic losses and threatening the ecological balance of forested ecosystems through secondary disturbances (Musah et al., 2022).

Individual windstorm events disrupt forest stands, resulting in decreased timber value, difficulty salvaging damaged timber, and increased harvest costs (Pye et al., 2010). Furthermore, the market value of salvaged downed timber following windstorm events falls significantly as markets are inundated by increased timber volume. Hurricanes Katrina and Rita caused $2.25 billion in timber losses in Alabama, Louisiana, Mississippi, and Texas (Musah et al., 2022; Prestemon & Holmes, 2010). Storm-damaged trees are advised to be removed as quickly as possible after the disturbance (de Groot et al., 2018), prioritizing salvaging higher-value timber to reduce decay-related losses (Pye et al., 2010). Five classes of harvesting windows have been recommended for storm-damaged pine trees (Bradley et al., 2018) (Table 1). The intensity,

nature, and extent of storm damage can vary greatly, therefore preliminary evaluation of damaged areas must be the primary step in windstorm damage assessment (Dickens & Moorhead, 2016).

Table 1: Windstorm-damaged pine trees harvesting window in Alabama (Based on Bradley et al., 2018)

Damage Class	Harvest Window	Comments
Minor bending or leaning	None	Trees may recover.
Uprooted	2-3 months	Stems may succumb to fungi and wood-boring insects.
Broken tops or trunks with less than four main live limbs left or severely bent	As soon as possible	Depending upon tree size and location of breakage, solid wood products may be produced. If ring shake or pulled fibers present, these trees may not be suitable for lumber of plywood.
Broken tops or trunks with more than four main live limbs left	None	Trees should be monitored for beetle attacks.
Major wounds	As soon as possible	Pine beetles will target damaged trees.

1.3.3. Application of Remote Sensing in Assessing Forest Parameters

One of the most important aspects of forest management is analyzing forest structure and damage following a disaster, which reduces the likelihood of future biological damage and sensitivity to post-disturbances (Einzmann et al., 2017; Hamdi et al., 2019). Damaged forests must be efficiently surveyed to collect accurate statistics and inventory information (Bouget & Duelli, 2004). With the emergence of remote sensing technologies, data acquisition methods at high precision and spatial resolution have supplemented traditional field measurement methods for forest inventory (Järnstedt et al., 2012; Stepper et al., 2014). The utilization of remotely sensed data has become increasingly prevalent in recent years for monitoring a wide range of

phenomena related to the earth's surface. These applications include, but are not limited to, monitoring land-cover changes, hydrological processes, damage caused by natural disasters, and understanding of natural resources and environmental phenomena (Taylor, 1996; Dalla Mura et al., 2015; Lechner et al., 2020; Schmugge et al., 2002). Various sensors and platforms can be utilized to gather remote sensing data. These sensors can be either passive, such as optical, multispectral, hyperspectral, and thermal sensors, or active, such as Synthetic Aperture Radar and lidar. Similarly, various platforms are available, such as Earth Observation satellites, manned aircraft, and UAVs, which can be equipped with these sensors to obtain a wide range of valuable information (Guo et al., 2023; Lechner et al., 2020).

Satellite or airborne systems, may include high operational costs, safety risks, and limited temporal and spatial resolution (Bhardwaj et al., 2016; Liebel & Körner, 2016; Mohan et al., 2021; Villa et al., 2013). The use of UAVs equipped with RGB cameras or lidar sensors can prove to be a valuable solution to address such challenges (Bhardwaj et al., 2016; Mohan et al., 2021). Lidar technology has emerged as one of the most capable tools for extensive research and quantifying the 3D structure of forests (Hudak et al., 2009; Næsset et al., 2004; Silva et al., 2017). Lidar is an active remote sensing technology that uses a pulsed laser to measure varying distances to the Earth (Guo et al., 2023). In addition to its low cost, high speed, flexibility in operating in diverse environments, and ability to capture highly precise information in all weather conditions, it provides higher spatial resolution compared to other remote sensing sources (Beland et al., 2019; Dassot et al., 2011; Lechner et al., 2020). Moreover, lidar technology can provide information from within the canopy, further enhancing the accuracy and comprehensiveness of data collection (Popescu, 2007). Due to its capability to rapidly provide

spatially precise, accurate, and detailed information across large inventory areas, lidar has emerged as the dominant tool for examining factors such as forest inventory attributes, fuel load distribution, and erosion susceptibility (Hudak et al., 2009; Leite et al., 2022; Silva et al., 2017). It has been widely used to obtain estimates of tree height, tree density, forest composition, crown diameter, basal area, growing stock volume, biomass, and leaf area index (Abdollahnejad et al., 2018; N~esset, 1997; Nothdurft et al., 2021; Silva et al., 2017; Xu et al., 2019).

Lidar can be operated on a variety of remote sensing platforms, including terrestrial, mobile, spaceborne, airborne, and UAV systems (Goodbody et al., 2017). UAV technological advancement has enabled the collection of high-resolution three-dimensional products for assessing forest attributes, easing the process of forest management (Abdollahnejad et al., 2018; Järnstedt et al., 2012). Given its ability to fly at lower altitudes, UAV-based lidar can generate significantly greater return (or point) densities compared to airborne and satellite platforms (d'Oliveira et al., 2020; Lin et al., 2019; Storch et al., 2022), allowing for precise measurement of individual trees and understory vegetation (Almeida et al., 2019; Wallace et al., 2014). It has, therefore, rapidly become a crucial means of data collection for forest ecosystem studies due to its ability to penetrate tree canopy and recreate vertical forest structures, as well as its great flexibility and lower cost (Lefsky et al., 2002; Bohlin et al., 2012; Messinger et al., 2016; Xu et al., 2019). Over the past decade, developments in lidar data processing software have led to increased adoption for supporting applications. Access to suitable lidar processing tools is essential for accurate and precise lidar data manipulation and analysis (Mohan et al., 2021). There are various lidar processing software alternatives available today, including free options like CloudCompare, SAGA GIS, R, and FUSION/LDV, as well as commercial software like

LAStools, LP360, ArcGIS Pro, Lidar360, and ENVI lidar. These tools include a variety of capabilities, such as lidar data display, filtering, cleaning, segmentation, and feature extraction, making it simple to analyze and understand lidar data for diverse ecological applications (Guo et al., 2023). Emerging remote sensing technologies, including UAV-lidar, therefore, hold significant promise for determining forest attributes at considerably reduced costs and with high precision.

1.3.4. Lidar and Remotely Sensed Imagery for Ecological Studies

The utilization of lidar-based remote sensing technology holds great promise in Forestry and environmental fields (Feng et al., 2015). With its capability to capture precise three-dimensional data on both the vertical and horizontal distribution of forest canopy elements, lidar is highly valued for its ability to classify vegetation, identify species, and classify land cover classes. As a result, its utilization has grown substantially (Michałowska & Rapiński, 2021).

Numerous studies have demonstrated the usefulness of lidar data in ecological studies. Thapa et al. (2023) used NAIP imagery and airborne lidar data to detect invasive plant species (Tallow tree and Chinese Privet) in coastal Alabama and Mississippi, employing three image classification techniques- ISODATA, Maximum Likelihood, and Random Forest. The integration of NAIP imagery with lidar-derived metrics (CHM and Topographic Wetness Index) yielded the highest accuracy of 87.5% using the Random Forest classifier, emphasizing the importance of combining spectral and structural data for precise mapping (Thapa et al., 2023). Similarly, Bandyopadhyay et al. (2013) used airborne lidar data and high-resolution aerial color imagery (0.15 meters resolution) to differentiate urban vegetation and buildings from other

objects. Employing region-growing algorithms for distinguishing between buildings and vegetation, they integrated lidar and RGB data, resulting in a classification accuracy of over 85%.

Recent advancements in UAV technology have enabled capturing high-quality imagery with exceptional spatial and temporal resolution. This has allowed for the detailed analysis of forest characteristics at a fine scale (Beland et al., 2019; Chuvieco, 2020). The captured imagery can be further processed to classify forest features and attributes (canopy cover, height, forest health, tree density, and distribution). Ultrahigh-resolution UAV-imagery (with spatial resolution in centimeters) incorporating complex surface details and textures provides an optimal platform for efficient vegetation studies, with proven efficiency at resolutions ranging from less than 2cm to 7cm (Feng et al., 2015; Lu & He, 2017; Poblete-Echeverría et al., 2017; Schiefer et al., 2020). Researchers such as Feng et al. (2015) and Lu & He (2017) have emphasized the usefulness of such imagery. The study conducted by Lu & He (2017) employed an octocopter UAV equipped with a modified digital camera to capture high-resolution imagery across the near-infrared, green, and blue bands of a tall grassland in Ontario, Canada. The results demonstrated the UAV's proficiency in examining fine-scale species composition in grasslands with 85% accuracy in species classification. This underscores the significant value of high spatial resolution data (with spatial resolution in centimeters) for detailed vegetation monitoring and ecological research, particularly compared to free and open satellite images with lower accuracy i.e., with spatial resolution ranging from 1m to 500m (Lu & He, 2017). Similarly Lee & Yu (2018) developed an innovative method to automatically detect dead or dying trees using UAV-imagery. The results of their study indicated that dead trees could be detected from UAV-imagery with a confidence

level of over 80%. Furthermore, spectral, textural, and morphological information extracted from ultrahigh-resolution UAV-imagery is highly valuable for monitoring urban forests and classifying urban tree species (Wang et al., 2021).

Integrating lidar data and imagery has become increasingly popular for environmental monitoring, forest management, and disaster response (Bandyopadhyay et al., 2013; Li et al., 2021; Secord et al., 2017). Numerous studies have emphasized integrating remotely sensed imagery with lidar-derived attributes. Lidar-derived metrics can significantly improve the accuracy and efficacy of vegetation mapping, species identification, and classification procedures, particularly when combined with advanced classification algorithms (Corte et al., 2020; Kim et al., 2020; Liang et al., 2020). Corte et al. (2020) used machine learning with high-dimensional UAV-lidar data to estimate dendrometric metrics for individual trees, such as total height, overall timber volume, and DBH. Li et al. (2021) collected high-resolution terrain data using UAV-lidar, which they used for flood modeling. The precision of lidar-generated DEM allowed for the seamless simulation of flash floods, and the study recommended that UAV-lidar techniques are a reliable and effective tool for high-accuracy flood simulation.

1.3.5. Image Classification Techniques

The classification of remotely sensed data is a crucial process for extracting valuable information. This involves grouping each pixel or cluster of pixels of an image into specific classes based on their spectral, spatial, and temporal characteristics. Classification techniques can be categorized into supervised and unsupervised methods. Supervised classification utilizes labeled training data, while unsupervised classification identifies clusters or groups of similar

spectral signatures without prior knowledge of class labels (Chuvieco, 2020; Sisodia et al., 2014). Maximum Likelihood (ML) classification is the most widely used method, assigning each pixel to a class based on the highest probability (Chuvieco, 2020; Lillesand et al., 2004; Mollick et al., 2023; Sisodia et al., 2014). Machine learning classifiers have gained widespread interest among researchers due to their ability to produce higher classification accuracy. These classifiers learn patterns and relationships from training data and apply the knowledge to new data during prediction (Ba et al., 2020). Nonparametric algorithms like Decision Trees (DTs) and Random Forest (RF) (Breiman, 2001) are particularly flexible and robust as they make no assumptions about the input data distribution and can effectively handle non-linear data (Fan, 2023; Frohn & Arellano-Neri, 2005; Li et al., 2013).

Data collected from various remote sensing platforms, including satellites, airborne systems, and UAVs, when integrated with diverse classification algorithms help in extracting valuable ecological information. Sharma et al. (2013) conducted a study showcasing a DT classification algorithm for classifying Landsat Thematic Mapper (TM) data. The study compared the accuracy of this method with traditional ISODATA clustering and supervised Maximum Likelihood Classifier methods. Results showed that the DT surpassed the other techniques in terms of higher classification accuracy, with an overall accuracy of 90% and a kappa value of 0.88. Another popular machine-learning algorithm for image classification is Random Forest, which, being an ensemble of DTs, is considered better than the traditional DT classifier (Breiman, 2001; Khatami et al., 2016). This algorithm is highly effective for classification and detecting outliers and requires minimal user input, making it a popular choice (Gislason et al., 2006; Guan et al., 2012). For instance, Li et al. (2013) utilized DT and RF

algorithms to classify forest types and monitor forest changes over time at the Huntington Wildlife Forest using Landsat TM data. They discovered that RF produced greater classification accuracy than DT.

The study by Long et al. (2023) utilized multi-temporal, high-spatial-resolution satellite images from Landsat 7, Spot-5, RapidEye, and Planet satellites to assess landslide progression in the Mianyuan River Basin, China. Utilizing both the Maximum Likelihood classification method and the Random Forest algorithm, the study revealed that while ML achieved an average accuracy of 73%, RF algorithm performed even better, with an average accuracy of 87%. Similarly, Billah et al. (2023) assessed flood damage using Sentinel-1 and Sentinel-2 satellite data, combining radar and optical imaging capabilities to accurately distinguish flood extents across land categories. They found that RF classifier performed better than ML in evaluating and identifying flood damages with 90% accuracy, emphasizing the need to integrate data types for better disaster management and preparation.

Kim et al. (2020) employed four distinct classification algorithms (RF, Maximum Likelihood, Mahalanobis Distance, and Support Vector Machine) for vegetation mapping of No Name Key, Florida. They used publicly available airborne lidar data and high-resolution NAIP imagery and conducted classification on two sets of datasets: NAIP imagery only and a combination of NAIP imagery and airborne lidar data. The RF classification on the stacked image with NAIP imagery and lidar achieved the highest overall accuracy (OA) and kappa coefficient. In a similar line, Zhang et al. (2019) investigated the best risk model for predicting hurricane-related damages. Four classification techniques were used: artificial neural network,

support vector machine, RF, and k-nearest neighbor. The findings revealed that RF was the most effective algorithm in predicting mangrove damage, with a correlation coefficient (r) of 0.84, outperforming the other classification methods.

UAVs equipped with imaging sensors, lidar sensors, and classification algorithms such as Random Forest, Maximum Likelihood, and Decision Trees have become crucial tools in forest management and ecological studies. Hartling et al. (2021) used a UAV-based multi-sensor method consisting of multispectral, hyperspectral, lidar, and thermal infrared data to classify urban trees of seven different species. They achieved the highest accuracy of 83.3% using the Random Forest classifier, highlighting the effectiveness of combining multiple sensor data for accurate classification. In a study conducted by Fan (2023), ground surface structures were classified using high-resolution UAV data captured by a DJI Phantom 3 equipped with an RGB camera. The images had a resolution of 2-5 cm/pixel, which allowed for detailed visibility. The study used Support Vector Machine, Random Forest, and Maximum Likelihood methods to classify the images. RF was found to be the most effective, with an accuracy of 91.78%, Kappa coefficient of 0.88, and AUC of 0.93, demonstrating its superiority in handling complex classification scenarios in high-resolution imagery analysis.

Similarly, Wang, et al. (2021) used high-resolution UAV (Unmanned Aerial Vehicle) images with a RGB camera to monitor urban forests on a single tree scale, combining spectral data, tree dimensions, and vegetation indices. They found that RF classifier outperformed the Maximum Likelihood Classification (MLC), attaining 91.3% accuracy. The study concluded that using RF in a multidimensional approach enhances the accuracy of forest monitoring,

demonstrating the effectiveness of combining advanced classification techniques with detailed UAV imagery.

Previous research has extensively used various classification techniques to map land cover changes and tree species (Balha & Singh, 2022; Hartling et al., 2021), detect invasive species (Thapa et al., 2023), and assess the impact of natural disasters like landslides and floods (Long et al., 2023; Billah et al., 2023). While some studies have employed airborne and terrestrial data sources to identify windstorm-downed trees (Blanchard et al., 2011; Polewski et al., 2015; Queiroz et al., 2019), the use of UAV-captured imagery and lidar data in mapping windstorm disturbances has been relatively unexplored. Given the increasing availability of high-resolution UAV imagery and lidar data, there is significant potential to further investigate their effectiveness in accurately detecting and classifying extensive windstorm damage in forested areas.

1.4. References

Abdollahnejad, A., Panagiotidis, D., & Surovỳ, P. (2018). Estimation and extrapolation of tree parameters using spectral correlation between UAV and Pléiades data. Forests, 9(2).

Akay, A. E., Oğuz, H., Karas, I. R., & Aruga, K. (2009). Using Lidar technology in forestry activities. Environmental Monitoring and Assessment, 151, 117–125. https://idp.springer.com/authorize/casa?redirect_uri=https://link.springer.com/article/10.1007/s10661-008-0254-1&casa_token=OuRqjgrTLhIAAAAA:imjI-iPRdYKS0aRtHdzjKS0fqM6fXr0p8jQE0tbBRDq10TmgT43avE_HUYxas9pubjYK0uiA0divUwTd

ALABAMA FORESTRY COMMISSION FOREST RESOURCE REPORT 2021. (2021).

Alberto Silva, C., Klauberg, C., de Pádua Chaves Carvalho, S., Hudak, A. T., & Carlos Estraviz Rodriguez, L. (2014). Mapping aboveground carbon stocks using Lidar data in Eucalyptus spp. plantations in the state of Sao Paulo, Brazil (Vol. 42).

Almeida, D. R. A., Broadbent, E. N., Zambrano, A. M. A., Wilkinson, B. E., Ferreira, M. E., Chazdon, R., Meli, P., Gorgens, E. B., Silva, C. A., Stark, S. C., Valbuena, R., Papa, D. A., & Brancalion, P. H. S. (2019). Monitoring the structure of forest restoration plantations with a drone-Lidar system. International Journal of Applied Earth Observation and Geoinformation, 79, 192–198. https://doi.org/10.1016/j.jag.2019.03.014

Asner, G. P., Knapp, D. E., Kennedy-Bowdoin, T., Jones, M. O., Martin, R. E., Boardman, J., & Hughes, R. F. (2008). Invasive species detection in Hawaiian rainforests using airborne imaging spectroscopy and Lidar. *Remote Sensing of Environment*, *112*(5), 1942–1955. https://doi.org/10.1016/j.rse.2007.11.016

Ba, A., Laslier, M., Dufour, S., & Hubert-Moy, L. (2020). Riparian trees genera identification based on leaf-on/leaf-off airborne laser scanner data and machine learning classifiers in northern France. *International Journal of Remote Sensing*, *41*(5), 1645–1667.

Bandyopadhyay, M., Van Aardt, J. A. N., & Cawse-Nicholson, K. (2013). *Classification and extraction of trees and buildings from urban scenes using discrete return Lidar and aerial color imagery* (M. D. Turner & G. W. Kamerman, Eds.; p. 873105). https://doi.org/10.1117/12.2015890

Banu, T. P., Borlea, G. F., & Banu, C. (2016). The use of drones in forestry. *Journal of Environmental Science and Engineering B*, *5*(11), 557-562.

Balha, A., & Singh, C. K. (2022). Comparison of Maximum Likelihood, Neural Networks, and Random Forests Algorithms in Classifying Urban Landscape. In V. P. Singh, S. Yadav, K. K. Yadav, G. A. Corzo Perez, F. Muñoz-Arriola, & R. N. Yadava (Eds.), *Application of Remote Sensing and GIS in Natural Resources and Built Infrastructure Management* (pp. 29–38). Springer International Publishing. https://doi.org/10.1007/978-3-031-14096-9_2

Beland, M., Parker, G., Sparrow, B., Harding, D., Chasmer, L., Phinn, S., Antonarakis, A., & Strahler, A. (2019). On promoting the use of Lidar systems in forest ecosystem research. *Forest Ecology and Management*, *450*, 117484. https://doi.org/10.1016/j.foreco.2019.117484

Beniaich, A., Silva, M. L. N., Avalos, F. A. P., Menezes, M. D. D., & Cândido, B. M. (2019). Determination of vegetation cover index under different soil management systems of cover plants by using an unmanned aerial vehicle with an onboard digital photographic camera. Semina: Ciências Agrárias, 40(1), 49. https://doi.org/10.5433/1679-0359.2019v40n1p49

Bhardwaj, A., Sam, L., Akanksha, Martín-Torres, F. J., & Kumar, R. (2016). UAVs as remote sensing platform in glaciology: Present applications and future prospects. *Remote Sensing of Environment*, *175*, 196–204. https://doi.org/10.1016/j.rse.2015.12.029

Bigelow, S. W., Looney, C. E., & Cannon, J. B. (2021). Hurricane effects on climate-adaptive silviculture treatments to longleaf pine woodland in southwestern Georgia, USA. Forestry: An International Journal of Forest Research, 94(3), 395–406. https://doi.org/10.1093/forestry/cpaa042

Blake, E. S., Rappaport, E. N., Landsea, C. W., & Miami, N. (2007). The deadliest, costliest, and most intense United States tropical cyclones from 1851 to 2006 (and other frequently requested hurricane facts). NOAA/National Weather Service, National Centers for Environmental Prediction

Bohlin, J., Wallerman, J., & Fransson, J. E. S. (2012). Forest variable estimation using photogrammetric matching of digital aerial images in combination with a high-resolution DEM. Scandinavian Journal of Forest Research, 27(7), 692–699. https://doi.org/10.1080/02827581.2012.686625

Booth, D. J., & Oldfield, R. B. (1989). A comparison of classification algorithms in terms of speed and accuracy after the application of a post-classification modal filter. *International Journal of Remote Sensing*, *10*(7), 1271–1276. https://doi.org/10.1080/01431168908903965

Bork, E. W., & Su, J. G. (2007). Integrating LIDAR data and multispectral imagery for enhanced classification of rangeland vegetation: A meta analysis. *Remote Sensing of Environment*, *111*(1), 11–24. https://doi.org/10.1016/j.rse.2007.03.011

Bouget, C., & Duelli, P. (2004). The effects of windthrow on forest insect communities: A literature review. Biological Conservation, 118(3), 281–299. https://doi.org/10.1016/j.biocon.2003.09.009

Bradley, S., A. Maggard, & B. Carter. (2018). Assessing and managing storm-damaged timber. Alabama Cooperative Extension System, FOR-2066. 4p.

Brandeis, T., Turner, J., Baeza Castro, A., Brown, M., & Lambert, S. (2022). Assessing forest resource damage following natural disasters using national forest inventory plots. https://doi.org/10.2737/SRS-RP-65

Breiman, L. (2001). Random Forests. *Machine Learning*, *45*(1), 5–32. https://doi.org/10.1023/A:1010933404324

Canadell, J. G., & Raupach, M. R. (2008). Managing forests for climate change mitigation. In Science (Vol. 320, Issue 5882, pp. 1456–1457). https://doi.org/10.1126/science.1155458

Cannon, J. B., Peterson, C. J., O'Brien, J. J., & Brewer, J. S. (2017). A review and classification of interactions between forest disturbance from wind and fire. In Forest Ecology and Management (Vol. 406, pp. 381–390). Elsevier B.V. https://doi.org/10.1016/j.foreco.2017.07.035

Chuvieco, E. (2020). *Fundamentals of satellite remote sensing: An environmental approach*. CRC press. https://www.taylorfrancis.com/books/mono/10.1201/9780429506482/fundamentals-satellite-remote-sensing-emilio-chuvieco

Conner, W. H., Day, J. W., Baumann, R. H., & Randall, J. M. (1989). Influence of hurricanes on coastal ecosystems along the northern Gulf of Mexico. *Wetlands ecology and Management*, *1*, 45-56.

Corte, A. P. D., Souza, D. V., Rex, F. E., Sanquetta, C. R., Mohan, M., Silva, C. A., Zambrano, A. M. A., Prata, G., Alves De Almeida, D. R., Trautenmüller, J. W., Klauberg, C., De Moraes, A., Sanquetta, M. N., Wilkinson, B., & Broadbent, E. N. (2020). Forest inventory with high-density UAV-Lidar: Machine learning approaches for predicting individual tree attributes. *Computers and Electronics in Agriculture*, *179*, 105815. https://doi.org/10.1016/j.compag.2020.105815

Dale, V. H., Joyce, L. A., McNulty, S., Neilson, R. P., Ayres, M. P., Flannigan, M. D., Hanson, P. J., Irland, L. C., Lugo, A. E., Peterson, C. J., Simberloff, D., Swanson, F. J., Stocks, B. J., & Wotton, B. M. (2001). Climate change and forest disturbances. In BioScience (Vol. 51, Issue 9, pp. 723–734). https://doi.org/10.1641/0006-3568(2001)051[0723:CCAFD]2.0.CO;2

Dalponte, M., Bruzzone, L., & Gianelle, D. (2008). Fusion of hyperspectral and LIDAR remote sensing data for classification of complex forest areas. IEEE Transactions on Geoscience and Remote Sensing, 46(5), 1416–1427. https://doi.org/10.1109/TGRS.2008.916480

Dalla Mura, M., Prasad, S., Pacifici, F., Gamba, P., Chanussot, J., & Benediktsson, J. A. (2015). Challenges and Opportunities of Multimodality and Data Fusion in Remote Sensing. *Proceedings of the IEEE*, *103*(9), 1585–1601. https://doi.org/10.1109/JPROC.2015.2462751

Dassot, M., Constant, T., & Fournier, M. (2011). The use of terrestrial Lidar technology in forest science: Application fields, benefits and challenges. *Annals of Forest Science*, *68*(5), Article 5. https://doi.org/10.1007/s13595-011-0102-2

de Groot, M., Ogris, N., & Kobler, A. (2018). The effects of a large-scale ice storm event on the drivers of bark beetle outbreaks and associated management practices. Forest Ecology and Management, 408, 195–201. https://doi.org/10.1016/j.foreco.2017.10.035

Department of Agriculture, U., & Resources Conservation Service, N. (2018). Title 190-Forestry Inventory Methods Technical Note Forestry Inventory Methods. www.ascr.usda.gov

Dickens, E. D., & Moorhead, D. (2016). Assessing hurricane and tornado storm damaged forest stands. Warnell School of Forestry and Natural Resources, The University of Athens, Georgia. https://bugwoodcloud.org/bugwood/productivity/pdfs/assessing_hurricane_and_tornado_damaged_forest_stands_Dec-2016_final. pdf.

d'Oliveira, M. V. N., Broadbent, E. N., Oliveira, L. C., Almeida, D. R. A., Papa, D. A., Ferreira, M. E., Zambrano, A. M. A., Silva, C. A., Avino, F. S., Prata, G. A., Mello, R. A., Figueiredo, E. O., de Castro Jorge, L. A., Junior, L., Albuquerque, R. W., Brancalion, P. H. S., Wilkinson, B., & Oliveira-da-Costa, M. (2020). Aboveground biomass estimation in Amazonian tropical forests: A comparison

of aircraft-and gatoreye UAV-borne LIDAR data in the Chico mendes extractive reserve in Acre, Brazil. Remote Sensing, 12(11). https://doi.org/10.3390/rs12111754

Duan, F., Wan, Y., & Deng, L. (2017). A novel approach for coarse-to-fine windthrown tree extraction based on unmanned aerial vehicle images. Remote Sensing, 9(4). https://doi.org/10.3390/rs9040306

Dumont, D., Casey, L., Glass, P., Baisden, B., Cartwright, W., Varner, A., Forester, S., Christie, B., Specialist, G., Mchugh, J., Wildlife, D., Coordinator, D., & Sisk, L. (n.d.). Alabama Statewide Forest Assessment and Resource Strategy i Neil Letson, Project Coordinator for Alabama Forestry Commission Developed with assistance from the Alabama Forest Resources Center Forest Assessment Team Alabama Forestry Commission.

Einzmann, K., Immitzer, M., Böck, S., Bauer, O., Schmitt, A., & Atzberger, C. (2017). Windthrow detection in European forests with very high-resolution optical data. *Forests*, *8*(1), 21.

Elsner, J. B., & Jagger, T. H. (2010). On the increasing intensity of the strongest Atlantic hurricanes. Hurricanes and Climate Change: Volume 2, 175-190.

Fan, C. L. (2023). Ground surface structure classification using UAV remote sensing images and machine learning algorithms. Applied Geomatics, 15(4), 919–931. https://doi.org/10.1007/s12518-023-00530-x

Feng, Q., Liu, J., & Gong, J. (2015). UAV Remote Sensing for Urban Vegetation Mapping Using Random Forest and Texture Analysis. *Remote Sensing*, *7*(1), 1074–1094. https://doi.org/10.3390/rs70101074

FOREST INVENTORY AND MONITORING GUIDELINES A Guidebook for NCF Members. (2014).

Fortuin, C. C., Montes, C. R., Vogt, J. T., & Gandhi, K. J. K. (2022). Predicting risks of tornado and severe thunderstorm damage to southeastern U.S. forests. Landscape Ecology, 37(7), 1905–1919. https://doi.org/10.1007/s10980-022-01451-7

Fortuin, C. C., Montes, C. R., Vogt, J. T., & Gandhi, K. J. K. (2021). Predicting Risks of Severe Windstorm Damage to Southeastern U.S. forests. https://doi.org/10.21203/rs.3.rs-1171624/v1

Frohn , R. & Arellano-Neri , O. 2005 . Improving Artificial Neural Networks Using Texture Analysis and Decision Trees for the Classification of Land Cover . GIScience and Remote Sensing , 42 (1) : 44 – 65

Gardiner, B., Blennow, K., Carnus, J.-M., Fleischer, P., Ingemarsson, F., Landmann, G., Lindner, M., Marzano, M., Nicoll, B., Orazio, C., Ingemarson, F., Lindner, M., Peyron, J.-L., Reviron, M.-P., Schelhaas, M.-J., Schuck, A., Spielmann, M., & Usbeck, T. (2010). Destructive storms in European forests: past and forthcoming impacts Final report to European Commission-DG Environment Destructive Storms in European Forests: Past and Forthcoming Impacts. https://hal.inrae.fr/hal-02824530

Global Forest Resources Assessment 2020. (2020). In Global Forest Resources Assessment 2020. FAO. https://doi.org/10.4060/ca8753en

Goodbody, T. R. H., Coops, N. C., Marshall, P. L., Tompalski, P., & Crawford, P. (2017). N o 1-THE FORESTRY CHRONICLE (Vol. 93).

Greenough, G., McGeehin, M., Bernard, S. M., Trtanj, J., Riad, J., & Engelberg, D. (2001). The potential impacts of climate variability and change on health impacts of extreme weather events in the United States. Environmental Health Perspectives, 109(suppl 2), 191–198. https://doi.org/10.1289/ehp.109-1240666

Guan, H., Yu, J., Li, J., & Luo, L. (2012). RANDOM FORESTS-BASED FEATURE SELECTION FOR LAND-USE CLASSIFICATION USING LIDAR DATA AND ORTHOIMAGERY. *The International Archives of the Photogrammetry, Remote Sensing and Spatial Information Sciences*, *XXXIX-B7*, 203–208. https://doi.org/10.5194/isprsarchives-XXXIX-B7-203-2012

Guo, Q., Su, Y., & Hu, T. (2023). *Lidar principles, processing and applications in forest ecology*. Academic Press. https://books.google.com/books?hl=en&lr=&id=NyWJEAAAQBAJ&oi=fnd&pg=PP1&dq=Lidar+Principles,+Processing+and+Applications+in+Forest+Ecology&ots=NnYlehVTg-&sig=j4rv5MR83Xtxk3XQOyTpFqtZlVA

Guo, Q., Su, Y., Hu, T., Zhao, X., Wu, F., Li, Y., Liu, J., Chen, L., Xu, G., Lin, G., Zheng, Y., Lin, Y., Mi, X., Fei, L., & Wang, X. (2017). An integrated UAV-borne Lidar system for 3D habitat mapping in three forest ecosystems across China. International Journal of Remote Sensing, 38(8–10), 2954–2972. https://doi.org/10.1080/01431161.2017.1285083

Hamdi, Z. M., Brandmeier, M., & Straub, C. (2019). Forest damage assessment using deep learning on high resolution remote sensing data. Remote Sensing, 11(17). https://doi.org/10.3390/rs11171976

Hartley, R. J. L., Leonardo, E. M., Massam, P., Watt, M. S., Estarija, H. J., Wright, L., Melia, N., & Pearse, G. D. (2020). An Assessment of High-Density UAV Point Clouds for the Measurement of Young Forestry Trials. Remote Sensing, 12(24), 4039. https://doi.org/10.3390/rs12244039

Hartling, S., Sagan, V., & Maimaitijiang, M. (2021). Urban tree species classification using UAV-based multi-sensor data fusion and machine learning. GIScience & Remote Sensing, 58(8), 1250–1275. https://doi.org/10.1080/15481603.2021.1974275

Honkavaara, E., Litkey, P., & Nurminen, K. (2013). Automatic storm damage detection in forests using high-altitude photogrammetric imagery. Remote Sensing, 5(3), 1405–1424. https://doi.org/10.3390/rs5031405

Hudak, A. T., Evans, J. S., & Smith, A. M. S. (2009). Lidar utility for natural resource managers. In Remote Sensing (Vol. 1, Issue 4, pp. 934–951). https://doi.org/10.3390/rs1040934

In, F., Hampshire, N., Merrens, E. J., & Peart, D. R. (1992). Effects of Hurricane Damage on Individual Growth and Stand Structure in a Hardwood. In Source: Journal of Ecology (Vol. 80, Issue 4).

Järnstedt, J., Pekkarinen, A., Tuominen, S., Ginzler, C., Holopainen, M., & Viitala, R. (2012). Forest variable estimation using a high-resolution digital surface model. ISPRS Journal of Photogrammetry and Remote Sensing, 74, 78–84. https://doi.org/10.1016/j.isprsjprs.2012.08.006

Jarrell, J. D., Miami Max Mayfield, T., Miami Edward Rappaport, T. N., Miami Christopher Landsea, T., Miami, H., Kelly, J. J., Assistant Administrator, J., Evans, D. L., & Lautenbacher, C. C. (2001). THE DEADLIEST, COSTLIEST, AND MOST INTENSE UNITED STATES HURRICANES FROM 1900 TO 2000 (AND OTHER FREQUENTLY REQUESTED HURRICANE FACTS). In NOAA Technical Memorandum NWS TPC (Issue 3).

Jaud, M., Grasso, F., le Dantec, N., Verney, R., Delacourt, C., Ammann, J., Deloffre, J., & Grandjean, P. (2016). Potential of UAVs for monitoring mudflat morphodynamics (Application to the Sein e Estuary, France). ISPRS International Journal of Geo-Information, 5(4). https://doi.org/10.3390/ijgi5040050

Khatami, R., Mountrakis, G., & Stehman, S. V. (2016). A meta-analysis of remote sensing research on supervised pixel-based land-cover image classification processes: General guidelines for practitioners and future research. *Remote Sensing of Environment*, *177*, 89–100. https://doi.org/10.1016/j.rse.2016.02.028

Kim, J., Popescu, S. C., Lopez, R. R., Wu, X. B., & Silvy, N. J. (2020). Vegetation mapping of No Name Key, Florida using Lidar and multispectral remote sensing. *International Journal of Remote Sensing*, *41*(24), 9469–9506. https://doi.org/10.1080/01431161.2020.1800125

Klauberg, C., Vogel, J., Dalagnol, R., Ferreira, M. P., Hamamura, C., Broadbent, E., & Silva, C. A. (2023). Post-Hurricane Damage Severity Classification at the Individual Tree Level Using Terrestrial Laser Scanning and Deep Learning. Remote Sensing, 15(4). https://doi.org/10.3390/rs15041165

Knutti, R., Arblaster, J., Dufresne, J., Fichefet, T., Friedlingstein, P., Gao, X., Gutowski, W., Johns, T., Krinner, G., Shongwe, M., Tebaldi, C., Weaver, A., Wehner, M., Qin, D., Plattner, G., Tignor, M., Allen, S., Boschung, J., Nauels, A., … Allen, M. R. (2013). Mxolisi Shongwe (South Africa), Claudia Tebaldi (USA).

Kupfer, J. A., Myers, A. T., McLane, S. E., & Melton, G. N. (2008). Patterns of forest damage in a southern Mississippi landscape caused by Hurricane Katrina. Ecosystems, 11(1), 45–60. https://doi.org/10.1007/s10021-007-9106-z

Lechner, A. M., Foody, G. M., & Boyd, D. S. (2020). Applications in Remote Sensing to Forest Ecology and Management. *One Earth*, *2*(5), 405–412. https://doi.org/10.1016/j.oneear.2020.05.001

Lee, S., & Yu, B.-H. (2018). Automatic detection of dead tree from UAV imagery. *Proceedings of the 39th Asian Conference on Remote Sensing, Kuala Lumpur, Malaysia*, 15–19. https://mycoordinates.org/automatic-detection-of-dead-tree-from-uav-imagery/

Lefsky, M. A., Cohen, W. B., Parker, G. G., & Harding, D. J. (2002). Lidar remote sensing for ecosystem studies: Lidar, an emerging remote sensing technology that directly measures the three-dimensional distribution of plant canopies, can accurately estimate vegetation structural attributes and should be of particular interest to forest, landscape, and global ecologists. BioScience, 52(1), 19-30.

Leite, R. V., Silva, C. A., Broadbent, E. N., Amaral, C. H. do, Liesenberg, V., Almeida, D. R. A. de, Mohan, M., Godinho, S., Cardil, A., Hamamura, C., Faria, B. L. de, Brancalion, P. H. S., Hirsch, A., Marcatti, G. E., Dalla Corte, A. P., Zambrano, A. M. A., Costa, M. B. T. da, Matricardi, E. A. T., Silva, A. L. da, … Klauberg, C. (2022). Large scale multi-layer fuel load characterization in tropical savanna using GEDI spaceborne Lidar data. Remote Sensing of Environment, 268. https://doi.org/10.1016/j.rse.2021.112764

Li, B., Hou, J., Li, D., Yang, D., Han, H., Bi, X., Wang, X., Hinkelmann, R., & Xia, J. (2021). Application of Lidar UAV for High-Resolution Flood Modelling. *Water Resources Management*, *35*(5), 1433–1447. https://doi.org/10.1007/s11269-021-02783-w

Li, M., Im, J., & Beier, C. (2013). Machine learning approaches for forest classification and change analysis using multi-temporal Landsat TM images over Huntington Wildlife Forest. *GIScience & Remote Sensing*, *50*(4), 361–384. https://doi.org/10.1080/15481603.2013.819161

Liang, W., Abidi, M., Carrasco, L., McNelis, J., Tran, L., Li, Y., & Grant, J. (2020). Mapping Vegetation at Species Level with High-Resolution Multispectral and Lidar Data Over a Large Spatial Area: A Case Study with Kudzu. *Remote Sensing*, *12*(4), 609. https://doi.org/10.3390/rs12040609

Liebel, L., & Körner, M. (2016). SINGLE-IMAGE SUPER RESOLUTION FOR MULTISPECTRAL REMOTE SENSING DATA USING CONVOLUTIONAL NEURAL NETWORKS. *The International Archives of the Photogrammetry, Remote Sensing and Spatial Information Sciences*, *XLI-B3*, 883–890. https://doi.org/10.5194/isprs-archives-XLI-B3-883-2016

Lillesand, T., Kiefer, R. W., & Chipman, J. (2015). Remote sensing and image interpretation. John Wiley & Sons.

Lu, B., & He, Y. (2017). Species classification using Unmanned Aerial Vehicle (UAV)-acquired high spatial resolution imagery in a heterogeneous grassland. *ISPRS Journal of Photogrammetry and Remote Sensing*, *128*, 73–85. https://doi.org/10.1016/j.isprsjprs.2017.03.011

Mancini, F., Dubbini, M., Gattelli, M., Stecchi, F., Fabbri, S., & Gabbianelli, G. (2013). Using unmanned aerial vehicles (UAV) for high-resolution reconstruction of topography: The structure from motion approach on coastal environments. Remote Sensing, 5(12), 6880–6898. https://doi.org/10.3390/rs5126880

Mcnulty, S. G. (2001). Hurricane impacts on US forest carbon sequestration. www.elsevier.com/locate/envpol

Messinger, M., Asner, G. P., & Silman, M. (2016). Rapid assessments of amazon forest structure and biomass using small unmanned aerial systems. Remote Sensing, 8(8). https://doi.org/10.3390/rs8080615

Michałowska, M., & Rapiński, J. (2021). A Review of Tree Species Classification Based on Airborne Lidar Data and Applied Classifiers. *Remote Sensing*, *13*(3), Article 3. https://doi.org/10.3390/rs13030353

Miranda, M.L., 1996. Final report: an evaluation of the Post-Hugo forest recovery programs: salvage, wildfire hazard mitigation and reforestation. In: Haymond, J.L., Hook, D.D., Harms, W.R. (Eds.). Hurricane Hugo: South Carolina Forest Land Research and Man- agement Related to the Storm (USDA Forest Service General Technical Report SRS-5). pp. 498–532.

Mitchell, R. J., Liu, Y., O'Brien, J. J., Elliott, K. J., Starr, G., Miniat, C. F., & Hiers, J. K. (2014). Future climate and fire interactions in the southeastern region of the United States. Forest Ecology and Management, 327, 316–326. https://doi.org/10.1016/j.foreco.2013.12.003

Mohan, M., Leite, R. V., Broadbent, E. N., Wan Mohd Jaafar, W. S., Srinivasan, S., Bajaj, S., Dalla Corte, A. P., Do Amaral, C. H., Gopan, G., Saad, S. N. M., Muhmad Kamarulzaman, A. M., Prata, G. A., Llewelyn, E., Johnson, D. J., Doaemo, W., Bohlman, S., Almeyda Zambrano, A. M., & Cardil, A. (2021). Individual tree detection using UAV-Lidar and UAV-SfM data: A tutorial for beginners. *Open Geosciences*, *13*(1), 1028–1039. https://doi.org/10.1515/geo-2020-0290

Musah, M., Diaz, J. H., Alawode, A. O., Gallagher, T., Peresin, M. S., Mitchell, D., Smidt, M., & Via, B. (2022). Field Assessment of Downed Timber Strength Deterioration Rate and Wood Quality Using Acoustic Technologies. Forests, 13(5). https://doi.org/10.3390/f13050752

N~esset, E. (1997). Determination of mean tree height of forest stands using airborne laser scanner data. In ISPRS Journal of Photogrammetry & Remote Sensing (Vol. 52).

Næsset, E., Gobakken, T., Holmgren, J., Hyyppä, H., Hyyppä, J., Maltamo, M., Nilsson, M., Olsson, H., Persson, Å., & Söderman, U. (2004). Laser scanning of forest resources: The nordic experience. Scandinavian Journal of Forest Research, 19(6), 482–499. https://doi.org/10.1080/02827580410019553

NOAA, 1997. The Deadliest, Costliest, and Most Intense United States Hurricanes of this Century (and Other Frequently Requested Hurricane Facts). NOAA Technical Memorandum NWS TPC-1 (updated February 1997).

Nothdurft, A., Gollob, C., Kraßnitzer, R., Erber, G., Ritter, T., Stampfer, K., & Finley, A. O. (2021). Estimating timber volume loss due to storm damage in Carinthia, Austria, using ALS/TLS and spatial regression models. Forest Ecology and Management, 502. https://doi.org/10.1016/j.foreco.2021.119714

Oza, M. P., & Sharma, S. A. (1990). A comparative study of supervised classifiers on a subscene in Junagadh district, Gujarat. *Journal of the Indian Society of Remote Sensing*, *18*(3), 18–24. https://doi.org/10.1007/BF03030729

Page, W. G., & Jenkins, M. J. (2007). Mountain pine beetle-induced changes to selected lodgepole pine fuel complexes within the intermountain region. *Forest Science*, *53*(4), 507-518.

Poblete-Echeverría, C., Olmedo, G. F., Ingram, B., & Bardeen, M. (2017). Detection and Segmentation of Vine Canopy in Ultra-High Spatial Resolution RGB Imagery Obtained from Unmanned Aerial Vehicle (UAV): A Case Study in a Commercial Vineyard. Remote Sensing, 9(3), Article 3. https://doi.org/10.3390/rs9030268

Popescu, S. C. (2007). Estimating biomass of individual pine trees using airborne Lidar. Biomass and Bioenergy, 31(9), 646–655. https://doi.org/10.1016/j.biombioe.2007.06.022

Popescu, S. C., Wynne, R. H., & Nelson, R. F. (2003). Measuring individual tree crown diameter with Lidar and assessing its influence on estimating forest volume and biomass. Canadian Journal of Remote Sensing, 29(5), 564–577. https://doi.org/10.5589/m03-027

Prestemon, J. P., & Holmes, T. P. (2010). Economic impacts of hurricanes on forest owners. *Pye, John M; Rauscher, H Michael; Sands, Yasmeen; Lee, Danny C*, 207-221.

Pye, J., Rauscher, H., Sands, Y., Lee, D., & Beatty, J. (2010). Advances in threat assessment and their application to forest and rangeland management—Volume 1 and. Gen. Tech. Rep. PNW-GTR-802. Portland, OR: US Department of Agriculture, Forest Service, Pacific Northwest and Southern Research Stations, 708.

Record-breaking Atlantic hurricane season draws to an end | National Oceanic and Atmospheric Administration. (2020, November 24). https://www.noaa.gov/media-release/record-breaking-atlantic-hurricane-season-draws-to-end

Renard, K. G. (1997). *Predicting soil erosion by water: a guide to conservation planning with the Revised Universal Soil Loss Equation (RUSLE)*. United States Government Printing.

Rijal, A., Cristan, R., & Parajuli, M. (2023). Application of Lidar in Forest Management. Alabama Cooperative Extension System. https://www.aces.edu/blog/topics/forestry/application-of-lidar-in-forest-management/

Rijal, A., Cristan, R., Gallagher, T., Narine, L. L., & Parajuli, M. (2023). Evaluating the feasibility and potential of unmanned aerial vehicles to monitor implementation of forestry best management practices in the coastal plain of the southeastern United States. Forest Ecology and Management, 545, 121280.

Rondeux, J., & Sanchez, C. (2010). Review of indicators and field methods for monitoring biodiversity within national forest inventories. Core variable: Deadwood. In Environmental Monitoring and Assessment (Vol. 164, Issues 1–4, pp. 617–630). https://doi.org/10.1007/s10661-009-0917-6

Rutledge, B. T., Cannon, J. B., McIntyre, R. K., Holland, A. M., & Jack, S. B. (2021). Tree, stand, and landscape factors contributing to hurricane damage in a coastal plain forest: Post-hurricane assessment in a longleaf pine landscape. Forest Ecology and Management, 481. https://doi.org/10.1016/j.foreco.2020.118724

Schiefer, F., Kattenborn, T., Frick, A., Frey, J., Schall, P., Koch, B., & Schmidtlein, S. (2020). Mapping forest tree species in high resolution UAV-based RGB-imagery by means of convolutional neural networks. ISPRS Journal of Photogrammetry and Remote Sensing, 170, 205–215. https://doi.org/10.1016/j.isprsjprs.2020.10.015

Schmugge, T. J., Kustas, W. P., Ritchie, J. C., Jackson, T. J., & Rango, A. (2002). Remote sensing in hydrology. *Advances in Water Resources*, *25*(8), 1367–1385. https://doi.org/10.1016/S0309-1708(02)00065-9

Seidl, R., Fernandes, P. M., Fonseca, T. F., Gillet, F., Jönsson, A. M., Merganičová, K., Netherer, S., Arpaci, A., Bontemps, J. D., Bugmann, H., González-Olabarria, J. R., Lasch, P., Meredieu, C., Moreira, F., Schelhaas, M. J., & Mohren, F. (2011). Modelling natural disturbances in forest ecosystems: A review. In Ecological Modelling (Vol. 222, Issue 4, pp. 903–924). https://doi.org/10.1016/j.ecolmodel.2010.09.040

Selvarajan, S. (2011). FUSION OF LIDAR AND AERIAL IMAGERY FOR THE ESTIMATION OF DOWNED TREE VOLUME USING SUPPORT VECTOR MACHINES CLASSIFICATION AND REGION BASED OBJECT FITTING.

Sharma, R., Ghosh, A., & Joshi, P. K. (2013). Decision tree approach for classification of remotely sensed satellite data using open source support. *Journal of Earth System Science*, *122*(5), 1237–1247. https://doi.org/10.1007/s12040-013-0339-2

Sharma, A., Ojha, S. K., Dimov, L. D., Vogel, J. G., & Nowak, J. (2021). Long-term effects of catastrophic wind on southern US coastal forests: Lessons from a major hurricane. PLoS ONE, 16(1 January). https://doi.org/10.1371/journal.pone.0243362

Shinoda, Y., & Akasaka, M. (2020). Interaction exposure effects of multiple disturbances: plant population resilience to ungulate grazing is reduced by creation of canopy gaps. Scientific Reports, 10(1). https://doi.org/10.1038/s41598-020-58672-6

Silva, C. A., Hudak, A. T., Vierling, L. A., Loudermilk, E. L., O'Brien, J. J., Hiers, J. K., Jack, S. B., Gonzalez-Benecke, C., Lee, H., Falkowski, M. J., & Khosravipour, A. (2016). Imputation of Individual Longleaf Pine (Pinus palustris Mill.) Tree Attributes from Field and Lidar Data. Canadian Journal of Remote Sensing, 42(5), 554–573. https://doi.org/10.1080/07038992.2016.1196582

Silva, C. A., Klauberg, C., Hudak, A. T., Vierling, L. A., Jaafar, W. S. W. M., Mohan, M., ... & Saatchi, S. (2017). Predicting stem total and assortment volumes in an industrial Pinus taeda L. forest plantation using airborne laser scanning data and random forest. *Forests*, *8*(7), 254.

Silva, C. A., Klauberg, C., Hudak, A. T., Vierling, L. A., Liesenberg, V., Carvalho, S. P. E., & Rodriguez, L. C. (2016). A principal component approach for predicting the stem volume in Eucalyptus plantations in Brazil using airborne Lidar data. *Forestry: An International Journal of Forest Research*, *89*(4), 422-433.

Sisodia, P. S., Tiwari, V., & Kumar, A. (2014). A comparative analysis of remote sensing image classification techniques. *2014 International Conference on Advances in Computing, Communications and Informatics (ICACCI)*, 1418–1421. https://doi.org/10.1109/ICACCI.2014.6968245

Sofonia, J. J., Phinn, S., Roelfsema, C., Kendoul, F., & Rist, Y. (2019). Modelling the effects of fundamental UAV flight parameters on Lidar point clouds to facilitate objectives-based planning. ISPRS Journal of Photogrammetry and Remote Sensing, 149, 105–118. https://doi.org/10.1016/j.isprsjprs.2019.01.020

Ståhl, G., Ringvall, A., & Fridman, J. (2001). Oikos Editorial Office Assessment of Coarse Woody Debris: A Methodological Overview.

Stepper, C., Straub, C., & Pretzsch, H. (2014). Using semi-global matching point clouds to estimate growing stock at the plot and stand levels: Application for a broadleaf-dominated forest in central Europe. Canadian Journal of Forest Research, 45(1), 111–123. https://doi.org/10.1139/cjfr-2014-0297

Storch, M., Jarmer, T., Adam, M., & de Lange, N. (2022). Systematic Approach for Remote Sensing of Historical Conflict Landscapes with UAV-Based Laserscanning. Sensors, 22(1), Article 1. https://doi.org/10.3390/s22010217

Tanner, E. V. J., Kapos, V., & Healey, J. R. (1991). Part A. Special Issue: Ecosystem, Plant, and Animal Responses to Hurricanes in the Caribbean (Vol. 23, Issue 4).

Taylor, A. R., Dracup, E., MacLean, D. A., Boulanger, Y., & Endicott, S. (2019). Forest structure more important than topography in determining windthrow during Hurricane Juan in Canada's Acadian Forest. Forest Ecology and Management, 434, 255–263. https://doi.org/10.1016/j.foreco.2018.12.026

Thapa, N., Narine, L. L., Fan, Z., Yang, S., & Tiwari, K. (2023). Detection of invasive plants using NAIP imagery and airborne Lidar in coastal Alabama and Mississippi, USA. *Annals of Forest Research*, *66*(1), 63–77. https://www.afrjournal.org/index.php/afr/article/view/2548

US Department of Commerce, N. (2021). Long-Track Tornadoes of March 25, 2021. NOAA's National Weather Service. Retrieved April 16, 2024, from https://www.weather.gov/bmx/event_03252021

USDA (United States Department of Agriculture), Forest Service, 1988. The South's Fourth Forest: Alternatives for the Future (Forest Resource Report No. 24 June 1988). Washington, DC, p. 511.

Van Alphen, R., Rains, K. C., Rodgers, M., Malservisi, R., & Dixon, T. H. (2024). UAV-Based Wetland Monitoring: Multispectral and Lidar Fusion with Random Forest Classification. Drones, 8(3), 113. https://doi.org/10.3390/drones8030113

Villa, G., Moreno, J., Calera, A., Amorós-López, J., Camps-Valls, G., Domenech, E., Garrido, J., González-Matesanz, J., Gómez-Chova, L., Martínez, J. Á., Molina, S., Peces, J. J., Plaza, N., Porcuna, A., Tejeiro, J. A., & Valcárcel, N. (2013). Spectro-temporal reflectance surfaces: A new conceptual framework for the integration of remote-sensing data from multiple different sensors. *International Journal of Remote Sensing*, *34*(9–10), 3699–3715. https://doi.org/10.1080/01431161.2012.716910

Wallace, L., Lucieer, A., Watson, C., & Turner, D. (2012). Development of a UAV-Lidar system with application to forest inventory. Remote Sensing, 4(6), 1519–1543. https://doi.org/10.3390/rs4061519

Wallace, L., Watson, C., & Lucieer, A. (2014). Detecting pruning of individual stems using airborne laser scanning data captured from an Unmanned Aerial Vehicle. International Journal of Applied Earth Observation and Geoinformation, 30(1), 76–85. https://doi.org/10.1016/j.jag.2014.01.010

Wang, X., Wang, Y., Zhou, C., Yin, L., & Feng, X. (2021). Urban forest monitoring based on multiple features at the single tree scale by UAV. Urban forestry & urban greening, 58, 126958.

Wear, D. N., & Greis, J. G. (2012). The Southern Forest Futures Project: Summary Report.

Wischmeier, W. H., & Smith, D. D. (1978). *Predicting rainfall erosion losses: a guide to conservation planning*. Department of Agriculture, Science and Education Administration.

Xi, W., Peet, R. K., & Urban, D. L. (2008). Changes in forest structure, species diversity and spatial pattern following hurricane disturbance in a Piedmont North Carolina forest, USA. Journal of Plant Ecology, 1(1), 43–57. https://doi.org/10.1093/jpe/rtm003

Xu, Z., Li, W., Li, Y., Shen, X., & Ruan, H. (2019). Estimation of secondary forest parameters by integrating image and point cloud-based metrics acquired from unmanned aerial vehicle. Journal of Applied Remote Sensing, 14(02), 1. https://doi.org/10.1117/1.jrs.14.022204

Zhang, X., Zhang, F., Qi, Y., Deng, L., Wang, X., & Yang, S. (2019). New research methods for vegetation information extraction based on visible light remote sensing images from an unmanned aerial vehicle (UAV). *International Journal of Applied Earth Observation and Geoinformation*, *78*, 215–226. https://doi.org/10.1016/j.jag.2019.01.001

Chapter 2. Effectiveness of Unmanned Aerial Vehicle-Based Lidar for Assessing the Impact of Catastrophic Windstorm Events on Timberland

2.1. Abstract

The southeastern United States (US) is known for its highly productive forests but faces increasing challenges from climate-induced windstorms like hurricanes and tornadoes. These storms are threatening the sustainability and economic viability of these critical ecosystems. To address the pressing need for efficient and accurate windstorm damage assessments, this study explored the effectiveness of using unmanned aerial vehicles (UAVs) equipped with Light Detection and Ranging (lidar) and RGB imagery in the detection, classification, and mapping of storm-damaged forest stands. The primary objective of the study was to conduct a comparative analysis of three distinct classification techniques: Maximum Likelihood (ML), Decision Tree (DT), and Random Forest (RF), using two datasets: RGB imagery and its derivatives integrated with lidar-derived Canopy Height Models (CHM) and without lidar-CHM. The study's findings indicated that the RF classifier outperformed ML and DT methods, achieving the highest average overall accuracy (OA) of 94.52% with the CHM-integrated dataset and the highest average OA of 77.56% without the CHM-integrated dataset. These findings demonstrated the potential of UAV-lidar and RGB imagery as efficient, accurate, and cost-effective tools for quickly assessing windstorm damage. This study provides a foundational step towards developing advanced remote sensing applications for environmental monitoring and disaster management, paving the way for future research in optimizing and scaling these methodologies across various forested landscapes and storm conditions.

Keywords: UAVs, lidar, hurricane, tornado CHM, random forest

2.2. Introduction

The southeastern US is home to some of the world's most productive forests, which contribute significantly to the country's local and national economies. These forests provide a significant source of softwood lumber, pulpwood, and other forest products while also serving as crucial habitats for a diverse range of wildlife (Oswalt et al., 2019; Parajuli et al., 2023; Wear & Greis, 2002; Wear & Greis, 2013). However, the escalating frequency of climate-induced disasters, including windstorm events, is adversely affecting the productivity, stability, and sustainability of forests within this region (Gardiner et al., 2010; Mitchel et al., 2014). An increase in the severity and frequency of extreme weather events, such as hurricanes and tornadoes, causes significant damage to forests. These events snap trees, uproot trees, break branches, alter soil structure, and cause erosion, leading to loss of timber, decreased carbon sequestration, and destruction of habitat (Fortuin et al., 2022; Sharma et al., 2021; Xi et al., 2008)

Hurricanes and tornadoes can destroy thousands of acres of forest land in a matter of days, removing more trees than what is typically harvested in a year which results in significant financial losses for landowners (Fortuin et al., 2022; McNulty, 2002; Mitchell et al., 2021). For instance, on March 25, 2021, ten tornadoes occurred in Alabama, causing extensive damage to the Oakmulgee National Forest and nearby private forestland (Mitchell et al., 2021; NWS, 2021). In 2018, hurricane Michael caused significant damage to 958,387 hectares of forest land in Georgia, with a pre-hurricane value of approximately $762 million USD (Georgia Forestry Commission, 2018). Similarly, Hurricane Laura caused severe destruction to Louisiana's Kisatchie National Forest in 2020, damaging almost half of its 242,811 hectares and impacted

nearly 323,748 hectares of timber in the state, with the total loss valued at $1.2 billion USD (Blazier, 2021; Mitchell et al., 2021).

Hurricanes and tornadoes cause significant damage to forests, resulting in financial losses if the timber is not recovered. These events impact wood quality and also reduce timber value since the market is flooded (Mitchell et al., 2021; Pye et al., 2010). This can result in landowners having to sell their timber at low prices or even the ability to get a logger on site before the wood quality diminishes. Bradley et al. (2018) emphasized the importance of timely salvage operations for storm-damaged pine trees, recommending immediate harvesting for trees with severe damage to maximize resource recovery, while suggesting a 2-3 month window for uprooted trees to prevent decay from fungi and pests. Moreover, increased storms can lead to more timber destruction, scattered downed timber, and secondary disturbances such as insect attacks, erosion, and wildfires (Musah et al., 2022). As a result, assessing storm damage is critical in determining the nature and scope of the damage. This can help determine if the stands are still viable and planning for salvage harvesting as needed. On-the-ground field surveys have traditionally been used to estimate windstorm damage. However, they are labor-intensive, time-consuming, expensive, and pose a safety risk to the surveyors due to the snapped and leaning trees and amount of debris on the ground (Bouget & Duelli, 2004; Ritter et al., 2022; Windrim et al., 2019). Remote sensing technologies have revolutionized the process of forest assessment and damage estimation by providing information without being physically present on-site or in a safe area near the damaged area (i.e., forest road) if using unmanned aerial vehicles (UAVs).

UAVs have become popular in remote sensing and forestry due to their capacity to offer detailed three-dimensional (3D) data (Banu et al., 2016, Rijal et al., 2023). UAVs have been used in a variety of forestry applications, including quantifying forest structure (Almeida et al., 2019; Alonzo et al., 2018), disaster management (Dassot et al., 2011; Li et al., 2021; Rajan et al., 2021), and disease mapping (Dash et al., 2017; Housman et al., 2018). Light Detection and Ranging (lidar), an active remote sensing technology that uses a pulsed laser to precisely measure the earth's surface (Dong & Chen, 2017; Guo et al., 2023), has been used in several studies to identify and map vegetation, land cover change, species identification, and other applications (Cao et al., 2019; Liu et al., 2018). For instance, Corte et al. (2020) demonstrated the effectiveness of UAV-based lidar technology in estimating individual tree dendrometric metrics when combined with machine learning techniques like Support Vector Regression, RF, Artificial Neural Networks, and Extreme Gradient Boosting.

UAV-lidar, also known as drone-lidar, has improved forest research by providing a rapid, precise, cost-effective, accessible, and versatile method for measuring the three-dimensional structure of forests. This technology offers various advantages over other remote sensing systems like satellite and airborne systems (Goodbody et al., 2017; Sofonia et al., 2019; Xu et al., 2019). Lidar-derived products, combined with remotely sensed imagery, are highly beneficial for vegetation classification, species identification, and land cover classification tasks (Bandyopadhyay et al., 2013; Secord et al., 2017; Shi et al., 2018). Aerial imagery complements lidar data by providing detailed visual information about tree crowns, canopy cover, and understory vegetation. The integration of these datasets enhances the accuracy of tree height and canopy structure estimation, which is crucial for forestry applications like post-disaster damage

assessments, timber volume estimation, and habitat modeling (Bork & Su, 2007; Ritter et al., 2022; Thapa et al., 2023).

Effective classification techniques are crucial for obtaining reliable information from remotely sensed data. Over the years, several classification approaches have been developed to facilitate the accurate and precise gathering of earth observation information. The most widely used image classification techniques include parametric classification methods like Maximum Likelihood (ML) classification (Chuvieco, 2020; Zhai et al., 2012) and non-parametric classification methods like traditional Decision Tree (DT) method (Otukei & Blaschke, 2010; Sharma et al., 2013) and machine learning approaches such as Random Forest (RF) (Balha & Singh, 2022; Breiman, 2001; Queiroz et al., 2019). Among these methods, researchers have gained considerable interest in machine learning classifiers due to their ability to handle non-linear data effectively, offer higher classification accuracy, and provide user flexibility (Ba et al., 2020; Kim et al., 2020; Li et al., 2013).

Few studies have been conducted using lidar data and aerial imagery to detect windthrown trees and map woody debris in windstorm-affected areas. Lidar data is considered more advantageous than other methods in such studies as it is not affected by canopy obstruction and can accurately identify individual windthrown trees (Niemi & Vauhkonen, 2016; Tran et al., 2018). Detecting and mapping windthrown trees and woody debris can be a challenging task. However, it can be addressed using various remote sensing platforms such as airborne, terrestrial, and UAVs. Blanchard et al. (2011) employed airborne lidar data and object-based image processing to detect and examine downed trees in forest areas. The study accurately

categorized 73% of digitized downed trees. However, misclassification occurred due to non-tree objects with similar lidar signatures and in areas with noncontiguous objects or data gaps, complicating accurate classification.

Polewski et al. (2015) suggested detecting fallen trees in airborne lidar point clouds by merging short segments into entire stems with the Normalized Cut algorithm. This approach demonstrated the ability to detect up to 90% of fallen stems in plots while retaining an accuracy rate greater than 80%. However, the study's rigorous and multiple steps for data processing might pose challenges regarding processing time and resource needs, particularly for big lidar data sets. Queiroz et al. (2019) focused on developing a methodology for detecting standing dead trees referred to as snags and downed coarse woody debris (CWD) using centimetric aerial imagery combined with airborne lidar data. The researchers employed RF machine learning classifier alongside a Geographic Object-Based Image Analysis (GEOBIA) approach, utilizing spectral, spatial, and lidar-derived height variables as predictors. The results demonstrated high accuracy in CWD detection within the application area, with a reported 93.4% completeness and 94.5% correctness when training samples were located within the application area. However, applying the trained model's effectiveness to different sites or forest types without retraining could be limited, especially if those areas have significantly different environmental conditions.

UAVs have emerged as a well-suited alternatives to airborne and terrestrial lidar systems for varying topography and have been used in some studies to detect fallen logs. Panagiotidis et al. (2019) utilized high-resolution RGB images from UAVs to identify fallen logs in forests by employing a line template matching algorithm based on Hough transformation. Likewise, Duan

et al. (2017), demonstrated the potential of high-resolution UAV imagery for recognizing fallen trees using the Hough transformation algorithm. The method achieved a completeness of 75.7% and a correctness of 92.5%, indicating high reliability in detecting fallen logs. However, the extraction process occasionally misclassified branches and objects with similar geometry as windthrown trees, indicating a limitation in distinguishing between tree trunks and objects of comparable shape. Inoue et al. (2014) conducted a study exploring the use of high-resolution imagery obtained from UAVs to survey fallen trees in a deciduous broadleaved forest in Eastern Japan. The study successfully identified 80% to 90% of fallen trees larger than 30 cm in diameter or a length greater than 10 m. However, detecting smaller fallen trees was challenging due to image resolution limitations and the complexity of the forest floor.

Prior studies have utilized airborne lidar, terrestrial lidar, airborne imagery, or UAV-imagery independently to detect fallen trees and woody debris. However, limited research has been conducted into the feasibility of using UAV-lidar in conjunction with UAV-derived imagery to map and classify storm-damaged forests. Windstorms such as hurricanes and tornadoes frequently cause massive damage to timberland in the southeastern US, making it critical to develop a faster, more efficient, and accurate approach for assessing the impacts and mapping storm-damaged forests. The advent of UAV technology provides an excellent and time-efficient opportunity to understand the pattern, nature, and severity of damage following any windstorm event. This provides landowners, foresters, and stakeholders with detailed observations and essential information for fine-scale post-disaster planning and decision-making.

The primary goal of this study was to examine the effectiveness of lidar and RGB imagery captured from a UAV in detecting, classifying, and mapping storm-damaged forest stands in windstorm-affected regions of the southeast US. The study classifies windstorm-damaged sites into four major classification categories based on their condition: downed trees, standing trees, ground (non-trees), and water. This classification is crucial for assessing the damage caused by windstorms and aids in efficiently allocating resources for recovery efforts.

2.3. Materials and Methods

2.3.1. Study Area

The study included ten sites (Figure 1) that were damaged by hurricanes and tornadoes in 2022 and 2023. Six of the ten sites were damaged by tornadoes in Alabama, two by tornadoes in Georgia, and two by hurricanes in Florida. Of the ten study sites, five sites were around 20 acres, and the remaining five were around 10 acres in area. The humid and subtropical climate, soil types, vegetation, topography, and historical land use patterns all contributed to the study area's distinctive ecosystems. All the study sites were located within proximity to the Atlantic Ocean and the Gulf of Mexico, which highly influences catastrophic weather events, making them vulnerable to windstorm hazards. The locations, combined with the climate of the study areas, further exposes them to frequent natural phenomena, including, thunderstorms, tornadoes, and hurricanes, particularly during the summer and fall months (Zabel et al., 2017). The most common tree species found in all the ten sites was *Pinus taeda* (loblolly pine), with only a few occurrences of hardwood species like *Quercus spp.* in some sites.

The National Weather Service (NWS) Damage Assessment Toolkit (DAT), which contains information on points, routes, track centerlines, and damage swaths of tornadoes and convective wind events, was used to identify study sites. The DAT is a GIS-based system that gathers, saves, and analyzes windstorm damage data using the Enhanced Fujita (EF) scale. Hurricane data were acquired from the National Oceanic and Atmospheric Administration's (NOAA) National Hurricane Center (NHC). The data were accessible through a user-friendly web-based graphical interface. Based upon the preliminary damage path analysis from NWS DAT and NOAA NHC, the following counties were found to be severely affected by tornados and hurricanes: Bibb, Tuscaloosa, and Coosa in Alabama; Troup in Georgia; and Perry in Florida. Field visits were conducted to confirm the damage and finalize the study area.

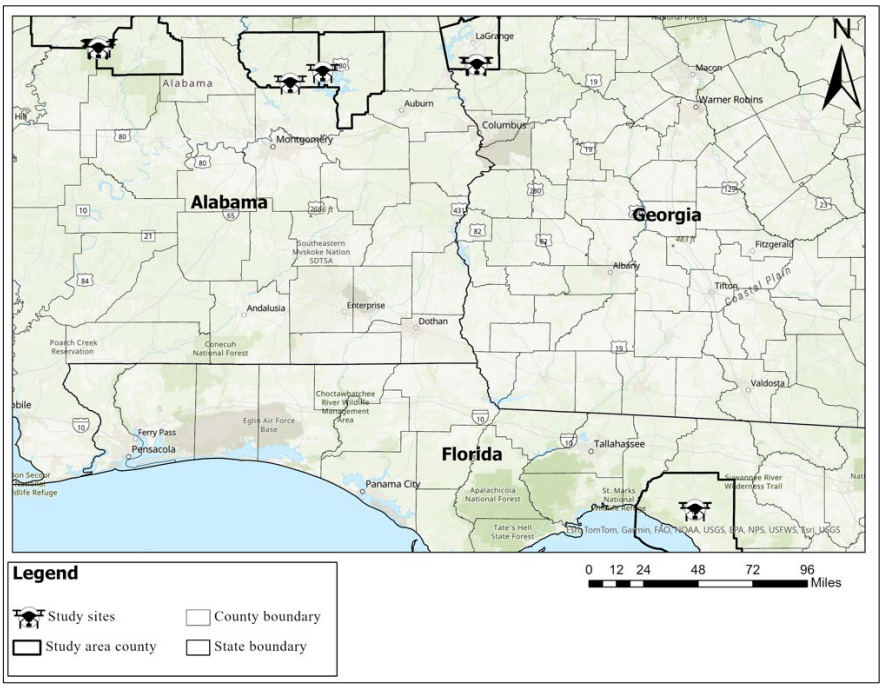

Figure 1. Study site locations.

2.3.2. Data Acquisition

2.3.2.1. Forest Inventory

Stand-level data was collected using 1/10th acre plots, and the number of sites included six plots randomly selected on sites between 11-20 acres and three plots on sites 10 acres and under (Department of Agriculture & Resources Conservation Service, 2018; Northwest Natural Resource Group, 2014). Tree measurements included tree count, tree species, diameter at breast height (DBH), diameter at both ends of fallen or uprooted trees, height of standing trees, and length of downed trees. Damage condition of trees were recorded and included snapped trees (trunk snapped with stem or crown broken), uprooted/fallen trees, bole only (stem breakage/no crown), and standing trees with no damage (Klauberg et al., 2023). DBH was measured using a diameter tape, tree height was measured using a clinometer for standing trees, and tree length was measured using a tape measure for fallen trees. Trimble's R2 GNSS receiver was used to acquire high-accuracy positioning of each sampled tree.

2.3.2.2. Remote Sensing Data Collection

The study utilized two forms of remotely sensed data - lidar data and RGB imagery. These data were captured using the DJI Matrice 300 (M300) Real-Time Kinematic (RTK) UAV equipped with the DJI Zenmuse L1 lidar sensor, which includes a Red-Green-Blue (RGB) camera. The M300 is equipped with a GNSS RTK receiver, providing high-accuracy positioning. The DJI Zenmuse L1 produces a true-color point cloud using the combined data from the RGB sensor and Inertial Measurement Unit (IMU). The DJI Pilot app was used to create and conduct flight plans. The M300 was flown at an altitude of 70 meters (230 feet) above ground level (AGL), with a speed of 5 m/s (11 mph), 70/60 percentage front and side overlap, 160 kHz

sampling rate, repetitive scanning mode, triple return/echo mode, and with elevation optimization and IMU calibration turned on. The direction of the flight plan was selected to minimize the flight duration. The Zenmuse L1 requires centimeter-level positional data for point cloud data processing, which can be collected using either RTK (Real-Time Kinematic) or PPK (Post-Processed Kinematic) methods. For this study, we used RTK networks hosted by the Alabama Department of Transportation (ALDOT), the Florida Department of Transportation (FDOT), and eGPS RTK Network in Georgia. All of these networks provide real-time corrections. The ALDOT and FDOT networks are free for users to set up and stream NTRIP from anywhere in Alabama and Florida. To connect to the NTRIP service, user accounts were created on the ALDOT and FDOT websites. The provided account information was entered into the RTK setting tab of the DJI Pilot app. To use the NTRIP service, the Custom Network RTK option was selected in the DJI Pilot app of the remote controller, and the account details were entered. It is important to set up the custom RTK information during the flight planning process. Once connected, the RTK status remained active throughout the flight. To maintain the RTK connection, the remote controller remained connected to the internet throughout the flight. Figure 2 illustrates the overall workflow of the study.

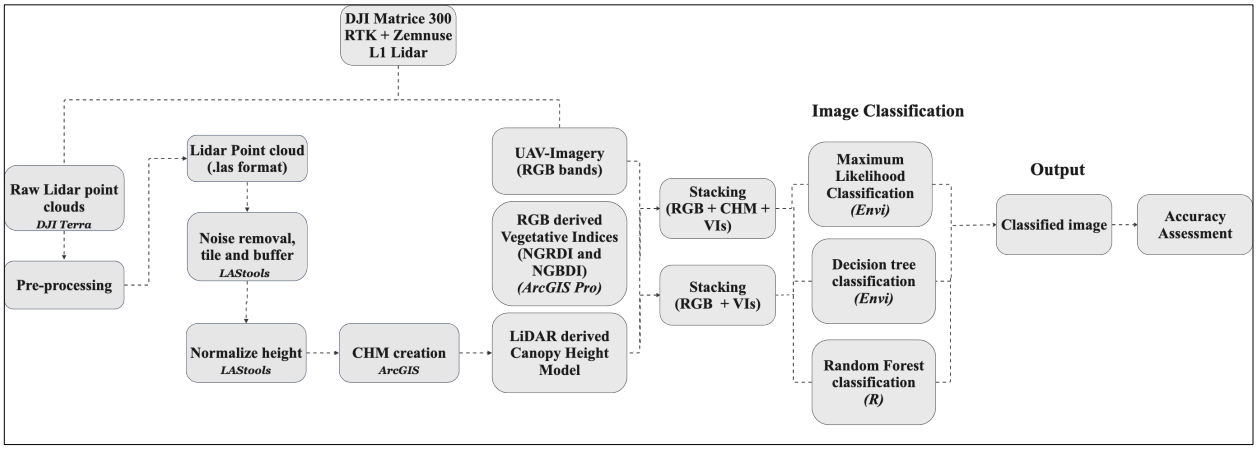

Figure 2. Workflow of the study

2.3.3. Data Processing

2.3.3.1. Lidar Data Pre-processing and Derived Products

Lidar data obtained from the DJI Zenmuse L1 was pre-processed using DJI Terra, which is a proprietary software that is used to process lidar data captured specifically by the DJI Zenmuse L1 sensor. A point cloud processing mission was first created, and raw data was entered into the program. The processing parameters were set to enable high-point cloud density and accuracy optimization. The output coordinate system was defined as WGS84/UTM zones, and the reconstruction output was set to PNTS and LAS format. A high point cloud density was selected, which used 100% of the data for processing. The point coordinates were geo-referenced using RTK data obtained through the defined custom network. After successfully processing the data, a '.las' file containing the point cloud data was created.

Lidar point cloud data was then processed to obtain normalized height, remove noise, and classify the ground using LAStools (Isenburg, 2012) software. Functions used within LAStools included lasnoise to remove noise from the point cloud data, lastile to create tiles and buffers to prevent edge artifacts during data processing, lasground classified the points as ground and non-ground points, lasheight to obtain normalized height (height above ground level) and filtering was done to remove heights below 0 m and above the height of the tallest tree recorded during the field survey. Lastile was used again to remove the buffer and lasmerge to merge the tiled lidar data.

The obtained normalized point cloud data was processed using Esri ArcGIS Pro 3.1.0 (Esri, 2023) to generate a Canopy Height Model (CHM) with grid sizes ranging from 2.5 to 3.5

cm. Additionally, Digital Elevation Models (DEMs) were also created and used to derive the slope and aspect products.

2.3.3.2. RGB Imagery Processing and Derived Products

The RGB imagery acquired by the DJI Zenmuse L1 was processed using ArcGIS Drone2Map software (ArcGIS Drone2Map, 2022). The orthomosaic resolution ranged from 2.5 to 3.5 cm, and depending on site location, each output was referenced to UTM Zone 16 N for Alabama and Georgia sites and UTM Zone 17 N for Florida sites.

Four vegetative indices were created using three bands of the RGB imagery (Red band (R), Green band (G), and Blue band (B)): Normalized Green Red Difference Index (NGRDI) (Du & Noguchi, 2017), Normalized Green Blue Difference Index (NGBDI) (Zhang et al., 2019), Excess Green Index (ExG), and Excess Red Index (ExR) (Beniaich et al., 2019; Meyer & Neto, 2008) (Table 2). NGBDI and NGRDI are two extensively used RGB-derived vegetative indices that are useful in detecting vegetation changes by highlighting the differences in the spectral signature of healthy, stressed, dead, or non-vegetated areas, with values ranging from -1 to 1. Values closer to 1 indicate healthy green vegetation, while values closer to -1 indicate lower or absence of vegetation (Du & Noguchi, 2017). The vegetative indices were calculated using ArcGIS Pro 3.1.0.

ffTable 2. Vegetation indices derived from RGB bands.

Vegetative Indices	Formula
Normalized Green Red Difference Index (NGRDI)	(G+R)/(G−R)
Normalized Green Blue Difference Index (NGBDI)	(G+B)/(G−B)

Excess Green Index (ExG)	2G−R−B
Excess Red Index (ExR)	1.4 R – G

2.3.4. Image Classification Scheme

The study focused on assessing the effectiveness of UAV-lidar in identifying and mapping windstorm damage. To achieve this, two datasets were created for the image classification process. The first dataset consisted of RGB bands, NGRDI, and NGBDI stacked together with lidar-derived CHM. Similarly, the second dataset included RGB imagery stacked with only vegetative indices NGRDI and NGBDI. The RGB imagery and its derived indices were resampled to match the spatial resolution of CHM before stacking. These two sets of data were then used separately as input for image classification, employing three different classification techniques: Maximum Likelihood Classification, Decision Tree classification, and Random Forest classification.

During the initial stages of our classification task, we attempted to integrate slope, aspect, and two RGB-derived indices, ExG and ExR, with other datasets (RGB bands, NGRDI, NGBDI, and lidar-CHM). This integration was tested at one of the study sites to assess their contributions to the classification of windstorm-damaged forest stands into four classes: downed trees, standing trees, ground (non-trees), and water. Although slope and aspect have been widely used in ecological studies, often for analyzing forest composition, species richness, and diversity, they did not significantly aid in this study (Méndez-Toribio et al., 2016; Sharma et al., 2010). We observed that the vegetative indices (ExG and ExR) exhibited high spectral similarity among the classes, increasing confusion among classes. Similarly, slope and aspect data were also of limited value. This lack of influence could be attributed to the assumption that the orientation (aspect)

and steepness (slope) of the terrain do not directly relate to the condition of the trees (whether downed or standing). Trees in various states can occupy terrains with identical slope and aspect characteristics, which might diminish the discriminatory capability of these variables in classifying tree status post-storm damage.

2.3.4.1. Definition of Classification Criteria and Training Sample Collection

Defining classes for image classification is a crucial process that is closely tied to the project's objectives, the study area, and the resolution and quality of the input data (Feng et al., 2015). High-resolution UAV-imagery is particularly effective for this task, enabling accurate differentiation between downed trees, standing trees, ground, and waterbodies. Given the varying conditions across the sites, four distinct classification categories were selected and included downed trees, standing trees, ground (non-trees), and water. Soils on four sites were saturated at the time of sampling, which resulted in water on portions of the sites.

Choosing appropriate training samples is a crucial step in implementing supervised image classification techniques. The aim is to capture the spectral variability by sampling representative pixels within the study area (Chuvieco, 2020). Training samples were randomly selected for each class at each study area based on visual interpretation of UAV imagery and prior knowledge of the study area gained during the site visit. The samples were selected to represent each class while appropriately capturing the necessary spectral variability. Training data and test data were defined based on the training data selection guideline from Fundamentals of Remote Sensing (Chuvieco, 2020). To prepare the training data, three regions of interest (ROIs) included downed trees, standing trees, and ground for six sites, while four ROIs included downed trees, standing

trees, ground, and water for the remaining four sites with water. The desired pixels for each ROI were acquired by zooming in on the UAV imagery using the ROI tool in ENVI. The Jeffries-Matusita distance and Transformed Divergence measure was used as a measure for spectral separability between classes, ranging from a scale of 0 to 2 (Sen et al., 2019). Classes with a spectral separability value of at least 1.9 were considered well-separated (Richards & Jia, 1999). Selection of the training samples and spectral separability was conducted in ENVI 5.6.2.

2.3.4.2. Image Classification

The first classification method used for the study was the Maximum Likelihood Classification, a popular supervised classification method that requires training data (Ok et al., 2012; Sharma et al., 2013; Sisodia et al., 2014). ML classifier assigns each pixel to a class based on the spectral and statistical properties of the training data. Two distinct datasets were utilized as input, the first dataset was integrated with lidar-CHM, RGB bands, NGRDI, and NGBDI, and the second included only the RGB bands, NGRDI, and NGBDI. The unimodal statistics of ROIs with spectral separability greater than 1.9 were obtained, and the classification was then performed using ENVI.

Decision Tree was the second classification method used and was also performed using ENVI 5.6.2 (Figure 3). DT is a flexible and simple non-parametric classifier capable of multistage classification by utilizing a series of binary decisions to assign pixels into distinct classes (Sharma et al., 2013; Zhai et al., 2012). With each new expression entered, a binary decision is generated, resulting in two new classes that can be divided into two more classes based on another expression (Sisodia et al., 2014). These expressions or rules include thresholds

on spectral bands and other auxiliary information such as elevation (Chuvieco, 2020). Each band within each dataset was unique, necessitating careful analysis to determine the threshold for dividing pixels into different classes. The recorded values for each image band from the training data were carefully examined to find the appropriate thresholds required to classify pixels into distinct groups for conducting DT classification. By identifying distinct values within each class, specific threshold values were defined. The pixel values differed across all ten sites. The CHM, NGRDI, and NGBDI bands displayed higher values for standing live trees, while significantly lower values were seen for downed trees, ground, and water. Conversely, the red and blue bands exhibited lower values in standing trees than in other classes. These distinct values served as the foundation for categorizing pixels into different classes while constructing the DT.

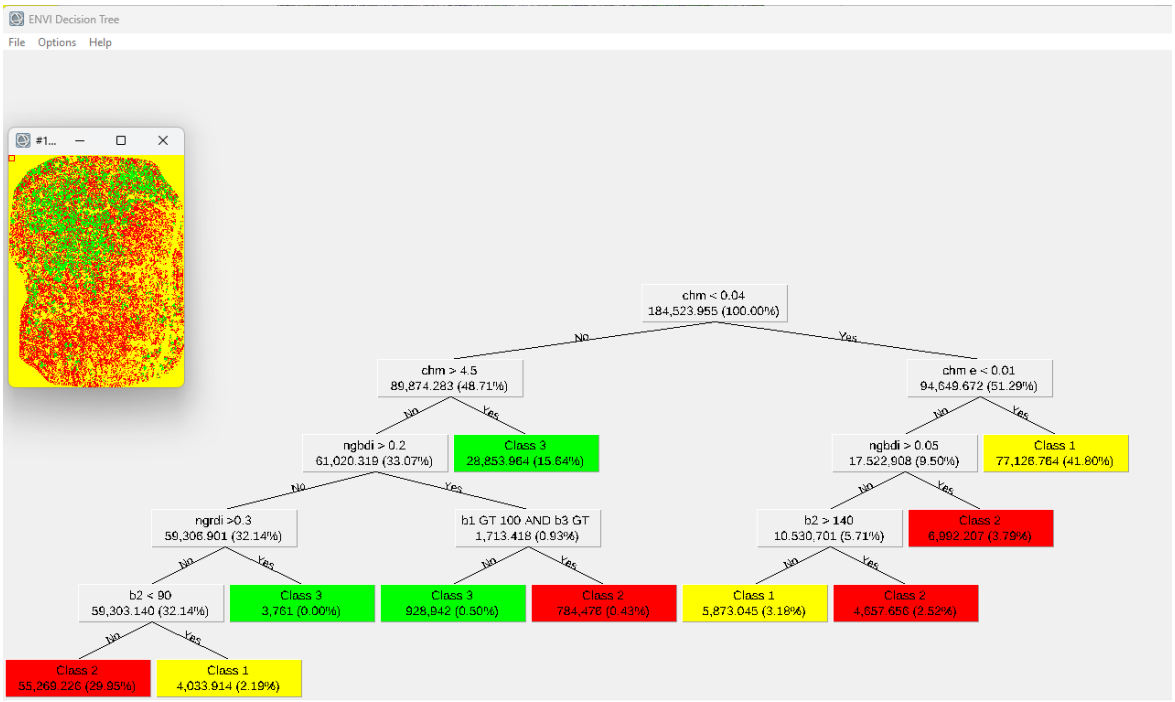

Figure 3. Decision tree implementation in ENVI.

The third approach used for was Random Forest, which was implemented using the R statistical software program (Breiman, 2001). Instead of generating a single tree, this method builds a forest (or group) of trees by randomly selecting input variables and training samples, usually reserving 80% for training and 20% for model testing. Out-of-bag (OOB) error samples (samples that are not used during tree construction) are employed to estimate the classification error (Guan et al., 2012). This algorithm is an advantageous classification method due to its computational efficiency, noise insensitivity, and resistance to overfitting. Furthermore, it can also determine the importance of each input variable (Feng et al., 2015). In this study, RF was implemented using ModelMap, a comprehensive and user-centric R package. ModelMap is specifically designed to streamline the processes of modeling and spatial mapping through a suite of functions such as model.build(), model.diagnostics(), model.mapmake(), model.importance.plot(), and model.interaction.plot() (Freeman et al., 2023). The predictor variables used for RF modeling RGB imagery bands: R, G, and B, NGRDI, NGBDI, and lidar-derived CHM.

2.3.4.3. Accuracy Assessment

To quantitatively analyze the classification performance of the three classifiers, ENVI software was utilized to create a confusion matrix for accuracy assessment using independent validation samples. ENVI's ROI tool was used to create the validation (testing) data. To evaluate the accuracy of each classification approach used in the study, the same sets of test data were used for all three classification methods on the same site. The location information collected by the Trimble R2 GNSS receiver was utilized for the selection of the test data. To measure the performance of all three classification algorithms, classification indicators within the confusion

matrix were calculated and examined, including overall accuracy (OA), Kappa coefficient (k), producer accuracy (PA), and user accuracy (UA). OA measures the proportion of correctly classified samples out of the total number of samples in the dataset. It is calculated as the ratio of the total number of correctly classified samples to the total number of samples. The Kappa coefficient is a measure of agreement between observed classification results and expected results by chance, with values ranging from -1 to 1. Here, 1 denotes full agreement, 0 denotes agreement equal to chance, while value closer to -1 indicates agreement poorer than chance. PA is a measure that determines the likelihood that a specific class on the ground is accurately classified in the map or model. While UA is a measure that assesses the probability that the model-identified class represents that class on the ground (Chuvieco, 2020).

2.4. Results

The study examined the effectiveness of RF, ML, and DT classifiers in mapping windstorm damages across six tornado-damaged sites in Alabama (Sites 1-6), two tornado-damaged sites in Georgia (Sites 7-8), and two hurricane-damaged sites in Florida (Sites 9-10). UAV-captured RGB and lidar data were used to generate two independent datasets used separately with all three classification methods (Section 2.3.4). Damage classification maps with four distinct categories (downed trees, standing trees, ground, and water) (Section 2.3.4.1) were generated (Figures 4-7). The classification accuracy was evaluated using a confusion matrix (Tables 5-9 and 11-14). The results were summarized according to the dataset and classification method utilized. (Tables 3, 4 and 10) summarizes the results comparing the accuracy attained, including overall accuracy, kappa coefficient, producer accuracy, and user accuracy across all sites.

The performance of different classification methods using RGB imagery combined with lidar-CHM, NGRDI, and NGBDI was assessed. With the CHM integrated dataset, the RF classifier consistently achieved the highest accuracy, with an average Overall Accuracy (OA) of 94.52% and a kappa value of 0.92. ML also demonstrated high accuracy with CHM, achieving an average OA of 89.52% and an average kappa value of 0.85. DT classifier performed less effectively than the other two methods, attaining an average OA of 81.78% and an average kappa value of 0.75 (Table 3).

Consistent patterns were observed across all individual sites, with the highest overall accuracy (98.63%) and kappa coefficient (0.98) achieved using the RF classifier in Site 3 (Duncanville, Alabama). Similar results were seen in other sites, where RF outperformed ML and DT classifiers (Table 3). ML classification closely followed, achieving the highest OA of 93.34% and a kappa coefficient of 0.90 in Site 3. DT yielded the maximum OA (94.99%) and kappa coefficient (0.92) in Site 6. When comparing the average performances of the classifiers in Alabama, Georgia, and Florida, RF showed the best accuracy across Alabama and Georgia, with average OAs of 95.99% and 94.22%, respectively. ML provided a slightly better average OA (91.60%) and kappa coefficient (0.89) compared to RF (OA= 90.4%) in Florida, along with an average kappa coefficient of 0.94 (Table 3).

Damage classification maps using the lidar-CHM integrated dataset were produced using three distinct classification categories: downed trees, standing trees, and ground, and were prepared using all three classifiers RF, ML, and DT for sites without water (Figure 4). Similarly,

sites with water had four distinct classification categories: downed trees, standing trees, ground, and water (Figure 5). Classification maps for the other sites can be found in Appendix A.

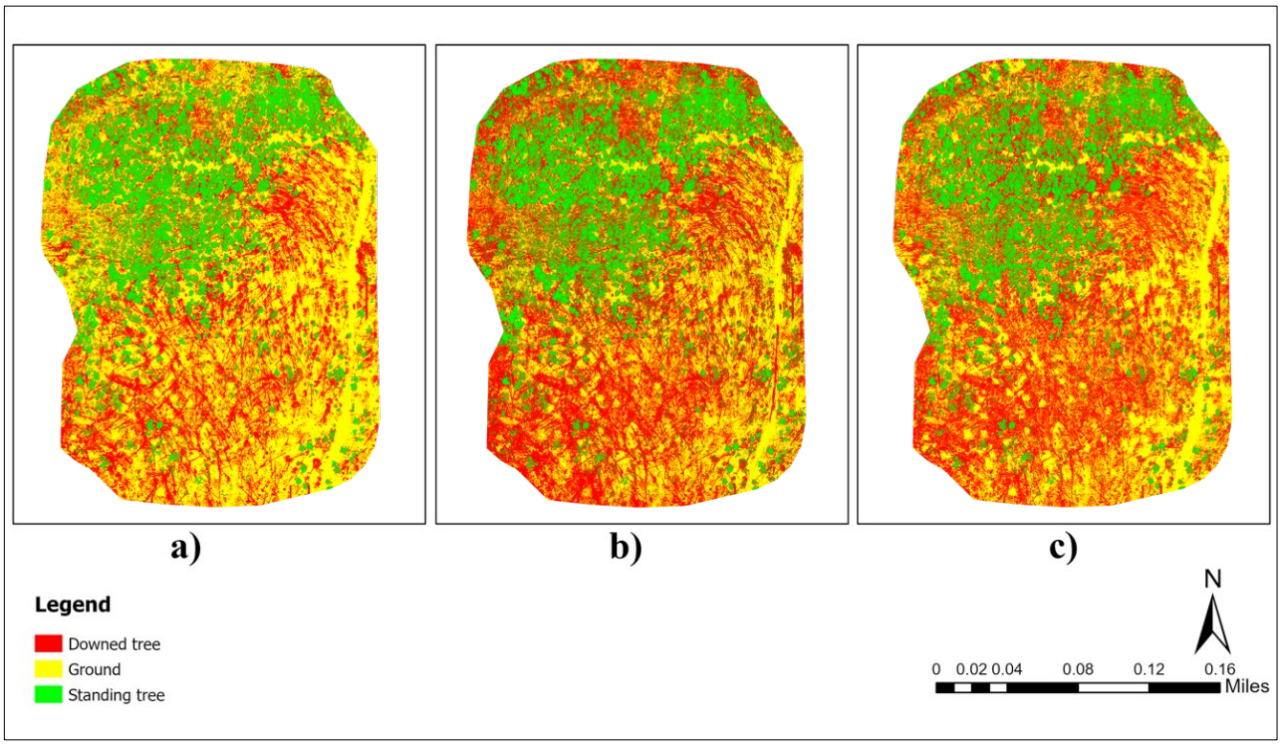

Figure 4. A map of the tornado-damaged in Duncanville, Alabama (site 1) prepared using a dataset integrated with lidar-CHM. Green represents standing trees, red represents downed trees, and yellow represents the ground. Panel (a) represents RF classification, (b) represents ML classification, and (c) represents DT classification.

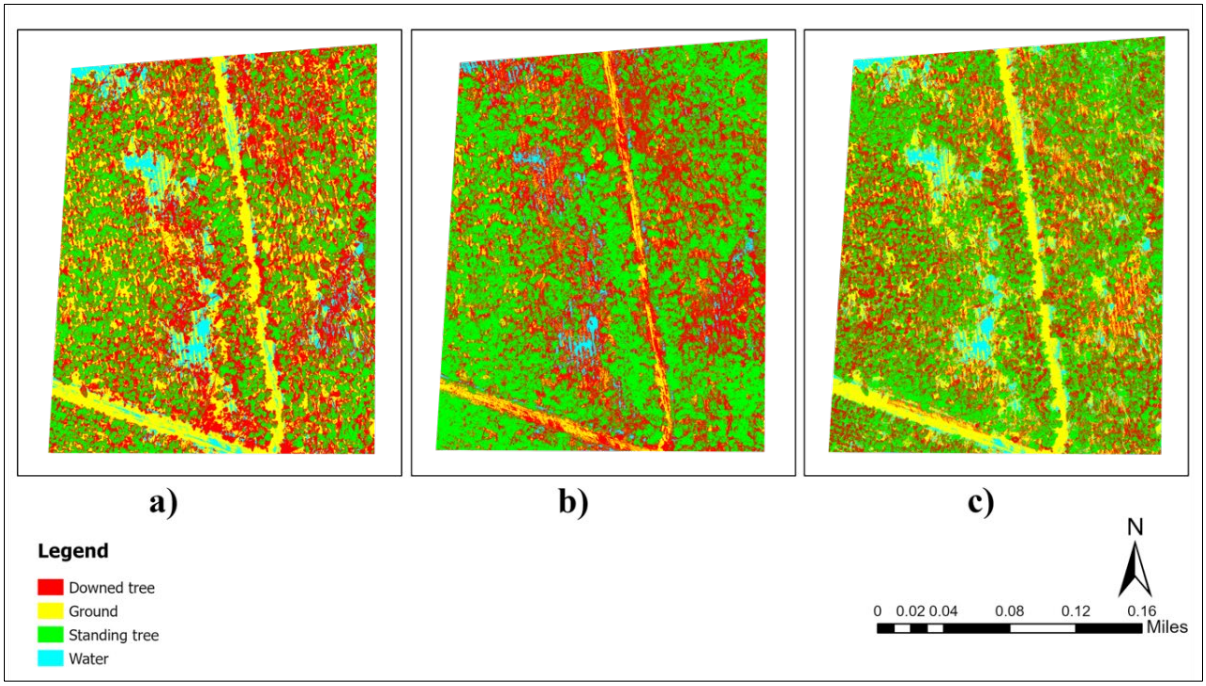

Figure 5. A map of a hurricane-damaged in Perry, Florida (site 9) prepared using a dataset integrated with lidar-CHM. Green represents standing trees, red represents downed trees, yellow represents the ground, and blue represents water. Panel (a) represents RF classification, (b) represents ML classification, and (c) represents DT classification.

Table 3. Comparison of classification methods (RF, ML, and DT) using CHM-included and CHM-excluded datasets for windstorm damage assessment in Alabama (Sites 1-6), Georgia (Sites 7-8), and Florida (Sites 9-10). Classification accuracies (Overall Accuracy and kappa coefficient) for each input dataset for each method are presented.

		With CHM						Without CHM					
		RF		ML		DT		RF		ML		DT	
Site Location		OA	k	OA	k	OA	k	OA	k	OA	k	OA	k
AL	Site 1	95.04	0.93	91.39	0.87	92.87	0.89	76.5	0.65	82.54	0.74	77.97	0.67
	Site 2	94.79	0.92	91.32	0.87	89.87	0.85	86.45	0.80	82.16	0.73	75.37	0.63
	Site 3	98.63	0.98	93.34	0.90	91.05	0.87	71.32	0.56	80.68	0.71	58.04	0.39
	Site 4	98.08	0.97	82.78	0.77	81.24	0.75	80.52	0.74	66.69	0.56	69.07	0.59
	Site 5	93.93	0.91	88.45	0.83	86.89	0.80	73.46	0.60	62.98	0.45	59.32	0.39
	Site 6	95.45	0.93	91.06	0.87	94.99	0.92	78.14	0.67	67.59	0.52	75.16	0.63
GE	Site 7	92.02	0.89	86.69	0.82	56.59	0.42	69.41	0.59	72.5	0.63	33.23	0.11
	Site 8	96.43	0.95	86.94	0.80	76.42	0.65	76.83	0.65	72.29	0.59	45.36	0.18
FL	Site 9	93.16	0.91	91.55	0.89	77.69	0.70	83.01	0.77	76.33	0.68	70.86	0.61
	Site 10	87.64	0.84	91.66	0.89	70.15	0.60	79.94	0.73	82.68	0.77	60.69	0.48
	Average	94.52	0.92	89.52	0.85	81.78	0.75	77.56	0.68	74.64	0.64	62.51	0.47

The performance of different classification methods using RGB imagery combined with only NGRDI and NGBDI (without lidar-CHM) was also assessed. The analysis of the dataset without lidar-CHM showed a noticeable decrease in the performance of all classifiers, as evidenced by reductions in overall accuracy (OA) and kappa coefficient. RF remained the most accurate method, with an average OA of 77.56% and a kappa coefficient of 0.68. The ML and DT methods followed, with average OAs of 74.64% and 62.51%, respectively, and corresponding kappa values of 0.64 and 0.47, respectively (Table 3).

Consistent patterns were observed across individual sites, with the highest overall accuracy (86.45%) and kappa coefficient (0.80) obtained using RF in Site 2 (Duncanville, Alabama). Similar results were seen in five other sites (Site 4, 5, 6, 8, and 9), where RF outperformed ML and DT classifiers. ML classification closely followed with the highest OA of 82.68% and kappa coefficient of 0.77 obtained in Site 10 (Table 3). The drop in classification accuracy in the absence of lidar-CHM was most noticeable for the DT method. For example, at Site 7, the DT classifier's OA decreased from 56.59% (with CHM) to 33.23% (without CHM) (see Section 1.1). RF consistently outperformed the other classifiers in Alabama, Georgia, and Florida, with an average OA of 77.73%, 73.12%, and 81.46%, respectively. In contrast, the DT had the lowest average OA (62.51%) and Kappa coefficient (0.47).

Damage classification maps using RGB imagery stacked with only NGRDI and NGBDI (no lidar-CHM) datasets were produced similarly as with CHM. Classification maps without water had three distinct classification categories: downed trees, standing trees, and ground prepared (Figure 6). Classification maps with water had four distinct classification categories:

downed trees, standing trees, ground, and water (Figure 7). These figures can be directly compared to Figure 4 and Figure 5, which present damage-classified maps prepared with lidar-CHM integrated imagery of the same sites. Classification maps for the other sites can be found in Appendix A.

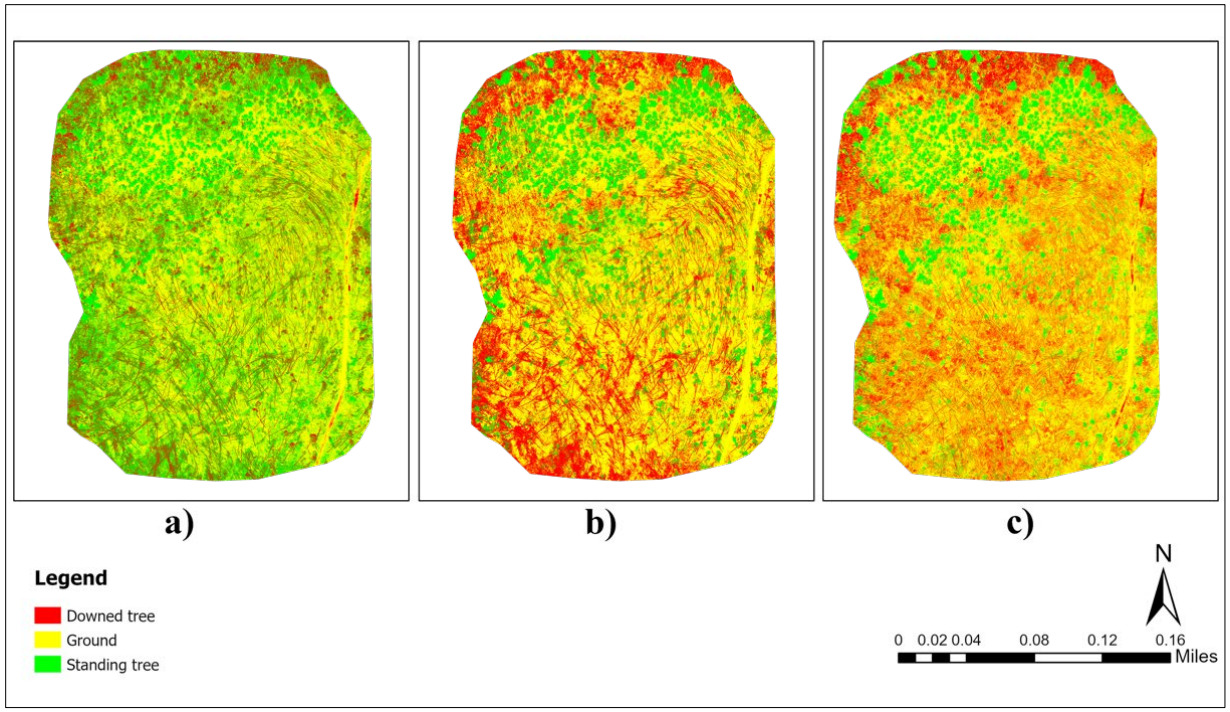

Figure 6: A map of the tornado-damaged in Duncanville, Alabama (site 1) prepared using a dataset integrated without lidar-CHM. Green represents standing trees, red represents downed trees, and yellow represents the ground. Panel (a) represents RF classification, (b) represents ML classification, and (c) represents DT classification.

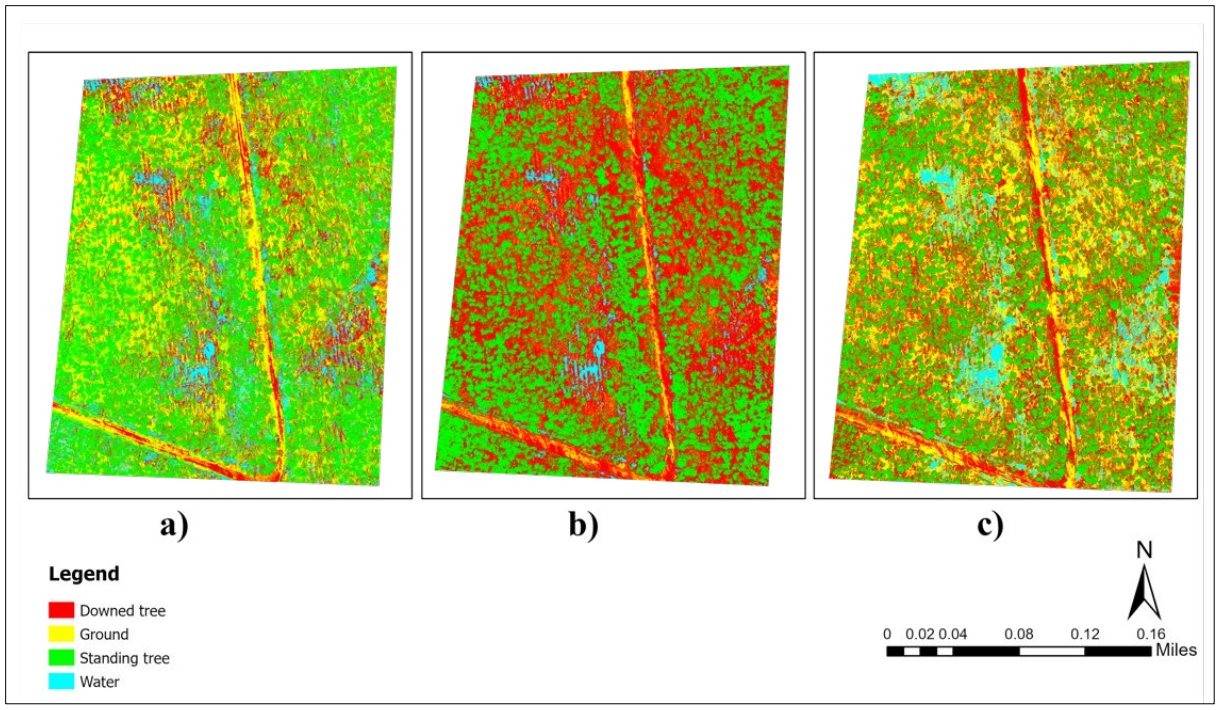

Figure 7: A map of a hurricane-damaged in Perry, Florida (site 9) prepared using a dataset integrated without lidar-CHM. Green represents standing trees, red represents downed trees, yellow represents the ground, and blue represents water. Panel (a) represents RF classification, (b) represents ML classification, and (c) represents DT classification.

Similarly, the Producer's Accuracy (PA) and User's Accuracy (UA) using the lidar-CHM integrated dataset for each classification category were obtained for each site. The maximum PA for classifying ground (100%) and downed trees (98.36%), as well as the maximum UA for classifying standing trees (100%), was obtained in Site 3 with RF (Table 4). ML also performed well, achieving a maximum UA of 99.63% for downed trees, while RF achieved a UA of 98.72%, highlighting its reliability. Although ML (89.52%) had lower overall accuracy compared to RF (94.52%), it achieved the maximum PA (100%) for classifying standing trees in Site 2 and maximum UA (100%) for classifying ground in Site 1 (Table 4). DT exhibited the lowest average PA (79.79%) for classifying downed trees compared to the other two classifiers.

Four sites showed the presence of water, adding it as a separate category alongside downed trees, standing trees, and ground. The highest producer's accuracy for water was achieved using RF (100%) in site 9, Florida, while the user's accuracy was 98.07%. ML had the highest average UA for classifying water at 98.88% for the same site. Overall, RF consistently demonstrated the best accuracy, with the highest average PA for classifying ground (97.20%), downed tree (89.63%), and water (98.51%), indicating the classifier's superior ability to label a true class correctly. Similarly, ML had an average PA of 85.08% for the ground class, 86.32% for the downed tree class, and 83.25% for the water class. In comparison to ML, DT exhibited a slightly higher average PA of 85.25% for the ground class but lower for the downed tree (79.79%) and water (74.12%) classes. RF also produced the highest average UA for standing trees (98.33%), ground (92.38%), and downed trees (95.16%). Similarly, for the downed tree class, ML achieved an average UA of 85.36, while DT achieved a UA of 73.86, which is lower compared to the UA obtained by RF for the same class (Table 4).

Table 4. Comparison of accuracies using lidar-CHM integrated imagery in windstorm-affected sites in Alabama (Sites 1-6), Georgia (Sites 7-8), and Florida (Sites 9-10). Classification accuracies (Producer's Accuracy (PA) and User's Accuracy (UA)) for each class for each site are presented.

		With CHM							
Methods	**Site**	**PA (Standing Tree)**	**UA (Standing Tree)**	**PA (Ground)**	**UA (Ground)**	**PA (Downed Tree)**	**UA (Downed Tree)**	**PA (Water)**	**UA (Water)**
	1	98.17	97.19	95.43	94.11	91.44	93.68		
	2	88.4	98.08	99.23	97.97	96.87	89.33		
Random	**3**	97.3	100	100	97.78	98.36	98.36		
Forest	**4**	99.76	98.58	99.75	95.51	96.49	98.72	96.22	99.74
(RF)	**5**	97	98.48	99.27	88.45	85.68	95.92		
	6	95.37	98.1	95.98	96.44	95.03	92.12		
	7	99.75	100	84.08	92.1	86.03	96.69	98.07	82.02
	8	99.31	100	98.29	91.67	91.8	97.76		
	9	98.53	95.93	100	98.76	74.39	98.07	100	98.07
	10	71.53	97.03	100	70.92	80.25	90.93	99.75	99.75
Average		94.51	98.34	97.20	92.37	89.63	95.16	98.51	94.89

	1	98.83	91.51	80.67	100	94.18	85.14		
	2	100	92.55	83.21	98.86	90.91	84.09		
Maximum	**3**	94.29	92.35	91.94	99.73	93.97	88.17		
Likelihood	**4**	99.52	76.01	67.48	79.31	84	81.75	79.9	99.38
(ML)	**5**	100	76.63	96.33	98.99	69.42	95.02		
	6	98.84	92.22	84.63	97.02	89.62	85.19		
	7	100	96.67	96.52	67.36	66.18	99.63	84.3	96.14
	8	100	94.55	70.22	89.56	89.46	78.12		
	9	98.53	94.58	91.71	98.92	93.41	77.69	82.6	100
	10	100	94.27	88.1	97.37	92	78.8	86.21	100
Average		99.00	90.13	85.08	92.71	86.31	85.36	83.25	98.88
	1	98.33	95.47	89.63	94.62	90.41	88.59		
	2	98.54	81.62	95.2	97.3	75.68	93.05		
	3	87.39	86.09	99.24	98.01	85.48	87.89		
Decision	**4**	65.46	77.21	94.62	87.95	73	63.76	92.21	98.66
Tree	**5**	92.75	81.18	98.04	91.55	70.15	88.65		
(DT)	**6**	96.06	95.62	95.98	96.9	93	92.58		
	7	37.35	68.16	66.67	53.39	59.56	45.08	62.8	70.84
	8	57.83	94.01	81.39	93.18	90.63	60		
	9	68.3	84.24	84.42	76.36	79.27	64.74	78.92	91.74
	10	88.32	78.4	47.35	77.83	80.75	54.29	62.56	82.74
Average		79.03	84.2	85.25	86.71	79.79	73.86	74.12	85.99

For each classification technique utilized, confusion matrices were generated for both the dataset integrated with lidar-CHM and the dataset without lidar-CHM. This analysis was conducted across all ten sites, resulting in a total of 60 confusion matrices: 30 for the CHM-integrated dataset and 30 for the dataset excluding lidar-CHM. Specifically highlighted are the confusion matrices from the Random Forest classification for the CHM-integrated dataset at two sites. Site 3 (with three distinct classification categories), which exhibited the highest overall classification accuracy, and Site 9 (with four distinct classification categories) are thoroughly analyzed in Tables 5-9, respectively.

The confusion matrix for RF in site 3 showed that the downed tree class had 365 ground truth pixels, 359 of which are correctly classified as downed trees (Table 5). Hence, the producer's accuracy was 359/365=98.36%, which means that 98.36% of the actual downed tree

pixels were correctly identified by the classifier as downed trees. Downed trees had a total of 365 classified pixels, 359 out of those classified pixels were again classified correctly by Random Forest as downed trees (Table 7). Hence, the UA was 359/365=98.36%, which means that 98.36% of the area in the classified image classified as downed trees were downed trees on the ground. Both PA and UA for the downed tree class shows that nearly all downed trees were correctly classified, and the classification was reliable. The most confused classes for RF in site 3 were between the ground and downed tree class where 6 ground truth pixels from the downed tree class were incorrectly classified as ground, making omission error for the downed tree class 6/365= 1.65%. Similarly, 6 standing tree truth pixels were classified as downed trees, making commission error for the downed tree class 6/365=1.65% (Table 6).

Table 5. Confusion matrix obtained for RF using dataset integrated with lidar-CHM for Site 3 (in pixels)

Ground Truth (Pixels)				
Class	Standing tree	Downed tree	Ground	Total
Standing tree	324	0	0	324
Downed tree	6	359	0	365
Ground	3	6	397	406
Total	333	365	397	1095

Table 6. Error of Commission and Omission obtained for RF using dataset integrated with lidar-CHM for Site 3

Class	Commission (%)	Omission (%)	Commission (Pixels)	Omission (Pixels)
Standing tree	0	2.70	0/324	9/333
Downed tree	1.64	1.64	6/365	6/365
Ground	2.22	0	9/406	0/397

Table 7. Producer and User Accuracies obtained for RF using dataset integrated with lidar-CHM for Site 3

Class	PA (%)	UA (%)	PA (Pixels)	UA (Pixels)
Standing tree	97.30	100	324/333	324/324
Downed tree	98.36	98.36	359/365	359/365
Ground	100	97.78	397/397	397/406

The confusion matrix for RF classifier in site 9 showed that 305 pixels out of 410 ground truth pixels were correctly classified as downed trees (Table 8). Hence, the PA was 305/410=74.39%, which means that 74.39% of the actual downed tree pixels were correctly identified by the classifier as downed trees. Downed trees had a total of 311 classified pixels, 305 out of those classified pixels were again classified correctly by Random Forest as downed trees (Table 8). Hence, the UA was 305/311=98.07%, which means that 98.07% of the area in the classified image classified as downed trees were downed trees on the ground. The most confused classes for RF in site 9 were between water and downed trees where 83 ground truth pixels of the downed tree class were incorrectly classified as water, followed by 17 pixels which were classified as standing trees, and 5 were classified as ground class, making omission error for downed tree class 83+17+5/410= 25.61%. Similarly, 6 standing tree truth pixels were classified as downed trees, making commission error for downed tree class 6/311=1.93% (Table 9).

Table 8. Confusion matrix obtained for RF using dataset integrated with lidar-CHM for Site 9 (in pixels)

	Ground Truth (Pixels)				
Class	Standing tree	Downed tree	Ground	Water	Total
Standing tree	401	17	0	0	418
Downed tree	6	305	0	0	311
Ground	0	5	398	0	403
Water	0	83	0	408	491
Total	407	410	398	408	1623

Table 9. Error of Commission and Omission obtained for RF using dataset integrated with lidar-CHM for Site 9

Class	Commission (%)	Omission (%)	Commission (Pixels)	Omission (Pixels)
Standing tree	4.07	1.47	17/418	6/407
Downed tree	1.93	25.61	6/311	105/410
Ground	1.24	0.00	5/403	0/398
Water	16.90	0.00	83/491	0/408

The Producer's Accuracy and User's Accuracy using the dataset without lidar-CHM (only RGB bands, NGRDI, and NGBDI) for each classification category were also obtained for each site. The maximum PA for classifying standing trees (100%) was obtained with RF in Site 10, with a UA of 99.7 (Table 10). Meanwhile, the maximum PA for classifying downed trees was 95.36% with an ML classifier at Site 9, but the RF model performed better with a 98.6% UA for classifying downed trees at Site 2. Although ML (74.64%) had slightly lower overall accuracy compared to RF (77.56%), it achieved the maximum PA (92.71%) for ground at Site 3, the maximum UA (97.94%) for ground at Site 1, and the maximum UA (100%) for standing trees at Site 10 (Table 10).

The highest accuracy for identifying water was achieved with DT (100%) in Site 9 and RF (100%) in Site 10. Additionally, the highest UA for water in the same site (Site 10) was achieved with ML (100%). Overall, ML demonstrated the best accuracy, with the highest average PA for classifying standing trees (83.94%) and downed trees (78.02%), as well as the highest average UA for standing trees (79.36%), ground (77.13%), and water (94.23%) (Table 4). The highest average PA for water (97.76%) was obtained with RF. Compared to the other two classifiers, DT showed the lowest overall PA (60.79%) and UA (51.39%) for classifying downed trees.

Table 10. Comparison of accuracies using imagery without lidar-CHM in windstorm-affected sites in Alabama (Sites 1-6), Georgia (Sites 7-8), and Florida (Sites 9-10). Classification accuracies (Producer's Accuracy (PA) and User's Accuracy (UA)) for each class for each site are presented.

		Without CHM							
Methods	**Site**	**PA (Standing Tree)**	**UA (Standing Tree)**	**PA (Ground)**	**UA (Ground)**	**PA (Downed Tree)**	**UA (Downed Tree)**	**PA (Water)**	**UA (Water)**
	1	76.64	66.32	59.81	94.64	93.53	76.73		
	2	100	73.8	95.81	95.24	63.75	98.6		
Random	**3**	70.33	74.57	81.46	66.34	62.54	73.19		
Forest	**4**	42.28	75.27	95.58	69.98	85.24	79.94	97.35	98.51
(RF)	**5**	85.89	66.82	61.28	76.12	74.14	79.88		
	6	91.84	71.75	77.47	85.2	64.88	79.85		
	7	63.92	61.96	52.6	56.17	66.18	75.08	94.03	81.73
	8	89.69	81.07	52.04	80.93	91.12	71.3		
	9	90.83	97.15	61.45	75.09	82.22	76.32	99.69	84.74
	10	100	99.7	38.64	71.2	82.13	58.04	100	97.08
Average		81.142	76.841	67.614	77.09	76.573	76.893	97.7675	90.515
	1	88.56	79.48	80.63	97.94	78.36	73.6		
	2	88.62	94.74	79.64	82.87	78.35	70.99		
Maximum	**3**	80.08	85.47	92.71	70.11	69.35	90.32		
Likelihood	**4**	64.31	71.58	47.81	64.06	61.01	43.16	93.79	99.37
(ML)	**5**	72.67	53.66	37.88	64.15	79.6	73.47		
	6	98.54	63.41	40.38	79.46	65.48	67.69		
	7	58.86	74.7	44.22	65.95	90.17	60.23	95.17	92.8
	8	96.88	73.29	33.79	82.12	90.26	68.18		
	9	98.22	97.36	37.15	93.66	95.36	57.63	73.99	84.75
	10	92.66	100	69.32	71	72.33	64.69	97.3	100
Average		83.94	79.369	56.353	77.132	78.027	66.996	90.0625	94.23
	1	93.43	77.11	72.64	92.02	67.66	67.66		
	2	82.46	97.81	85.03	61.21	58.54	77.11		
	3	48.58	95.22	69.6	44.21	60.68	52.27		
Decision	**4**	44.92	81.56	53.35	55.96	84.23	56.49	93.2	94.03
Tree	**5**	55.56	64.01	40.39	65.02	82.47	54.36		
(DT)	**6**	80.76	89.64	61.54	83.9	84.23	60.6		
	7	33.86	40.68	34.97	30.4	4.91	4.42	58.81	65.92
	8	42.81	80.59	39.51	47.39	53.87	33.57		
	9	89.35	96.49	41.34	49.5	57.73	52.58	100	87.53
	10	87.16	57.81	52.21	62.54	53.6	54.87	50.75	73.16
Average		65.889	78.092	55.058	59.215	60.792	51.393	75.69	80.16

30 confusion matrices were produced for the dataset excluding lidar-CHM. Specifically highlighted are the confusion matrices from the Random Forest classification for the CHM-integrated dataset at two sites. Site 2 (with three distinct classification categories), which

exhibited the highest overall classification accuracy, and Site 9 (with four distinct classification categories) are thoroughly analyzed in Tables 11-14, respectively.

The confusion matrix for RF classifier in site 2 showed that 211 pixels out of 331 ground truth pixels were correctly classified as downed trees (Table 11). Hence, the PA for the downed tree class was 211/331=63.75%, which means that 63.75% of the actual downed tree pixels were correctly identified by the classifier as downed trees. Downed trees had a total of 211 classified pixels, 214 out of those classified pixels were again classified correctly by Random Forest as downed trees (Table 11). Hence, the UA was 211/214=98.6%, which means that 98.6% of the area in the classified image classified as downed trees were downed trees on the ground. The most confused classes for RF in site 2 without CHM-integrated dataset were between standing trees and downed trees where 104 ground truth pixels of the downed tree class were incorrectly classified as standing trees, followed by 16 pixels that were classified as ground, making omission error for the downed tree class 104+16/331= 36.25%. Similarly, 3 pixels belonging to the ground class were classified as downed trees, making commission error for the downed tree class 3/214=1.40% (Table 12).

Table 11. Confusion matrix obtained for RF using dataset integrated without lidar-CHM for Site 2 (in pixels)

Ground Truth (Pixels)				
Class	Standing tree	Downed tree	Ground	Total
Standing tree	324	104	11	439
Downed tree	0	211	3	214
Ground	0	16	320	336
Total	324	331	334	989

Table 12. Error of Commission and Omission obtained for RF using dataset integrated without lidar-CHM for Site 2

Class	Commission (%)	Omission (%)	Commission (Pixels)	Omission (Pixels)
Standing tree	26.20	0.00	115/439	0/324
Downed tree	1.40	36.25	3/214	120/331
Ground	4.76	4.19	16/336	14/334

The confusion matrix for RF classifier in site 9 showed that 319 pixels out of 388 ground truth pixels were correctly classified as downed trees (Table 13). Hence, the PA was 319/388= 82.22%, which means that 82.22% of the actual downed tree pixels were correctly identified by the classifier as downed trees. Downed trees had a total of 418 classified pixels, 319 out of those classified pixels were classified correctly by Random Forest as downed trees (Table 13). Hence, the UA was 319/418=76.32%, which means that 76.32% of the area in the classified image classified as downed trees were downed trees on the ground. The most confused classes for RF in site 9 were between ground and downed trees where 48 ground truth pixels of the downed tree class were incorrectly classified as ground, followed by 13 pixels which were classified as water, and 8 were classified as standing trees, making omission error for the downed tree class 48+13+8/388= 17.78%. Similarly, 2 standing tree truth pixels were classified as downed trees, 96 pixels belonging to the ground class were classified as downed trees, and 1 water class ground truth pixel was classified as downed tree, making commission error for the downed tree class 2+96+1/418=23.68% (Table 14).

Table 13. Confusion matrix obtained for RF using dataset integrated without lidar-CHM for Site 9 (in pixels)

	Ground Truth (Pixels)				
Class	Standing tree	Downed tree	Ground	Water	Total
Standing tree	307	8	1	0	316
Downed tree	2	319	96	1	293

Ground	25	48	220	0	380
Water	4	13	41	322	418
Total	338	388	358	323	1407

Table 14. Error of Commission and Omission obtained for RF using dataset integrated without lidar-CHM for Site 9

Class	Commission (%)	Omission (%)	Commission (Pixels)	Omission (Pixels)
Standing tree	2.85	9.17	9/316	31/338
Downed tree	23.68	17.78	99/418	69/388
Ground	24.91	38.55	73/293	138/358
Water	15.26	0.31	58/380	1/323

Incorporating CHM data improved classification accuracies across all three methods, as demonstrated by higher OA and Kappa Coefficient values (see Table 3). For example, Site 3 achieved an overall accuracy (OA) of 98.63% and a kappa value of 0.98 for RF when including CHM, demonstrating an increase from its performance without CHM, which had an OA of 71.32% and a kappa value of 0.56. This trend was consistent across all sites, highlighting the significance of CHM data in enhancing classification accuracy. RF consistently outperformed ML and DT, with corresponding kappa values following the trends in OA. The RF classifier also consistently demonstrated high PA and UA for all tree damage categories when integrated with lidar-CHM data, particularly for standing trees and downed trees (Tables 4 and 10). The ML classifier performed well with datasets integrated with lidar-CHM but had comparatively lower performance than RF.

The RF model provided insight into the importance of each input variable by ranking them in order of their significance in predicting the model's accuracy. Figure 8 illustrates the variable importance plot for Site 1 using a dataset integrated with lidar-CHM, highlighting the

relevance of each input variable across all classes. CHM emerged as the most crucial variable for distinguishing between ground, downed trees, and standing trees, as illustrated in all three plots (Figure 8). When comparing the role of variables across all ten sites, CHM remained the most influential variable across all four categories. The importance of spectral bands and indices (NGBDI, NGRDI, R, G, and B) varied depending on the category, with vegetative indices (NGDBI and NGRDI) having a secondary role compared to CHM. Variables importance plots for the other sites can be found in Appendix B.

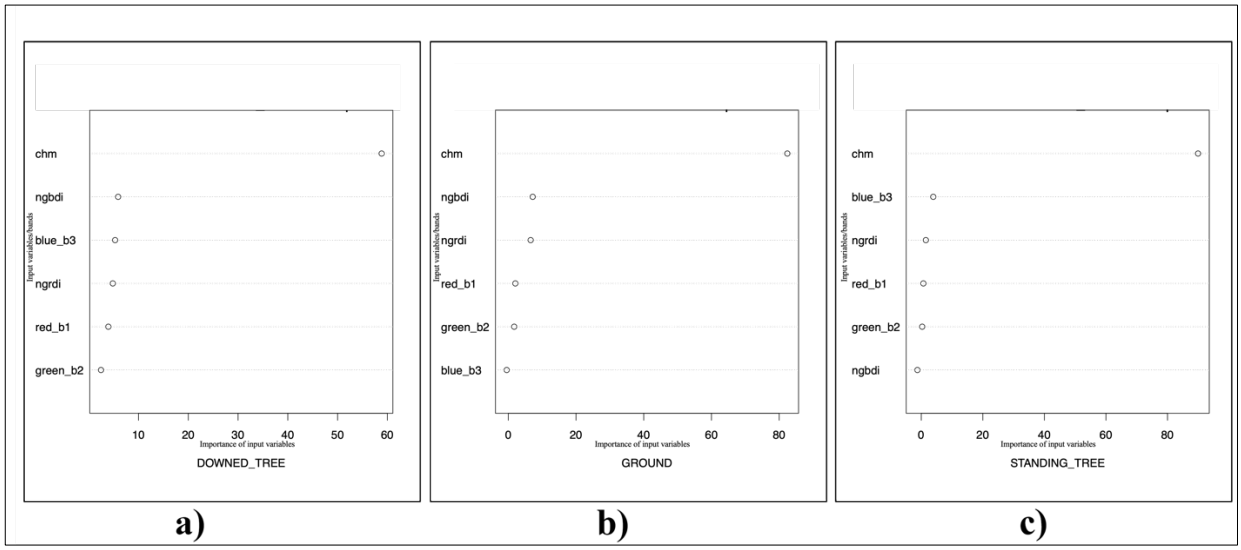

Figure 8. Variable importance plots generated using the ModelMap package in R, displaying the relative importance of each input variable for classifying windstorm damage using lidar-CHM integrated dataset: a) downed tree, b) ground, c) standing tree.

Figure 9 illustrates the variable importance plot for Site 1 using a dataset integrated without lidar-CHM, highlighting the relevance of each input variable across all classes. NGBDI and NGRDI emerged as the two most crucial variables for distinguishing between ground, downed trees, and standing trees, as illustrated in all three plots (Figure 9). When comparing the role of variables across all ten sites, different spectral bands and indices had varying levels of

importance depending on the category being predicted. Notably, NGRDI and NGBDI consistently emerged as the most influential variables across all four categories. Variables importance plots for the other sites can be found in Appendix B.

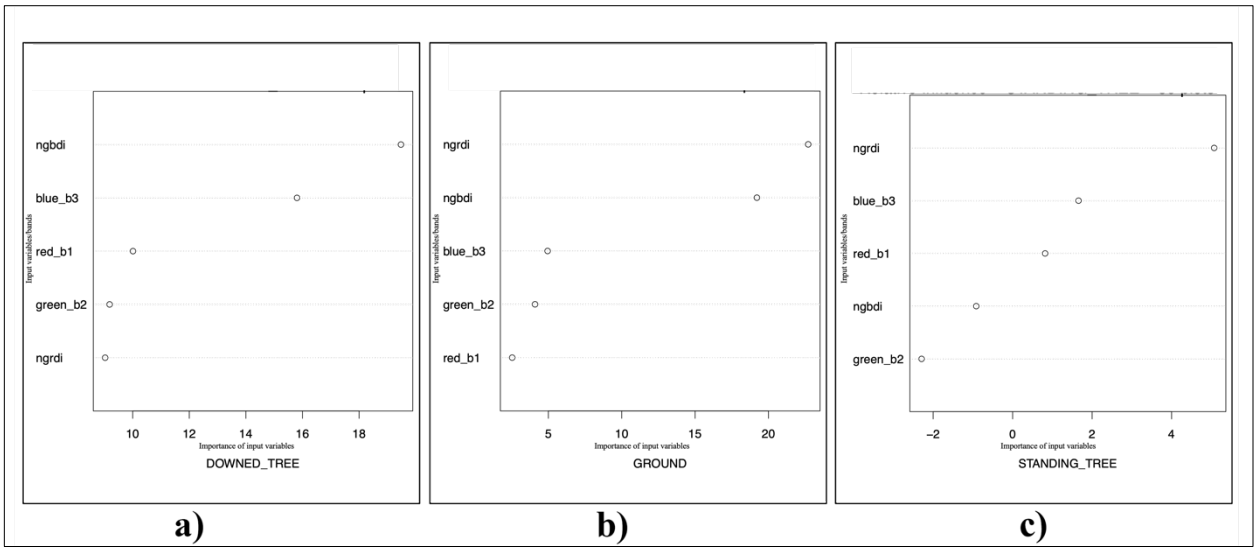

Figure 9. Variable importance plots generated using the ModelMap package in R, displaying the relative importance of each input variable for classifying windstorm damage using dataset without lidar-CHM: a) downed tree, b) ground, c) standing tree.

2.5. Discussion

This study explored the effectiveness of Random Forest, Maximum Likelihood, and Decision Tree techniques in classifying and mapping windstorm damages across Alabama, Georgia, and Florida. The combination of RGB bands, NGRDI, and NGBDI with and without lidar-CHM was examined for each classification approach. The findings showed that the RF classifier outperformed ML and DT across several metrics, including overall accuracy, kappa coefficient, producer's accuracy, and user's accuracy.

RF resulted in the best performance, both with the inclusion of lidar-CHM, achieving an average overall accuracy of 95.52%, and in its absence, with an average overall accuracy of 77.56%. These results align with prior research by Hartling et al. (2021) and Fan (2023), highlighting the effectiveness of machine learning techniques, particularly RF, in remote sensing applications, underscoring RF classifier's superiority in managing multiple data types and complex feature sets, making it particularly suitable for tasks involving extensive data fusion and classification tasks using data captured from UAV platform. This superiority is quantitatively supported by the consistently higher OA and kappa values compared to other classification algorithms, across different study sites within this study. The findings are also consistent with Li et al. (2013) who emphasized the proficiency of RF classifier in classifying environmental features. Feng et al. (2015) demonstrated the utility of UAV-RGB imagery and texture features in urban vegetation mapping, achieving classification accuracies of 90.6% and 86.2%. In contrast, this study achieved an even higher average overall accuracy (94.52%) using RGB imagery integrated with CHM data. Furthermore, both studies underscore the effectiveness of the RF algorithm in processing UAV-captured datasets. Feng et al. (2015) noted significant accuracy improvements when integrating texture features compared to using RGB data alone. Similarly, this research found that integrating CHM with RGB imagery and employing RF classification notably outperformed other methods (ML and DT), highlighting the robustness of this approach in handling varied and complex environmental data sets.

Queiroz et al. (2019) successfully utilized RF within a Geographic Object-Based Image Analysis (GEOBIA) setup to identify coarse woody debris through high-resolution aerial images and lidar data. Their findings also noted that the combination of remote sensing data and

advanced classification methods, such as RF, offers distinct advantages over traditional approaches like ML and DT algorithms when processing complex datasets. This has also been documented in studies by Ok et al. (2012) and Li et al. (2013). Moreover, Thapa et al. (2023) also provided support for the effectiveness of the RF classifier in handling intricate datasets, surpassing traditional methods like ISODATA clustering and ML in terms of overall accuracy and kappa coefficient.

Similar to the RF classifier, the ML classifier achieved an overall accuracy of 89.52% when utilizing datasets with the Canopy Height Model and 74.64% without lidar-CHM. The DT classifier recorded an OA of 81.78% with CHM datasets and 62.51% without lidar-CHM. These results consistently indicate that integrating lidar-derived data significantly enhances classification accuracy, regardless of the chosen algorithm. Kim et al. (2020) further supports this observation, showing that combining aerial imagery with lidar data significantly improves vegetation mapping accuracy. The insights on the importance of input variables, particularly the significance of CHM in distinguishing between classes, are consistent across studies by Qin et al. (2022) and Shi et al. (2018), emphasizing the critical role of structural data provided by lidar in environmental remote sensing applications.

The study results highlight the substantial increase in classification accuracy with including lidar-CHM. This improvement can be attributed to the combination of lidar-derived structural data with high-resolution RGB, where the structural features from lidar complement the spectral features from RGB in accurately classifying downed timber. This aligns with the findings of Goodbody et al. (2017), Corte et al. (2020), Kim et al. (2020) and Liu et al. (2018) on

the advantages of UAV-lidar in providing detailed three-dimensional information for precise identification and classification of features in forested landscapes. Our study's high classification accuracy, especially for the RF (average OA of 94.52% with CHM and 77.56% without CHM), further validates the effectiveness of combining lidar data with high-resolution RGB imagery for vegetation classification and post-disaster damage assessment. Hartling et al. (2021) underscored the effectiveness of employing UAVs equipped with lidar technology for detailed ecological classifications. Their research, alongside ours, demonstrated the significant utility of the RF in adeptly managing complex datasets captured via UAVs. Hartling et al. (2021) achieved a high overall accuracy of 83.3% using a fusion of features from all sensors (multispectral, hyperspectral, lidar, and thermal infrared imagery), highlighting the effectiveness of integrating multiple data types to enhance classification accuracy. Similarly, this study achieved an average overall accuracy of 94.52% by combining RGB and lidar data, underscoring the potential of lidar technology in improving environmental classification tasks. Similarly, the study by Alphen et al. (2024) also supports the role of UAV-lidar technology in enhancing the precision and efficiency of environmental monitoring.

The significance of lidar data in improving the accuracy of forest damage assessments has been highlighted by decreased model performance when CHM data was excluded from the analysis. This three-dimensional structural information provided by lidar plays a pivotal role in distinguishing between different forest damage categories, aligning with the findings of Blanchard et al. (2011), Polewski et al. (2015), and Tran et al. (2015). These studies emphasized the importance of lidar data in detecting downed logs and fallen trees, even in challenging environments. Blanchard et al. (2011), in particular, focused on Object-Based Image Analysis

(OBIA) combined with lidar data to detect and quantify downed logs in disturbed forest areas, demonstrating the significant aid of lidar-derived metrics in identifying and categorizing downed logs with approximately 73% accuracy. Our study similarly showed that including CHM data increased the average producer's accuracy for classifying downed trees (78.03% to 89.63% accuracy).

Furthermore, the use of RGB-derived indices, such as the NGRDI and NGBDI, has been shown to enhance the differentiation between categories by increasing the contrast between living vegetation (standing trees) and non-vegetative materials (such as downed trees, water, and ground). This approach is supported by previous studies that have applied these indices to improve the classification and identification of vegetation classes, especially in studies utilizing unmanned aerial vehicles UAVs. For example, Lee et al. (2013) used a combination of the RF classification and NGRDI to automatically identify dead trees in UAV imagery captured using only an RGB sensor. The inclusion of NGRDI as an additional feature improved the accuracy of dead tree detection, achieving a confidence level of over 80% in identifying dead trees from UAV imagery. Similarly, the study by Srivastava et al. (2022) demonstrated that vegetated areas could be differentiated using indices derived from the red, green, and blue bands of orthomosaic images. The authors suggested that combining various indices with the CHM makes it possible to use machine learning and deep learning algorithms to distinguish between types or species of vegetation.

Our study further explored the difficulties in distinguishing between classes, especially when CHM data were excluded. The confusion between classes in the absence of CHM

highlighted the need for advanced algorithms that could effectively utilize spectral and textural information to differentiate between closely related classes. Evaluation of the confusion matrix revealed significant misclassification between ground, water, and downed trees, as well as between downed and standing trees. This misclassification could be attributed to the presence of green leaves on trees that were downed by windstorms, making it challenging to distinguish between downed and standing trees without CHM data. Additionally, the proximity of downed trees and water to the ground likely contributed to the confusion between these two classes. Tarasova et al. (2012) also identified similar issues in land cover classification, particularly the confusion between water and bare land classes. They highlighted that the spectral properties of water pixels sometimes closely resembled those of bare land, especially in shadowed areas. In their study, confusion was also observed in differentiating the shrublands class from mixed (deciduous), herbaceous, and bare lands, suggesting difficulties distinguishing shrublands from adjacent land cover types due to overlapping spectral signatures of the imagery. Furthermore, in the study by Duan et al. (2017), there were instances where branches and objects with similar shapes were mistakenly identified as windthrown trees, revealing a limitation in distinguishing between tree trunks and similarly shaped objects.

During our study, we encountered various logistical and technical challenges that had a significant impact on the data collection and processing phases. One of the primary challenges we faced during the UAV data collection period was maintaining an active RTK status throughout the flight to ensure high-quality lidar data. The need for a reliable WiFi connection in rural areas was a persistent difficulty. To overcome this issue, we utilized portable WiFi hotspots that helped to improve internet connectivity for RTK operations while minimizing disruptions

caused by connectivity concerns. If cell service is an issue, a mobile base station receiver like the D-RTK 2 would work and provides high-precision GNSS receiver capabilities and generates centimeter-level positional data, offering improved relative accuracy and reliability (Czyża et al., 2023). Frequent weather changes, particularly strong gusts, created substantial challenges to RTK connectivity and UAV flight operations. This issue was particularly troublesome during UAV data-collection phases, often leading to delays. Rijal et al. (2023) also found that sudden weather changes, mainly wind gusts, made it difficult to conduct stable and reliable flights. To address this issue, we conducted weather checks during the flight planning process and continuously monitored weather conditions during data collection, utilizing weather forecasting apps tailored to these specific tasks. The collection of field data was further complicated due to the physical conditions of the sites. The extensive debris from downed timbers and the overall harsh site conditions posed significant risks to the safety of the field crew for collecting the plot-level data for ground truthing. As a result, the data collection process required more time than initially planned.

Once collected, the high-resolution lidar data from the ten study sites required substantial storage capacity and significant computational power for processing. These demands highlighted the need for robust computational resources to effectively handle tasks. Upgrades to our data storage and processing infrastructure were essential, including the acquisition of more powerful computing systems to process large datasets efficiently. Although there were challenges, our study successfully applied UAV-based lidar and RGB imaging, showcasing the potential of these technologies in environmental monitoring and disaster management.

2.6. Conclusion

This study demonstrated the feasibility and advantages of using UAV-lidar with UAV-derived RGB imagery for rapid, accurate, and cost-effective windstorm damage assessment. This study not only supports previous findings on the effectiveness of machine learning algorithms and the significance of lidar-derived data but also contributes to the practical applications of these technologies in post-disaster management and decision-making processes. Moreover, this study addresses a significant gap in current research by demonstrating the feasibility and effectiveness of using UAV-lidar in conjunction with UAV-derived RGB imagery for mapping and classifying storm-damaged forests. While previous studies have focused on detecting fallen timber and woody debris using airborne lidar, terrestrial lidar, and aerial imagery (Duan et al., 2017; Inoue et al., 2014; Panagiotidis et al., 2019), limited research has explored the combined use of UAV-lidar and RGB imagery for this purpose. Our findings suggest that this integrated approach can offer a rapid, and accurate means for assessing storm impacts and mapping losses. This can also directly contribute to minimizing economic impacts by enabling quicker response and timber recovery. Furthermore, the detailed damage classifications provided by these technologies can assist in the sustainable management of forest resources, which are crucial for maintaining biodiversity, carbon sequestration, and ecosystem services.

The findings of the study also highlight the need for additional research to improve scalability and applicability in diverse ecosystems and under different storm conditions. The study suggests the development of a single classification model that can be applied across different regions. Furthermore, integrating additional remote sensing data, such as multispectral imagery, or hyperspectral imagery, may enhance classification accuracy by providing more

information. Ultimately, employing advanced classification algorithms such as deep learning to classify and segment lidar data can be essential for accurately estimating the volume of downed timber, which is crucial for effective post-disaster management.

2.7. References

Akay, A. E., Oğuz, H., Karas, I. R., & Aruga, K. (2009). Using Lidar technology in forestry activities. Environmental Monitoring and Assessment, 151, 117–125. https://idp.springer.com/authorize/casa?redirect_uri=https://link.springer.com/article/10.1007/s10661-008-0254-1&casa_token=OuRqjgrTLhIAAAAA:imjI-iPRdYKS0aRtHdzjKS0fqM6fXr0p8jQE0tbBRDq10TmgT43avE_HUYxas9pubjYK0uiA0divUwTd

Almeida, D. R. A., Broadbent, E. N., Zambrano, A. M. A., Wilkinson, B. E., Ferreira, M. E., Chazdon, R., Meli, P., Gorgens, E. B., Silva, C. A., Stark, S. C., Valbuena, R., Papa, D. A., & Brancalion, P. H. S. (2019). Monitoring the structure of forest restoration plantations with a drone-Lidar system. International Journal of Applied Earth Observation and Geoinformation, 79, 192–198. https://doi.org/10.1016/j.jag.2019.03.014

Alonzo, M., Andersen, H.-E., Morton, D. C., & Cook, B. D. (2018). Quantifying boreal forest structure and composition using UAV structure from motion. *Forests*, *9*(3), 119.

ArcGIS Drone2Map. (2022). (Version 2022.1.2) Esri. https://www.esri.com/en-us/arcgis/products/arcgis-drone2map

Ba, A., Laslier, M., Dufour, S., & Hubert-Moy, L. (2020). Riparian trees genera identification based on leaf-on/leaf-off airborne laser scanner data and machine learning classifiers in northern France. *International Journal of Remote Sensing*, *41*(5), 1645–1667.

Balha, A., & Singh, C. K. (2022). Comparison of Maximum Likelihood, Neural Networks, and Random Forests Algorithms in Classifying Urban Landscape. In V. P. Singh, S. Yadav, K. K. Yadav, G. A. Corzo Perez, F. Muñoz-Arriola, & R. N. Yadava (Eds.), *Application of Remote Sensing and GIS in Natural Resources and Built Infrastructure Management* (pp. 29–38). Springer International Publishing. https://doi.org/10.1007/978-3-031-14096-9_2

Banu, T. P., Borlea, G. F., & Banu, C. (2016). The use of drones in forestry. *Journal of Environmental Science and Engineering B*, *5*(11), 557-562.

Beniaich, A., Silva, M. L. N., Avalos, F. A. P., Menezes, M. D. D., & Cândido, B. M. (2019). Determination of vegetation cover index under different soil management systems of cover plants by using an unmanned aerial vehicle with an onboard digital photographic camera. Semina: Ciências Agrárias, 40(1), 49. https://doi.org/10.5433/1679-0359.2019v40n1p49

Billah, M., Islam, A. K. M. S., Mamoon, W. B., & Rahman, M. R. (2023). Random forest classifications for landuse mapping to assess rapid flood damage using Sentinel-1 and Sentinel-2 data. Remote Sensing Applications: Society and Environment, 30, 100947. https://doi.org/10.1016/j.rsase.2023.100947

Blanchard, S. D., Jakubowski, M. K., & Kelly, M. (2011). Object-Based Image Analysis of Downed Logs in Disturbed Forested Landscapes Using Lidar. *Remote Sensing*, *3*(11), 2420–2439. https://doi.org/10.3390/rs3112420

Blazier, M. (2021). Louisiana's forest losses from the 2020 hurricanes. Louisiana State University AgCenter. 4p. Accessed on 6/11/2021 at: https://www.lsuagcenter.com/articles/page1623184643144

Bork, E. W., & Su, J. G. (2007). Integrating LIDAR data and multispectral imagery for enhanced classification of rangeland vegetation: A meta analysis. *Remote Sensing of Environment*, *111*(1), 11–24. https://doi.org/10.1016/j.rse.2007.03.011

Bradley, S., A. Maggard, & B. Carter. (2018). Assessing and managing storm-damaged timber. Alabama Cooperative Extension System, FOR-2066. 4p.

Breiman, L. (2001). Random Forests. *Machine Learning*, *45*(1), 5–32. https://doi.org/10.1023/A:1010933404324

Bouget, C., & Duelli, P. (2004). The effects of windthrow on forest insect communities: A literature review. Biological Conservation, 118(3), 281–299. https://doi.org/10.1016/j.biocon.2003.09.009

Cao, L., Liu, K., Shen, X., Wu, X., & Liu, H. (2019). Estimation of Forest Structural Parameters Using UAV-Lidar Data and a Process-Based Model in Ginkgo Planted Forests. *IEEE Journal of Selected Topics in Applied Earth Observations and Remote Sensing*, *12*(11), 4175–4190. https://doi.org/10.1109/JSTARS.2019.2918572

Chuvieco, E. (2020). *Fundamentals of satellite remote sensing: An environmental approach*. CRC press. https://www.taylorfrancis.com/books/mono/10.1201/9780429506482/fundamentals-satellite-remote-sensing-emilio-chuvieco

Corte, A. P. D., Souza, D. V., Rex, F. E., Sanquetta, C. R., Mohan, M., Silva, C. A., Zambrano, A. M. A., Prata, G., Alves De Almeida, D. R., Trautenmüller, J. W., Klauberg, C., De Moraes, A., Sanquetta, M. N., Wilkinson, B., & Broadbent, E. N. (2020). Forest inventory with high-density

UAV-Lidar: Machine learning approaches for predicting individual tree attributes. *Computers and Electronics in Agriculture*, *179*, 105815. https://doi.org/10.1016/j.compag.2020.105815

Czyża, S., Szuniewicz, K., Kowalczyk, K., Dumalski, A., Ogrodniczak, M., & Zieleniewicz, Ł. (2023). Assessment of Accuracy in Unmanned Aerial Vehicle (UAV) Pose Estimation with the REAL-Time Kinematic (RTK) Method on the Example of DJI Matrice 300 RTK. Sensors, 23(4), 2092. https://doi.org/10.3390/s23042092

Dash, J. P., Watt, M. S., Pearse, G. D., Heaphy, M., & Dungey, H. S. (2017). Assessing very high resolution UAV imagery for monitoring forest health during a simulated disease outbreak. *ISPRS Journal of Photogrammetry and Remote Sensing*, *131*, 1-14.

Dassot, M., Constant, T., & Fournier, M. (2011). The use of terrestrial Lidar technology in forest science: Application fields, benefits and challenges. *Annals of Forest Science*, *68*(5), Article 5. https://doi.org/10.1007/s13595-011-0102-2

Department of Agriculture, U., & Resources Conservation Service, N. (2018). Title 190-Forestry Inventory Methods Technical Note Forestry Inventory Methods. www.ascr.usda.gov

Dong, P., & Chen, Q. (2017). *Lidar remote sensing and applications*. CRC Press. https://www.taylorfrancis.com/books/mono/10.4324/9781351233354/Lidar-remote-sensing-applications-pinliang-dong-qi-chen

Du, M., & Noguchi, N. (2017). Monitoring of Wheat Growth Status and Mapping of Wheat Yield's within-Field Spatial Variations Using Color Images Acquired from UAV-camera System. *Remote Sensing*, *9*(3), 289. https://doi.org/10.3390/rs9030289

Duan, F., Wan, Y., & Deng, L. (2017). A Novel Approach for Coarse-to-Fine Windthrown Tree Extraction Based on Unmanned Aerial Vehicle Images. *Remote Sensing*, *9*(4), 306. https://doi.org/10.3390/rs9040306

Esri. (2022). *ArcGIS*. Retrieved 10/21/2022 from https://www.esri.com/en-us/arcgis/about-arcgis/overview

Esri. (2022). *ArcGIS Pro* (Version 3.1.0) from https://www.esri.com/en-us/arcgis/products/arcgis-pro/overview

Fan, C. L. (2023). Ground surface structure classification using UAV remote sensing images and machine learning algorithms. Applied Geomatics, 15(4), 919–931. https://doi.org/10.1007/s12518-023-00530-x

Feng, Q., Liu, J., & Gong, J. (2015). UAV Remote Sensing for Urban Vegetation Mapping Using Random Forest and Texture Analysis. *Remote Sensing*, *7*(1), 1074–1094. https://doi.org/10.3390/rs70101074

FOREST INVENTORY AND MONITORING GUIDELINES A Guidebook for NCF Members. (2014).

Fortuin, C. C., Montes, C. R., Vogt, J. T., & Gandhi, K. J. K. (2022). Predicting risks of tornado and severe thunderstorm damage to southeastern U.S. forests. *Landscape Ecology*, *37*(7), 1905–1919. https://doi.org/10.1007/s10980-022-01451-7

Freeman, E. A., Frescino, T. S., & Moisen, G. G. (2023). *ModelMap: An R Package for Model Creation and Map Production*.

Gardiner, B., Blennow, K., Carnus, J.-M., Fleischer, P., Ingemarsson, F., Landmann, G., Lindner, M., Marzano, M., Nicoll, B., Orazio, C., Ingemarson, F., Lindner, M., Peyron, J.-L., Reviron, M.-P., Schelhaas, M.-J., Schuck, A., Spielmann, M., & Usbeck, T. (2010). Destructive storms in European forests: past and forthcoming impacts Final report to European Commission-DG Environment Destructive Storms in European Forests: Past and Forthcoming Impacts. https://hal.inrae.fr/hal-02824530

Georgia Forestry Commission. (2018). Timber impact assessment: Hurricane Michael, October 10-11, 2018. 12p. Retrieved from: http://gatrees.net/forest-management/storm-damage/Hurricane%20MichaelTimber%20Impact%20Assessment%20Georgia%20October%2010-11%202018%20(2).pdf

Goodbody, T. R. H., Coops, N. C., Marshall, P. L., Tompalski, P., & Crawford, P. (2017). N o 1-THE FORESTRY CHRONICLE (Vol. 93).

Guan, H., Yu, J., Li, J., & Luo, L. (2012). RANDOM FORESTS-BASED FEATURE SELECTION FOR LAND-USE CLASSIFICATION USING LIDAR DATA AND ORTHOIMAGERY. *The International Archives of the Photogrammetry, Remote Sensing and Spatial Information Sciences*, *XXXIX-B7*, 203–208. https://doi.org/10.5194/isprsarchives-XXXIX-B7-203-2012

Guo, Q., Su, Y., & Hu, T. (2023). *Lidar principles, processing and applications in forest ecology*. Academic Press. https://books.google.com/books?hl=en&lr=&id=NyWJEAAAQBAJ&oi=fnd&pg=PP1&dq=Lidar+Principles,+Processing+and+Applications+in+Forest+Ecology&ots=NnYlehVTg-&sig=j4rv5MR83Xtxk3XQOyTpFqtZlVA

Hartley, R. J. L., Leonardo, E. M., Massam, P., Watt, M. S., Estarija, H. J., Wright, L., Melia, N., & Pearse, G. D. (2020). An Assessment of High-Density UAV Point Clouds for the Measurement of Young Forestry Trials. Remote Sensing, 12(24), 4039. https://doi.org/10.3390/rs12244039

Hartling, S., Sagan, V., & Maimaitijiang, M. (2021). Urban tree species classification using UAV-based multi-sensor data fusion and machine learning. GIScience & Remote Sensing, 58(8), 1250–1275. https://doi.org/10.1080/15481603.2021.1974275

Housman, I. W., Chastain, R. A., & Finco, M. V. (2018). An evaluation of forest health insect and disease survey data and satellite-based remote sensing forest change detection methods: case studies in the United States. *Remote Sensing*, *10*(8), 1184.

Isenburg, M. (2012). *LASTools - Software for Lidar processing*. rapidlasso from https://rapidlasso.com/lastools/

Inoue, T., Nagai, S., Yamashita, S., Fadaei, H., Ishii, R., Okabe, K., Taki, H., Honda, Y., Kajiwara, K., & Suzuki, R. (2014). Unmanned Aerial Survey of Fallen Trees in a Deciduous Broadleaved Forest in Eastern Japan. *PLoS ONE*, *9*(10), e109881. https://doi.org/10.1371/journal.pone.0109881

Kim, J., Popescu, S. C., Lopez, R. R., Wu, X. B., & Silvy, N. J. (2020). Vegetation mapping of No Name Key, Florida using Lidar and multispectral remote sensing. *International Journal of Remote Sensing*, *41*(24), 9469–9506. https://doi.org/10.1080/01431161.2020.1800125

Klauberg, C., Vogel, J., Dalagnol, R., Ferreira, M. P., Hamamura, C., Broadbent, E., & Silva, C. A. (2023). Post-Hurricane Damage Severity Classification at the Individual Tree Level Using Terrestrial Laser Scanning and Deep Learning. Remote Sensing, 15(4). https://doi.org/10.3390/rs15041165

Lee, S., & Yu, B.-H. (2018). Automatic detection of dead tree from UAV imagery. Proceedings of the 39th Asian Conference on Remote Sensing, Kuala Lumpur, Malaysia, 15–19. https://mycoordinates.org/automatic-detection-of-dead-tree-from-uav-imagery/

Li, B., Hou, J., Li, D., Yang, D., Han, H., Bi, X., Wang, X., Hinkelmann, R., & Xia, J. (2021). Application of Lidar UAV for High-Resolution Flood Modelling. *Water Resources Management*, *35*(5), 1433–1447. https://doi.org/10.1007/s11269-021-02783-w

Li, M., Im, J., & Beier, C. (2013). Machine learning approaches for forest classification and change analysis using multi-temporal Landsat TM images over Huntington Wildlife Forest. *GIScience & Remote Sensing*, *50*(4), 361–384. https://doi.org/10.1080/15481603.2013.819161

Liu, K., Shen, X., Cao, L., Wang, G., & Cao, F. (2018). Estimating forest structural attributes using UAV-Lidar data in Ginkgo plantations. *ISPRS Journal of Photogrammetry and Remote Sensing*, *146*, 465–482. https://doi.org/10.1016/j.isprsjprs.2018.11.001

Lopes Queiroz, G., McDermid, G. J., Castilla, G., Linke, J., & Rahman, M. M. (2019). Mapping Coarse Woody Debris with Random Forest Classification of Centimetric Aerial Imagery. *Forests*, *10*(6), 471. https://doi.org/10.3390/f10060471

Lu, B., & He, Y. (2017). Species classification using Unmanned Aerial Vehicle (UAV)-acquired high spatial resolution imagery in a heterogeneous grassland. *ISPRS Journal of Photogrammetry and Remote Sensing*, *128*, 73–85. https://doi.org/10.1016/j.isprsjprs.2017.03.011

McNulty, S. G. (2002). Hurricane impacts on US forest carbon sequestration. *Environmental Pollution*, *116*, S17–S24. https://doi.org/10.1016/S0269-7491(01)00242-1

Méndez-Toribio, M., Meave, J. A., Zermeño-Hernández, I., & Ibarra-Manríquez, G. (2016). Effects of slope aspect and topographic position on environmental variables, disturbance regime and tree community attributes in a seasonal tropical dry forest. Journal of Vegetation Science, 27(6), 1094–1103. https://doi.org/10.1111/jvs.12455

Meyer, G. E., & Neto, J. C. (2008). Verification of color vegetation indices for automated crop imaging applications. Computers and Electronics in Agriculture, 63(2), 282–293. https://doi.org/10.1016/j.compag.2008.03.009

Mitchell, R. J., Liu, Y., O'Brien, J. J., Elliott, K. J., Starr, G., Miniat, C. F., & Hiers, J. K. (2014). Future climate and fire interactions in the southeastern region of the United States. Forest Ecology and Management, 327, 316–326. https://doi.org/10.1016/j.foreco.2013.12.003

Mitchell, D., Smidt, M., McDonald, T., & Elder, T. (2021). Issues and Opportunities for Salvaging Storm Damaged Wood. *2021 ASABE Annual International Virtual Meeting, July 12-16, 2021*. 2021 ASABE Annual International Virtual Meeting, July 12-16, 2021. https://doi.org/10.13031/aim.202101231

Musah, M., Diaz, J. H., Alawode, A. O., Gallagher, T., Peresin, M. S., Mitchell, D., Smidt, M., & Via, B. (2022). Field Assessment of Downed Timber Strength Deterioration Rate and Wood Quality Using Acoustic Technologies. Forests, 13(5). https://doi.org/10.3390/f13050752

Northwest Natural Resource Group. (2014). Forest inventory and monitoring guidelines: A guidebook for NCF members. Northwest Certified Forestry. http://nnrg.org/ecosystem-services

Niemi, M. T., & Vauhkonen, J. (2016). Extracting canopy surface texture from airborne laser scanning data for the supervised and unsupervised prediction of area-based forest characteristics. *Remote Sensing*, *8*(7), 582.

Ok, A. O., Akar, O., & Gungor, O. (2012). Evaluation of random forest method for agricultural crop classification. *European Journal of Remote Sensing*, *45*(1), 421–432. https://doi.org/10.5721/EuJRS20124535

Oswalt, S. N., Smith, W. B., Miles, P. D., & Pugh, S. A. (2019). Forest resources of the United States, 2017. *General Technical Report-US Department of Agriculture, Forest Service. Forest Service*.

Otukei, J. R., & Blaschke, T. (2010). Land cover change assessment using decision trees, support vector machines and maximum likelihood classification algorithms. *International Journal of Applied Earth Observation and Geoinformation*, *12*, S27–S31. https://doi.org/10.1016/j.jag.2009.11.002

Panagiotidis, D., Abdollahnejad, A., Surovỳ, P., & Kuželka, K. (2019). Detection of fallen logs from high-resolution UAV images. *New Zealand Journal of Forestry Science*, *49*. http://nzjforestryscience.nz/index.php/nzjfs/article/view/26

Parajuli, M., Gallagher, T., Cristan, R., Daniel, M. J., Mitchell, D., & McDonald, T. (2023). Opportunities and challenges of woody biomass harvesting practices in the Southeastern region of the United States. *International Journal of Forest Engineering*, *34*(3), 303–316. https://doi.org/10.1080/14942119.2023.2238149

Poblete-Echeverría, C., Olmedo, G. F., Ingram, B., & Bardeen, M. (2017). Detection and Segmentation of Vine Canopy in Ultra-High Spatial Resolution RGB Imagery Obtained from Unmanned Aerial Vehicle (UAV): A Case Study in a Commercial Vineyard. Remote Sensing, 9(3), Article 3. https://doi.org/10.3390/rs9030268

Polewski, P., Yao, W., Heurich, M., Krzystek, P., & Stilla, U. (2015). Detection of fallen trees in ALS point clouds using a Normalized Cut approach trained by simulation. *ISPRS Journal of Photogrammetry and Remote Sensing*, *105*, 252–271. https://www.sciencedirect.com/science/article/pii/S0924271615000271?casa_token=ff6_v8ADQdkAAAAA:Pb5Kn0qMHRcKGVAZiyncQ_g-ARuWPtPByT3CMpfxEutNIsqxzMPh1cC2c4L_EroWGiv7u13Rkw

Qin, H., Zhou, W., Yao, Y., & Wang, W. (2022). Individual tree segmentation and tree species classification in subtropical broadleaf forests using UAV-based Lidar, hyperspectral, and ultrahigh-resolution RGB data. *Remote Sensing of Environment*, *280*, 113143. https://doi.org/10.1016/j.rse.2022.113143

Rajan, J., Shriwastav, S., Kashyap, A., Ratnoo, A., & Ghose, D. (2021). Disaster management using unmanned aerial vehicles. In *Unmanned Aerial Systems* (pp. 129–155). Elsevier. https://doi.org/10.1016/B978-0-12-820276-0.00013-3

Record-breaking Atlantic hurricane season draws to an end | National Oceanic and Atmospheric Administration. (2020, November 24). https://www.noaa.gov/media-release/record-breaking-atlantic-hurricane-season-draws-to-end

Reed, K. A., Wehner, M. F., & Zarzycki, C. M. (2022). Attribution of 2020 hurricane season extreme rainfall to human-induced climate change. Nature Communications, 13(1), 1905. https://doi.org/10.1038/s41467-022-29379-1

Rijal, A., Cristan, R., & Parajuli, M. (2023). Application of Lidar in Forest Management. Alabama Cooperative Extension System.

Rijal, A., Cristan, R., Gallagher, T., Narine, L. L., & Parajuli, M. (2023). Evaluating the feasibility and potential of unmanned aerial vehicles to monitor implementation of forestry best management practices in the coastal plain of the southeastern United States. *Forest Ecology and Management*, *545*, 121280.

Ritter, T., Gollob, C., Kraßnitzer, R., Stampfer, K., & Nothdurft, A. (2022). A Robust Method for Detecting Wind-Fallen Stems from Aerial RGB Images Using a Line Segment Detection Algorithm. *Forests*, *13*(1), Article 1. https://doi.org/10.3390/f13010090

Schiefer, F., Kattenborn, T., Frick, A., Frey, J., Schall, P., Koch, B., & Schmidtlein, S. (2020). Mapping forest tree species in high resolution UAV-based RGB-imagery by means of convolutional neural networks. ISPRS Journal of Photogrammetry and Remote Sensing, 170, 205–215. https://doi.org/10.1016/j.isprsjprs.2020.10.015

Secord, J., & Zakhor, A. (2007). Tree detection in urban regions using aerial Lidar and image data. *IEEE Geoscience and Remote Sensing Letters*, *4*(2), 196-200.

Sen, R., Goswami, S., & Chakraborty, B. (2019). Jeffries-Matusita distance as a tool for feature selection. *2019 International Conference on Data Science and Engineering (ICDSE)*, 15–20. https://doi.org/10.1109/ICDSE47409.2019.8971800

Sharma, A., Ojha, S. K., Dimov, L. D., Vogel, J. G., & Nowak, J. (2021). Long-term effects of catastrophic wind on southern US coastal forests: Lessons from a major hurricane. *PLOS ONE*, *16*(1), e0243362. https://doi.org/10.1371/journal.pone.0243362

Sharma, C. M., Baduni, N. P., Gairola, S., Ghildiyal, S. K., & Suyal, S. (2010). Effects of slope aspects on forest compositions, community structures and soil properties in natural temperate forests of Garhwal Himalaya. Journal of Forestry Research, 21(3), 331–337. https://doi.org/10.1007/s11676-010-0079-y

Sharma, R., Ghosh, A., & Joshi, P. K. (2013). Decision tree approach for classification of remotely sensed satellite data using open source support. *Journal of Earth System Science*, *122*(5), 1237–1247. https://doi.org/10.1007/s12040-013-0339-2

Shi, Y., Skidmore, A. K., Wang, T., Holzwarth, S., Heiden, U., Pinnel, N., Zhu, X., & Heurich, M. (2018). Tree species classification using plant functional traits from Lidar and hyperspectral data. *International Journal of Applied Earth Observation and Geoinformation*, *73*, 207–219. https://doi.org/10.1016/j.jag.2018.06.018

Sisodia, P. S., Tiwari, V., & Kumar, A. (2014). A comparative analysis of remote sensing image classification techniques. *2014 International Conference on Advances in Computing,*

Communications and Informatics (ICACCI), 1418–1421. https://doi.org/10.1109/ICACCI.2014.6968245

Srivastava, S. K., Seng, K. P., Ang, L. M., Pachas, A. 'Nahuel' A., & Lewis, T. (2022). Drone-Based Environmental Monitoring and Image Processing Approaches for Resource Estimates of Private Native Forest. *Sensors*, *22*(20), 7872. https://doi.org/10.3390/s22207872

Sofonia, J. J., Phinn, S., Roelfsema, C., Kendoul, F., & Rist, Y. (2019). Modelling the effects of fundamental UAV flight parameters on Lidar point clouds to facilitate objectives-based planning. ISPRS Journal of Photogrammetry and Remote Sensing, 149, 105–118. https://doi.org/10.1016/j.isprsjprs.2019.01.020

Ståhl, G., Ringvall, A., & Fridman, J. (2001). Oikos Editorial Office Assessment of Coarse Woody Debris: A Methodological Overview.

Storch, M., Jarmer, T., Adam, M., & de Lange, N. (2022). Systematic Approach for Remote Sensing of Historical Conflict Landscapes with UAV-Based Laserscanning. Sensors, 22(1), Article 1. https://doi.org/10.3390/s22010217

Thapa, N., Narine, L. L., Fan, Z., Yang, S., & Tiwari, K. (2023). Detection of invasive plants using NAIP imagery and airborne Lidar in coastal Alabama and Mississippi, USA. *Annals of Forest Research*, *66*(1), 63–77. https://www.afrjournal.org/index.php/afr/article/view/2548

Tran, T. H. G., Ressl, C., & Pfeifer, N. (2018). Integrated Change Detection and Classification in Urban Areas Based on Airborne Laser Scanning Point Clouds. *Sensors*, *18*(2), Article 2. https://doi.org/10.3390/s18020448

US Department of Commerce, N. (2021). Long-Track Tornadoes of March 25, 2021. NOAA's National Weather Service. Retrieved April 16, 2024, from https://www.weather.gov/bmx/event_03252021

Van Alphen, R., Rains, K. C., Rodgers, M., Malservisi, R., & Dixon, T. H. (2024). UAV-Based Wetland Monitoring: Multispectral and Lidar Fusion with Random Forest Classification. Drones, 8(3), 113. https://doi.org/10.3390/drones8030113

Wang, X., Wang, Y., Zhou, C., Yin, L., & Feng, X. (2021). Urban forest monitoring based on multiple features at the single tree scale by UAV. *Urban forestry & urban greening*, *58*, 126958.

Wear, D. N., & Greis, J. G. (2002). *Southern Forest Resource Assessment* (SRS-GTR-53; p. SRS-GTR-53). U.S. Department of Agriculture, Forest Service, Southern Research Station. https://doi.org/10.2737/SRS-GTR-53

Wear, D. N., & Greis, J. G. (2012). The Southern Forest Futures Project: Summary Report.

Windrim, L., Bryson, M., McLean, M., Randle, J., & Stone, C. (2019). Automated Mapping of Woody Debris over Harvested Forest Plantations Using UAVs, High-Resolution Imagery, and Machine Learning. *Remote Sensing*, *11*(6), Article 6. https://doi.org/10.3390/rs11060733

Xi, W., Peet, R. K., & Urban, D. L. (2008). Changes in forest structure, species diversity and spatial pattern following hurricane disturbance in a Piedmont North Carolina forest, USA. Journal of Plant Ecology, 1(1), 43–57. https://doi.org/10.1093/jpe/rtm003

Xu, Z., Li, W., Li, Y., Shen, X., & Ruan, H. (2019). Estimation of secondary forest parameters by integrating image and point cloud-based metrics acquired from unmanned aerial vehicle. Journal of Applied Remote Sensing, 14(02), 1. https://doi.org/10.1117/1.jrs.14.022204

Zhai, L., Sun, J., Sang, H., Yang, G., & Jia, Y. (2012). LARGE AREA LAND COVER CLASSIFICATION WITH LANDSAT ETM+ IMAGES BASED ON DECISION TREE. *The International Archives of the Photogrammetry, Remote Sensing and Spatial Information Sciences*, *XXXIX-B7*, 421–426. https://doi.org/10.5194/isprsarchives-XXXIX-B7-421-2012

Zhang, X., Zhang, F., Qi, Y., Deng, L., Wang, X., & Yang, S. (2019). New research methods for vegetation information extraction based on visible light remote sensing images from an unmanned aerial vehicle (UAV). *International Journal of Applied Earth Observation and Geoinformation*, *78*, 215-226.

Chapter 3. Conclusions and Future Directions on the Use of UAVs and Lidar Technology for Windstorm Damage Assessment

This study highlights the successful utilization of unmanned aerial vehicles (UAVs) equipped with Light Detection and Ranging (lidar) and red, green, blue (RGB) imagery in evaluating the impact of windstorm damage on forest stands. Through a comparative analysis of three distinct classification techniques- Maximum Likelihood (ML), Decision Tree (DT), and Random Forest (RF) - significant insights were gained into the classification methods that could be utilized for accurate forest mapping and damage assessment. The Random Forest (RF) technique emerged as the most effective method, offering superior accuracy and robustness using the lidar-derived Canopy Height Model (CHM) and RGB imagery. These findings demonstrate the potential of RF in enhancing forest assessment in post-disaster settings, which is crucial for timely and effective forest management and recovery strategies.

Notably, all three classifiers used in this study achieved the highest accuracy with the lidar-CHM integrated dataset, highlighting the role of lidar-derived structural information in facilitating detailed and fine-scale assessments of storm-damaged forests. The study also emphasized the importance of each input variable, as indicated by the variable importance plots derived from the Random Forest model, with CHM emerging as a critical variable in accurately distinguishing between classification categories. By providing a comprehensive evaluation of different classification techniques and emphasizing the advantages of integrating UAV-lidar and RGB imagery, this research proposes a rapid, accurate, and efficient framework for storm damage assessment in forested landscapes. This finding underscores the possibility of further

optimizing classification models by focusing on the combined benefits of spectral and structural data, advancing our understanding of remote sensing applications, and paving the way for future innovations in disaster management and recovery planning.

The study presents findings regarding the effectiveness of UAV-lidar and RGB imagery in forest damage assessment. However, further research is necessary to investigate the scalability of these methods across different forest ecosystems and storm conditions. Additionally, the study's focus on the southeastern US presents an opportunity to explore the applicability of these findings in other regions vulnerable to similar natural disasters. In doing so, it would be useful to explore the inclusion of other remote sensing data, like multispectral data, hyperspectral data, or synthetic aperture radar (SAR) and their derivatives. These data sources may provide additional information, especially in areas with cloud cover, dense canopy, downed timbers, and understory vegetation. This approach could potentially improve classification accuracy by providing more diverse information, helping to create a more comprehensive understanding of forest conditions and damage levels.

For this study, classification algorithms have been employed independently for each of the ten different sites that were damaged by storms. The algorithms were trained with site-specific data. This method, while effective for small-scale and localized assessments, might cause challenges when replicating to other storm-damaged sites. To create a more standardized and consistent approach across various sites, a single classification model, such as a single Random Forest model, could be developed. This model would use a comprehensive dataset derived from all sites to train a single RF classifier. Once developed, a single model could be

applied to the separate datasets from each of the ten sites without further adjustments. This approach would help to improve the reliability, scalability, comparability, and time efficiency of the methodology used to compare results across different forest conditions and storm impacts.

In this study, the downed tree class was frequently misclassified as the standing tree class, which could be because of the spectral similarity caused by the presence of green leaves on the downed trees. Additionally, there was notable confusion between the downed tree, ground, and water classes, likely due to their close proximity to the bare ground. The integration of data from multiple sensors, such as RGB and NIR bands, along with advancements in image processing techniques and machine learning algorithms can potentially provide solutions to the challenges of distinguishing among such closely related classification categories. This can further improve the accuracy and reliability of assessments of forest damage. While integrating UAV-lidar and RGB imagery presents a promising avenue for forest damage assessment, it also introduces challenges, particularly regarding data processing complexity. Future research should explore the application of deep learning and computer vision techniques to further enhance classification accuracy.

The acquired UAV-lidar data can be useful for determining the volume of damaged or fallen trees. This is crucial for efficient post-disaster restoration efforts. Computer vision algorithms can be employed to classify and segment the lidar point cloud data. These algorithms may be examined for distinguishing among varying levels of damage and identifying specific areas impacted by the storm. By utilizing volumetric analysis techniques on the segmented point

cloud, accurate calculations of the affected forest stands can be conducted to determine the volume of fallen timber.

There is potential for integrating satellite and airborne data to study storm-damaged forest stands. These platforms offer various data types that can supplement the high-resolution but localized data from UAVs equipped with lidar and RGB cameras. By doing so, damage across a broader area could be investigated to support efficient resource allocation for recovery efforts. For instance, imagery acquired from satellites can provide extensive coverage of regions affected by storms. This can be crucial for initial broad-scale damage assessments and for monitoring changes over time. Following a hurricane, satellite imagery may be used to quickly assess the extent of forest damage across hundreds of thousands of acres, identifying critical areas where UAVs should be deployed for a detailed examination.

Appendix A (Damage Classification Maps)

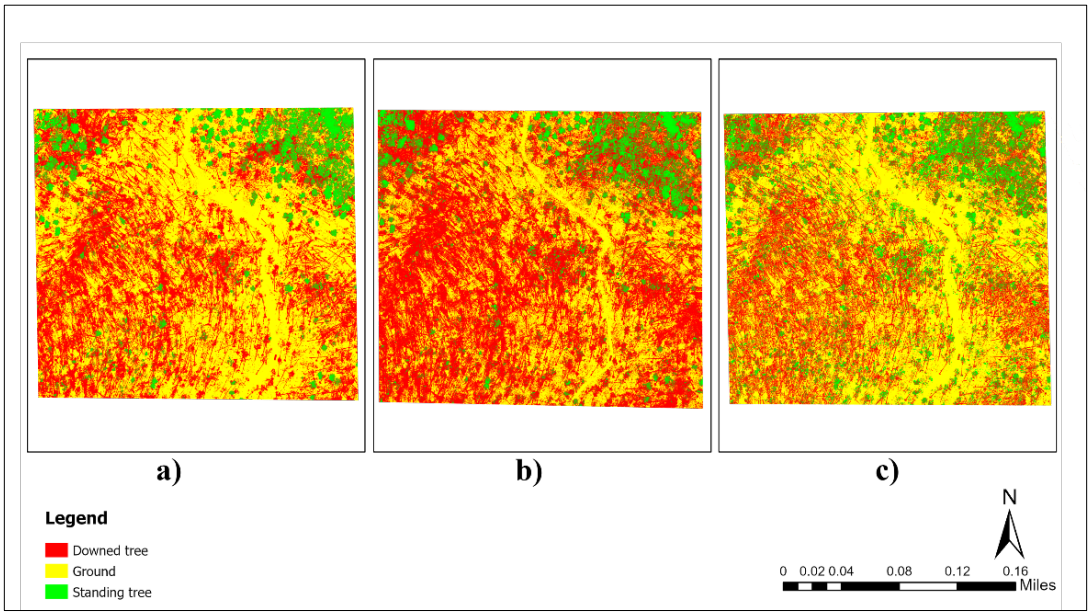

Figure 10. A map of the tornado-damaged in Duncanville, Alabama (site 2) prepared using a dataset integrated with lidar-CHM. Green represents standing trees, red represents downed trees, and yellow represents the ground. Panel (a) represents RF classification, (b) represents ML classification, and (c) represents DT classification.

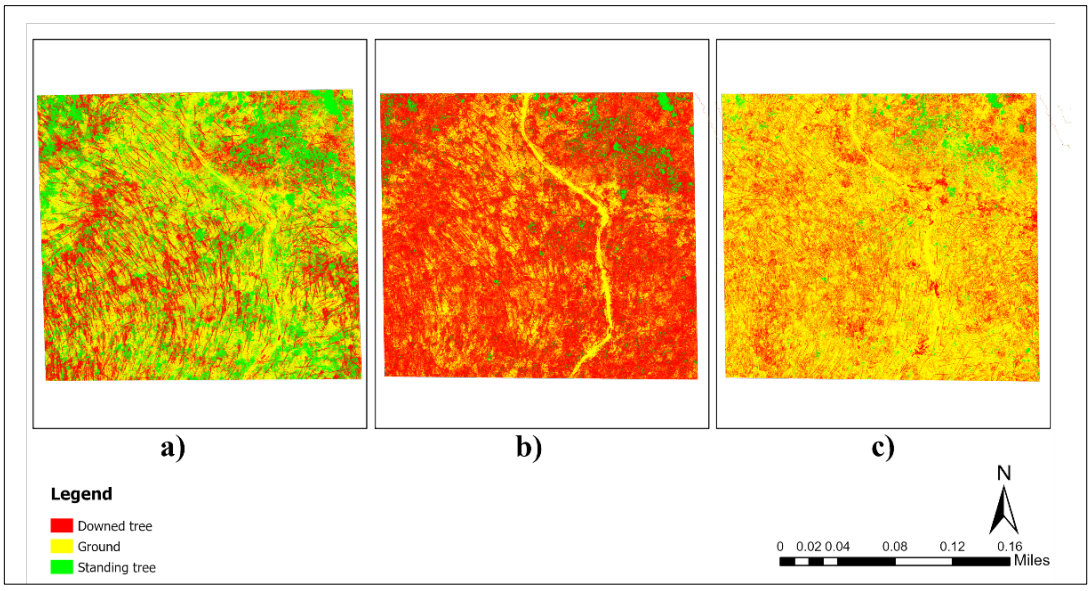

Figure 11. A map of the tornado-damaged in Duncanville, Alabama (site 2) prepared using a dataset integrated without lidar-CHM. Green represents standing trees, red represents downed trees, and yellow represents the ground. Panel (a) represents RF classification, (b) represents ML classification, and (c) represents DT classification.

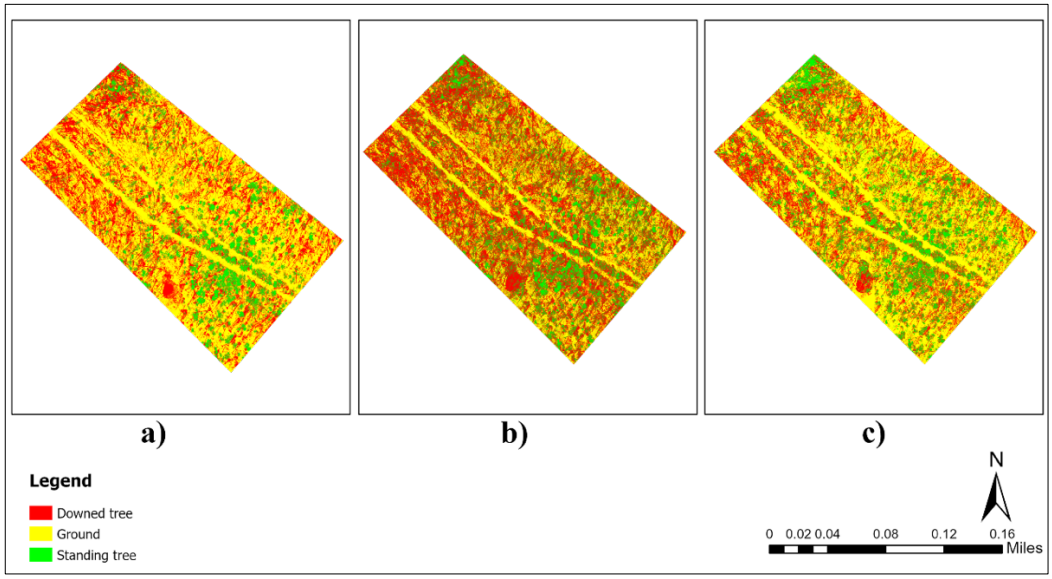

Figure 12. A map of the tornado-damaged in Duncanville, Alabama (site 3) prepared using a dataset integrated with lidar-CHM. Green represents standing trees, red represents downed trees, and yellow represents the ground. Panel (a) represents RF classification, (b) represents ML classification, and (c) represents DT classification.

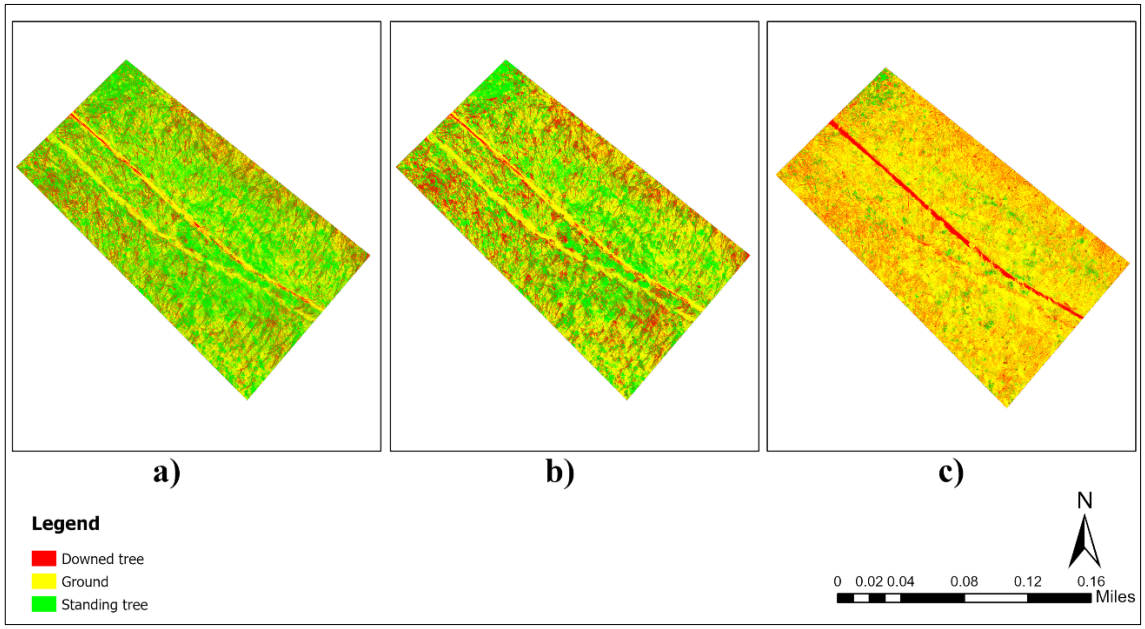

Figure 13. A map of the tornado-damaged in Duncanville, Alabama (site 3) prepared using a dataset integrated without lidar-CHM. Green represents standing trees, red represents downed trees, and yellow represents the ground. Panel (a) represents RF classification, (b) represents ML classification, and (c) represents DT classification.

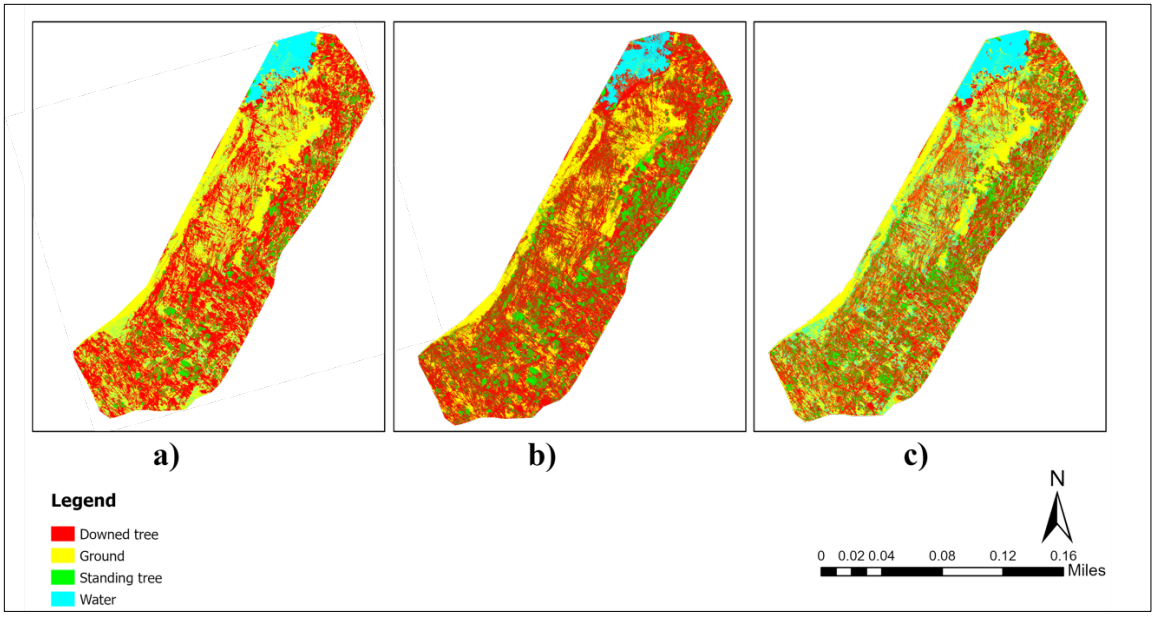

Figure 14. A map of the tornado-damaged in Duncanville, Alabama (site 4) prepared using a dataset integrated with lidar-CHM. Green represents standing trees, red represents downed trees, yellow represents the ground, and blue represents water. Panel (a) represents RF classification, (b) represents ML classification, and (c) represents DT classification.

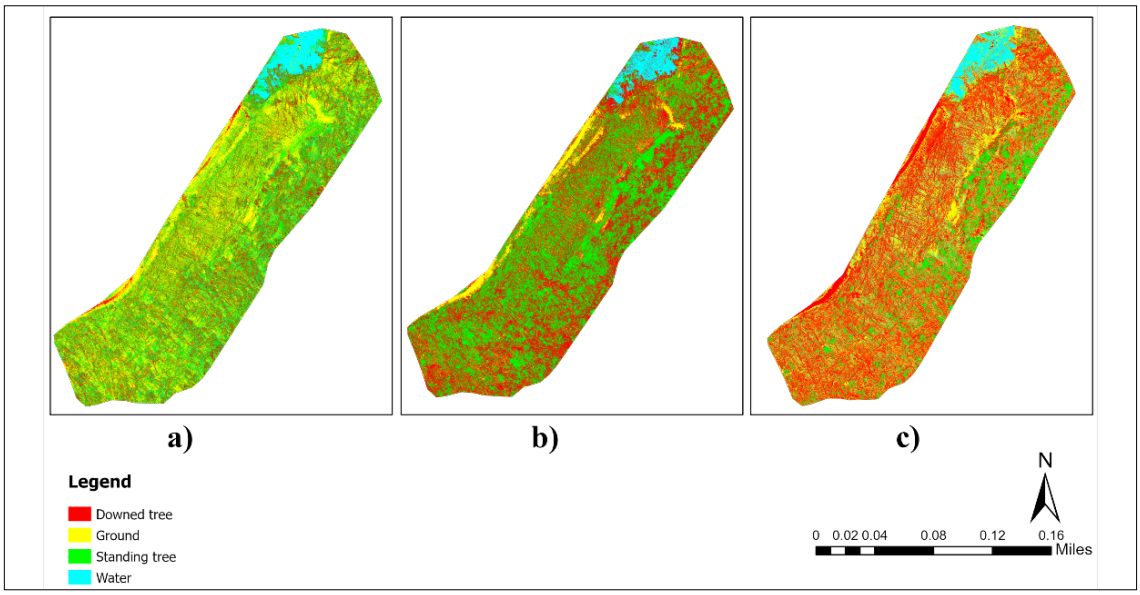

Figure 15. A map of the tornado-damaged in Duncanville, Alabama (site 4) prepared using a dataset integrated without lidar-CHM. Green represents standing trees, red represents downed trees, yellow represents the ground, and blue represents water. Panel (a) represents RF classification, (b) represents ML classification, and (c) represents DT classification.

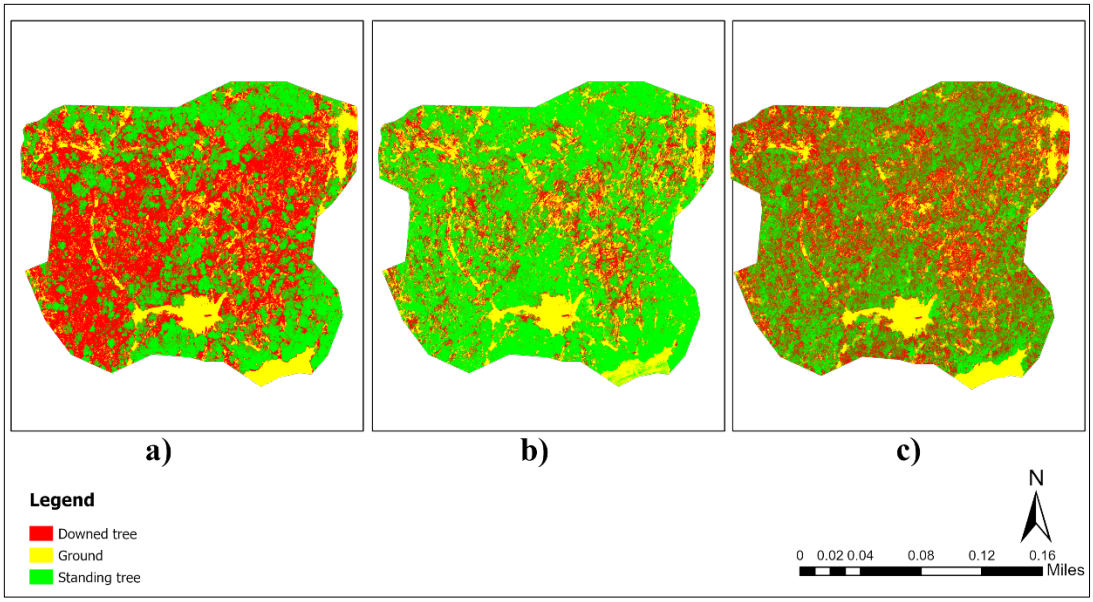

Figure 16. A map of the tornado-damaged in Duncanville, Alabama (site 5) prepared using a dataset integrated with lidar-CHM. Green represents standing trees, red represents downed trees, and yellow represents the ground. Panel (a) represents RF classification, (b) represents ML classification, and (c) represents DT classification.

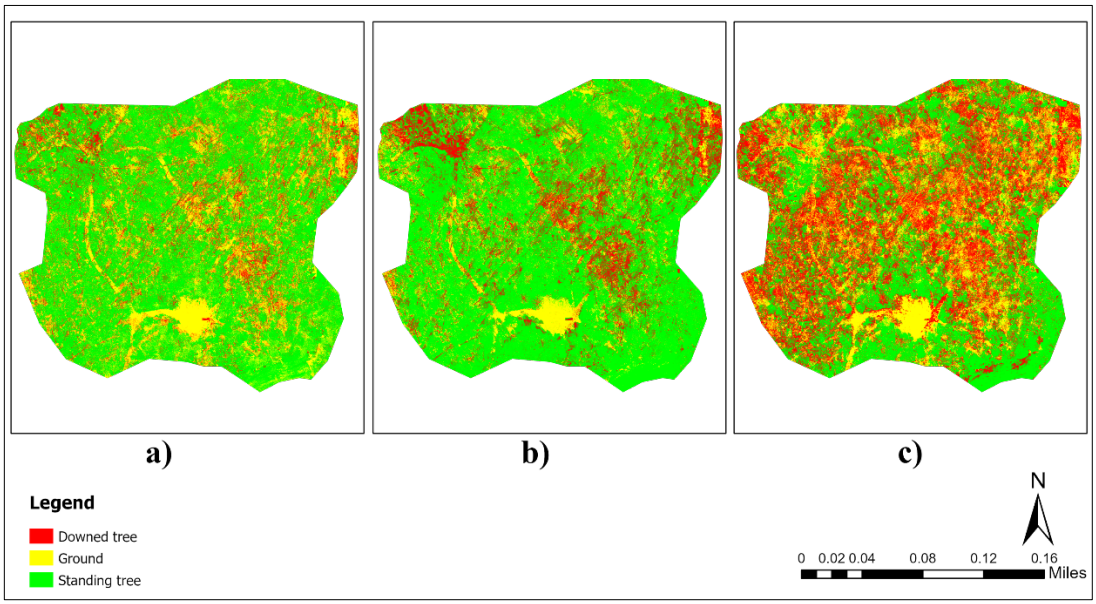

Figure 17. A map of the tornado-damaged in Duncanville, Alabama (site 5) prepared using a dataset integrated without lidar-CHM. Green represents standing trees, red represents downed trees, and yellow represents the ground. Panel (a) represents RF classification, (b) represents ML classification, and (c) represents DT classification.

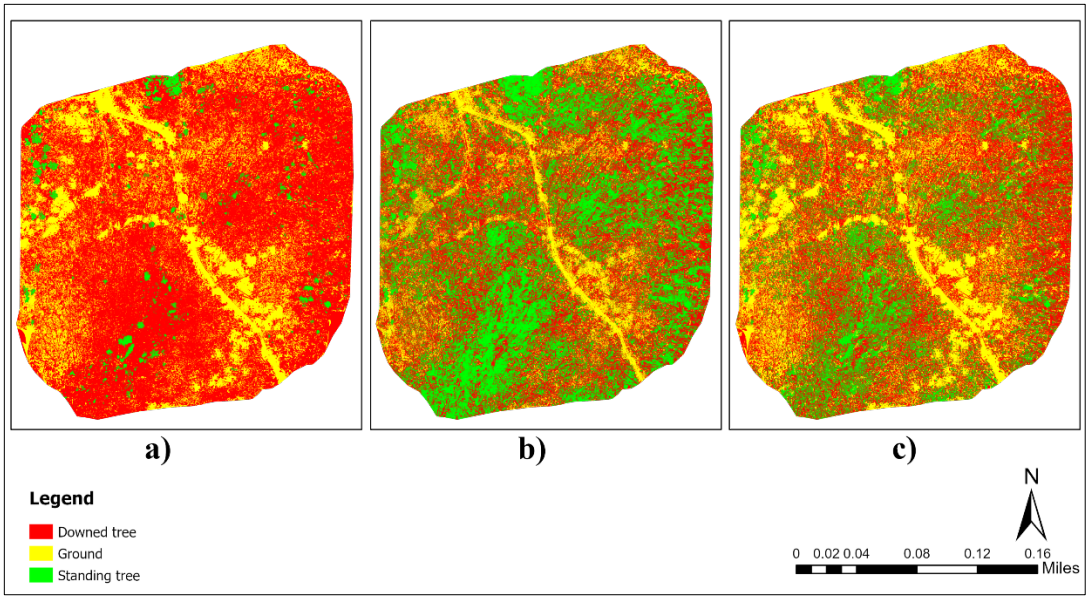

Figure 18. A map of the tornado-damaged in Duncanville, Alabama (site 6) prepared using a dataset integrated with lidar-CHM. Green represents standing trees, red represents downed trees, and yellow represents the ground. Panel (a) represents RF classification, (b) represents ML classification, and (c) represents DT classification.

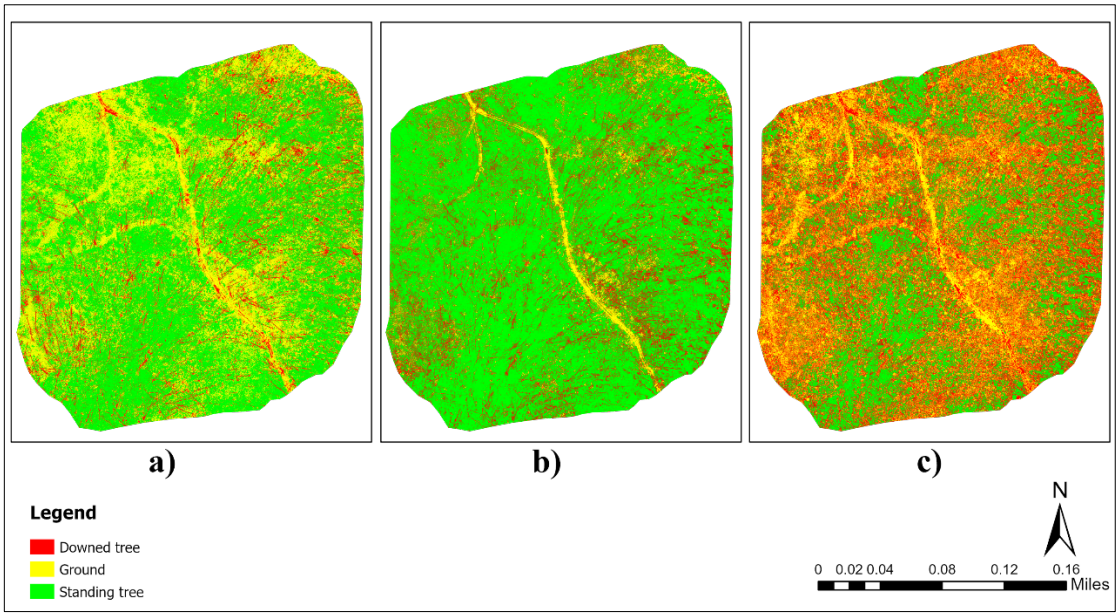

Figure 19. A map of the tornado-damaged in Duncanville, Alabama (site 6) prepared using a dataset integrated without lidar-CHM. Green represents standing trees, red represents downed trees, and yellow represents the ground. Panel (a) represents RF classification, (b) represents ML classification, and (c) represents DT classification.

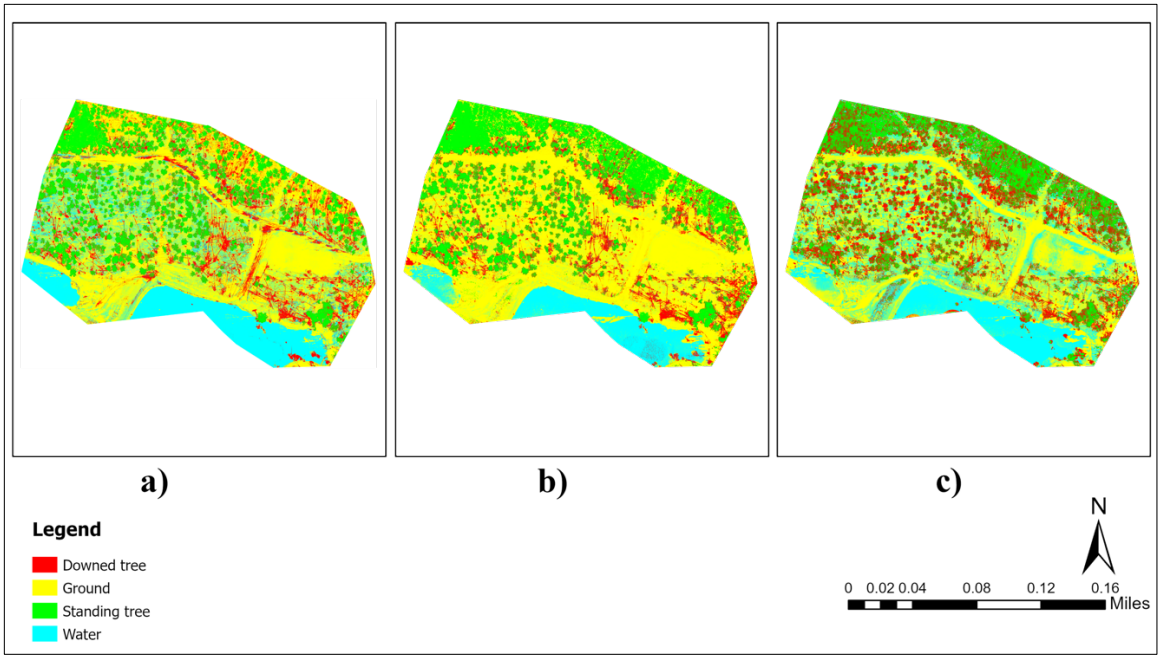

Figure 20. A map of the tornado-damaged in Duncanville, Alabama (site 7) prepared using a dataset integrated with lidar-CHM. Green represents standing trees, red represents downed trees, yellow represents the ground, and blue represents water. Panel (a) represents RF classification, (b) represents ML classification, and (c) represents DT classification.

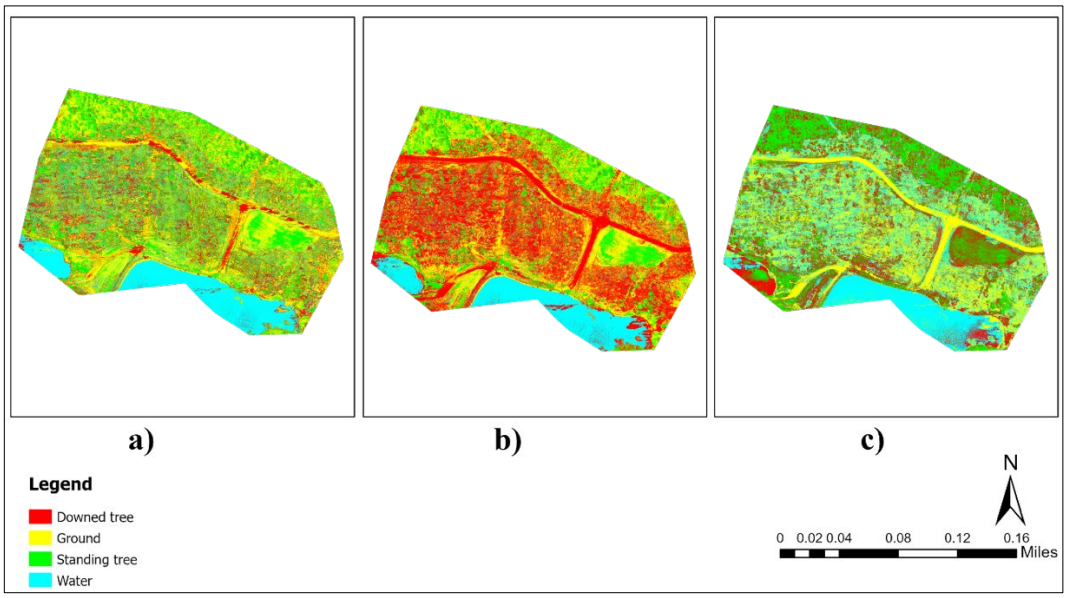

Figure 21. A map of the tornado-damaged in Duncanville, Alabama (site 7) prepared using a dataset integrated without lidar-CHM. Green represents standing trees, red represents downed trees, yellow represents the ground, and blue represents water. Panel (a) represents RF classification, (b) represents ML classification, and (c) represents DT classification.

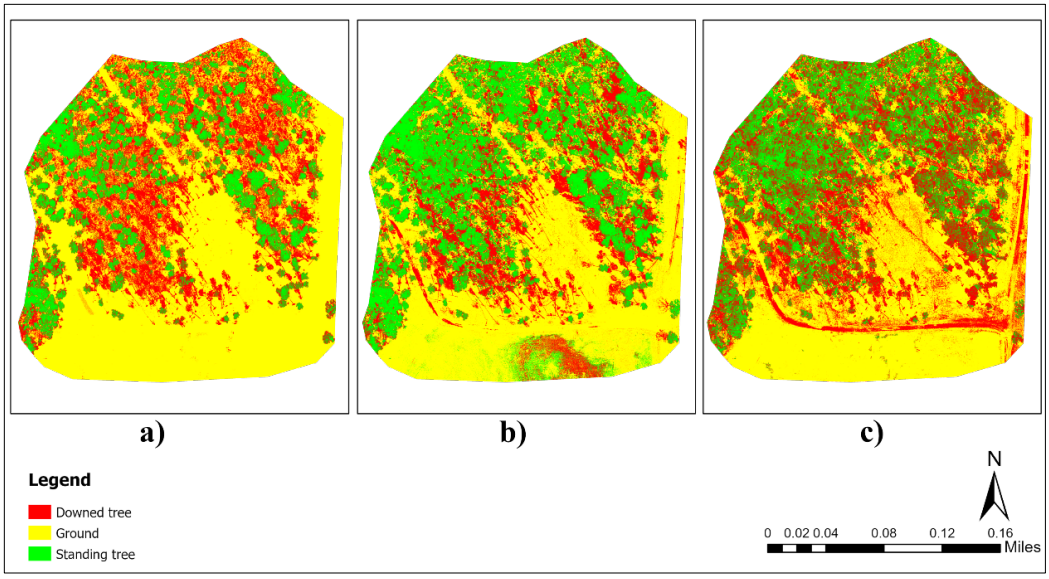

Figure 22. A map of the tornado-damaged in Duncanville, Alabama (site 8) prepared using a dataset integrated with lidar-CHM. Green represents standing trees, red represents downed trees, and yellow represents the ground. Panel (a) represents RF classification, (b) represents ML classification, and (c) represents DT classification.

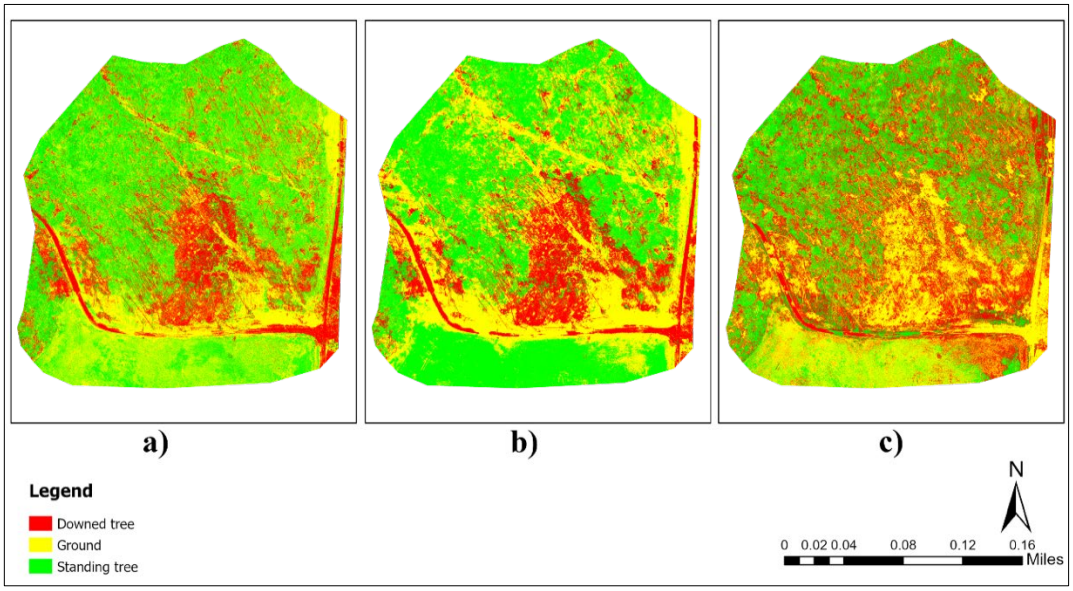

Figure 23. A map of the tornado-damaged in Duncanville, Alabama (site 8) prepared using a dataset integrated without lidar-CHM. Green represents standing trees, red represents downed trees, and yellow represents the ground. Panel (a) represents RF classification, (b) represents ML classification, and (c) represents DT classification.

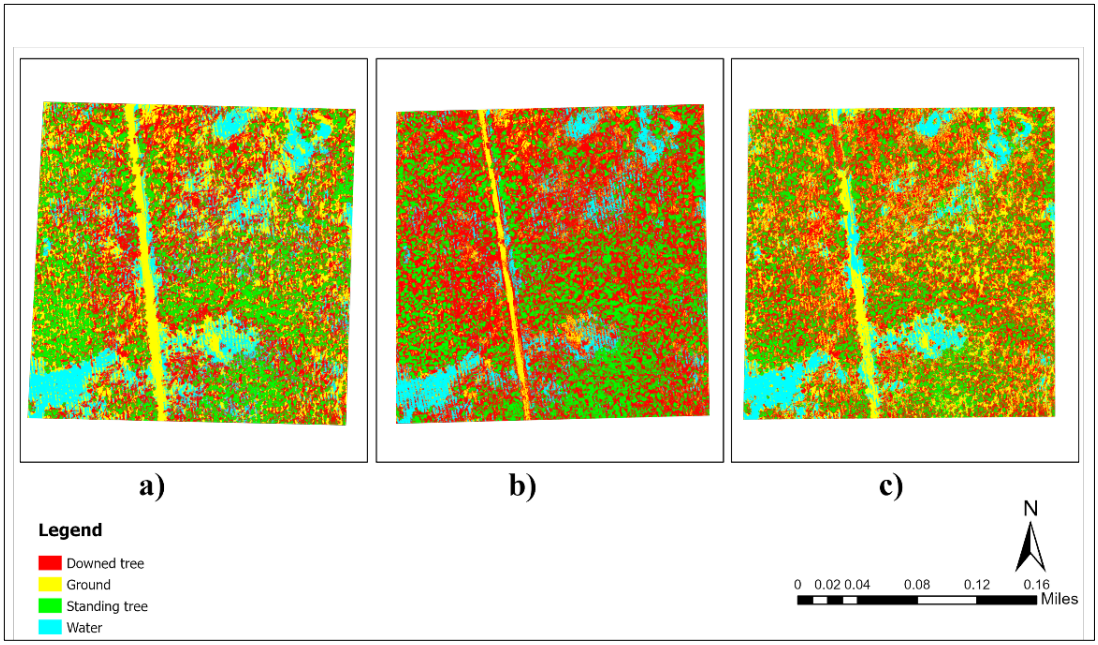

Figure 24. A map of the tornado-damaged in Duncanville, Alabama (site 10) prepared using a dataset integrated with lidar-CHM. Green represents standing trees, red represents downed trees, and yellow represents the ground. Panel (a) represents RF classification, (b) represents ML classification, and (c) represents DT classification.

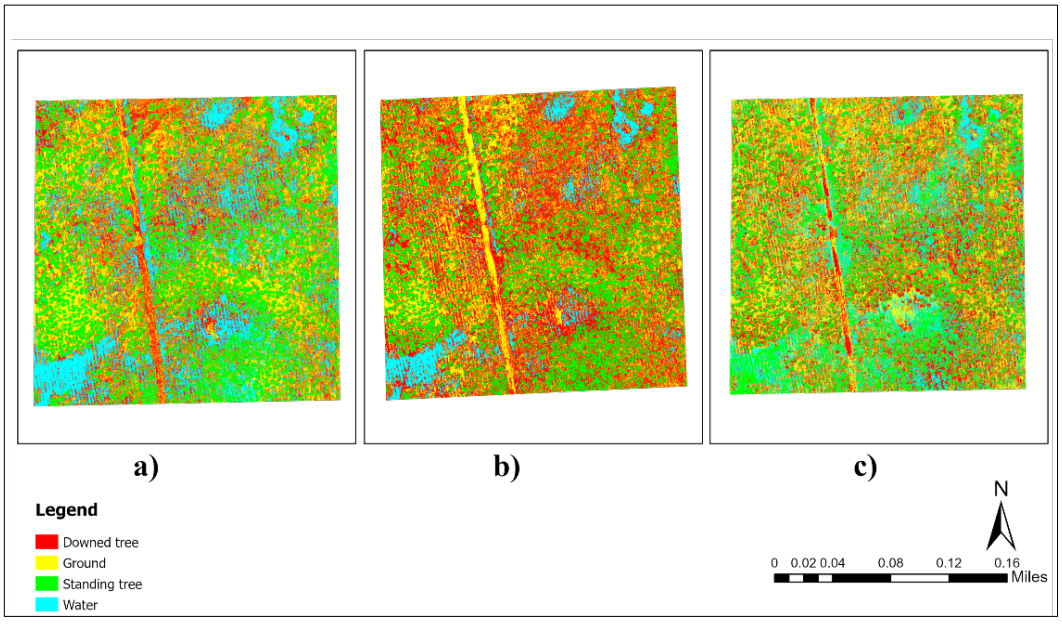

Figure 25. A map of the tornado-damaged in Duncanville, Alabama (site 10) prepared using a dataset integrated without lidar-CHM. Green represents standing trees, red represents downed trees, and yellow represents the ground. Panel (a) represents RF classification, (b) represents ML classification, and (c) represents DT classification.

Appendix B (Variable Importance Plots)

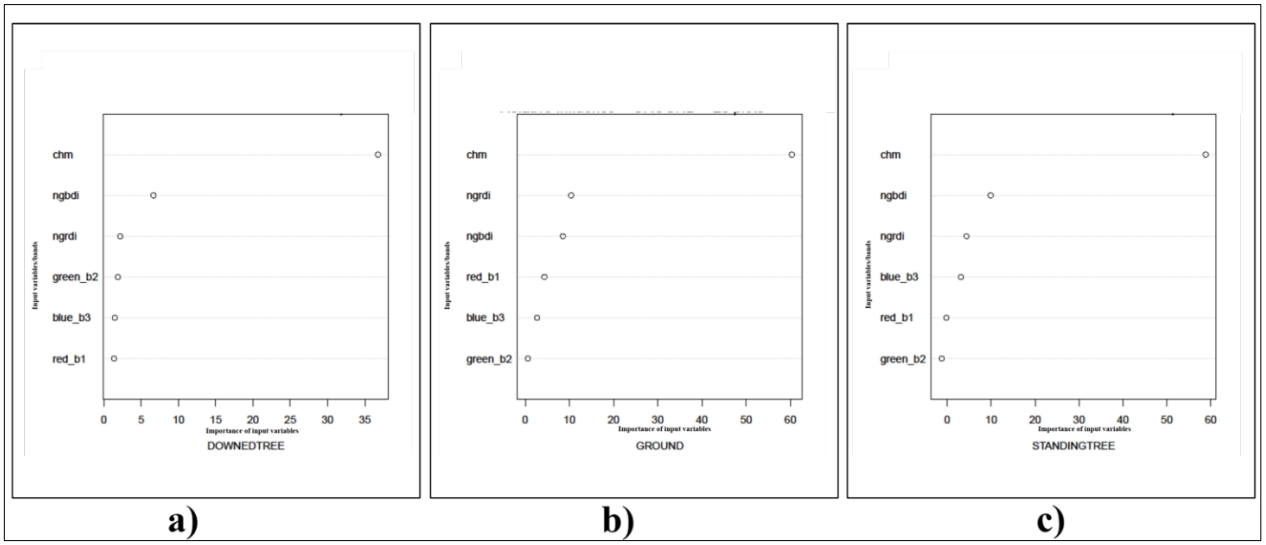

Figure 26. Variable importance plots generated using the ModelMap package in R, displaying the relative importance of each input variable for classifying windstorm damage (Site 2) using lidar-CHM integrated dataset: a) downed tree, b) ground, c) standing tree.

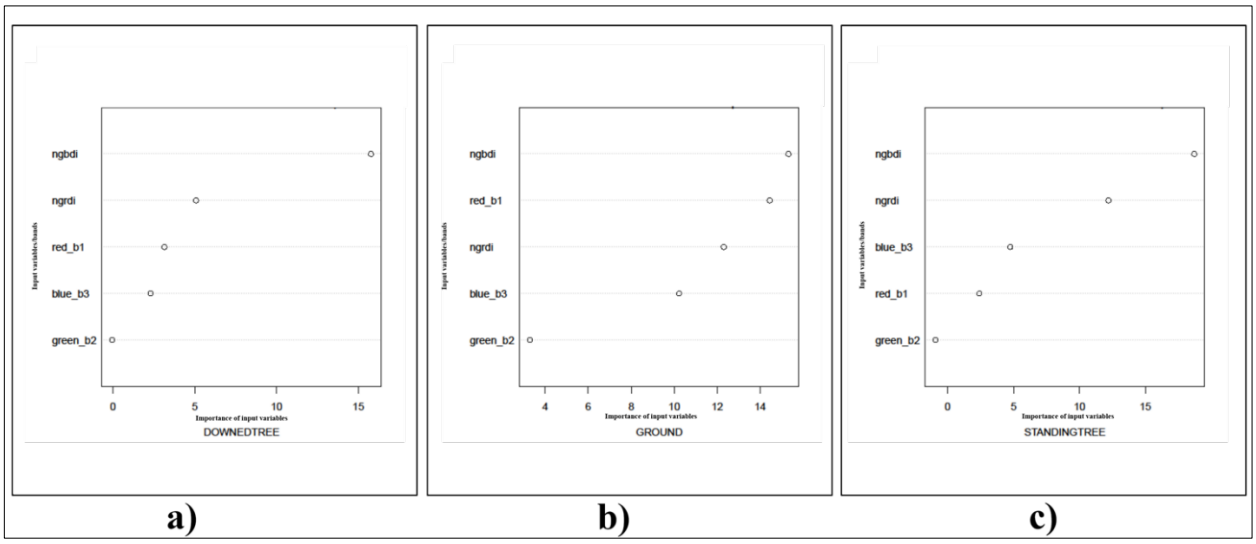

Figure 27. Variable importance plots generated using the ModelMap package in R, displaying the relative importance of each input variable for classifying windstorm damage (Site 2) using dataset without lidar-CHM: a) downed tree, b) ground, c) standing tree.

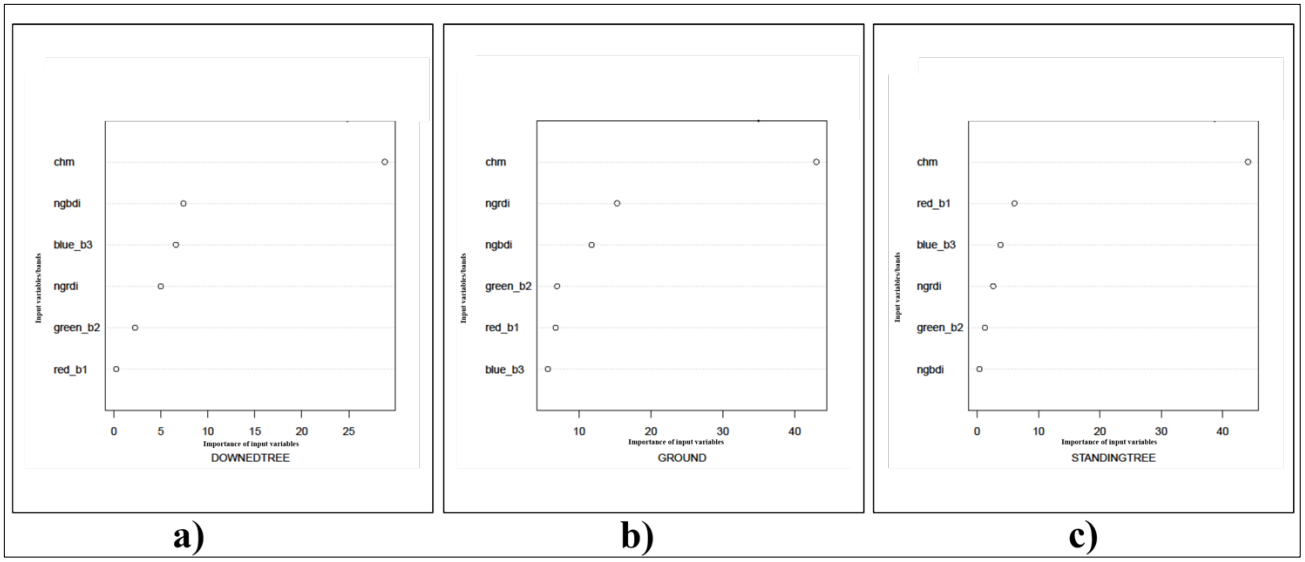

Figure 28. Variable importance plots generated using the ModelMap package in R, displaying the relative importance of each input variable for classifying windstorm damage (Site 3) using lidar-CHM integrated dataset: a) downed tree, b) ground, c) standing tree.

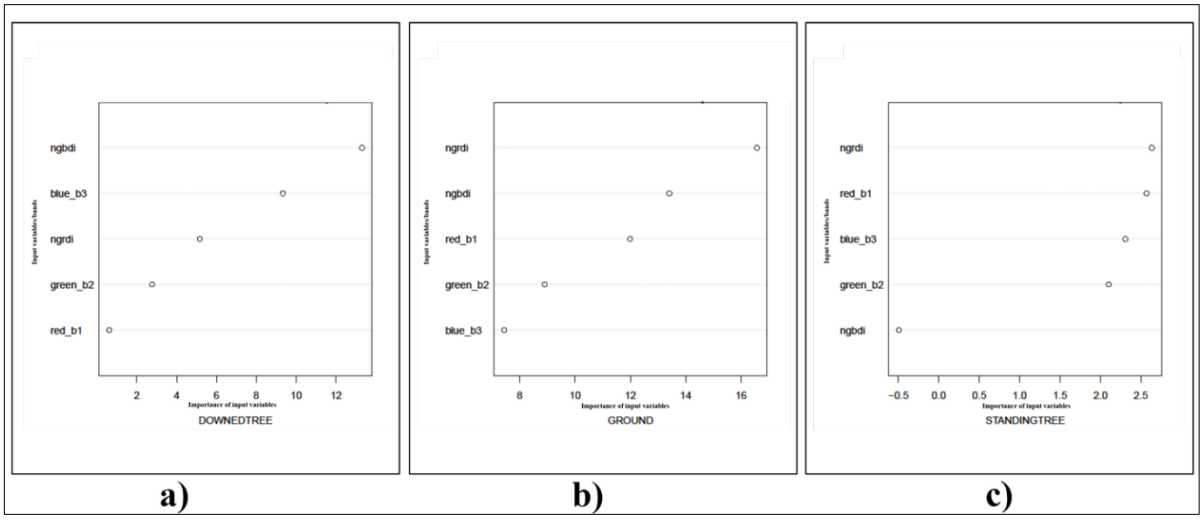

Figure 29. Variable importance plots generated using the ModelMap package in R, displaying the relative importance of each input variable for classifying windstorm damage (Site 3) using dataset without lidar-CHM: a) downed tree, b) ground, c) standing tree.

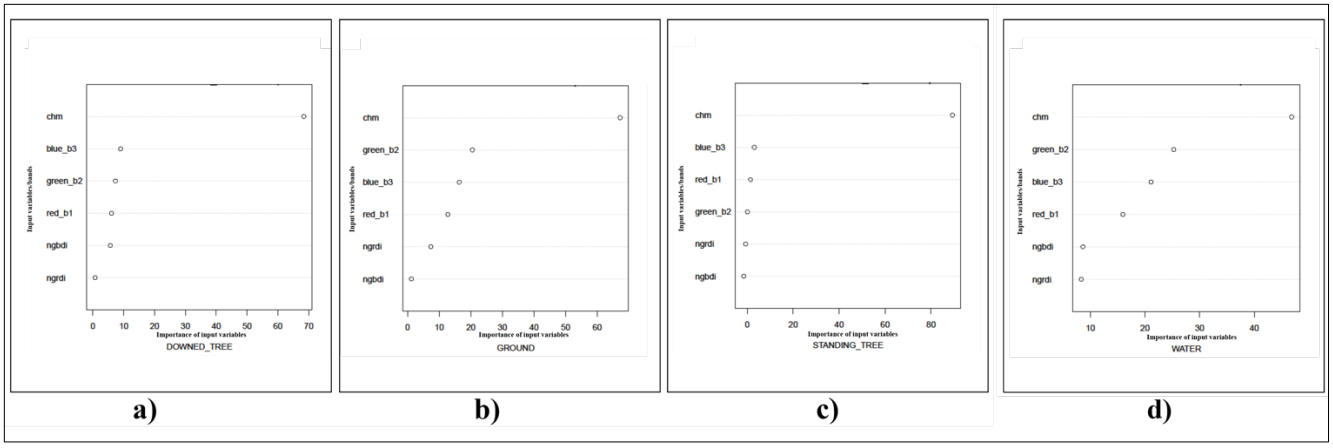

Figure 30. Variable importance plots generated using the ModelMap package in R, displaying the relative importance of each input variable for classifying windstorm damage (Site 4) using lidar-CHM integrated dataset: a) downed tree, b) ground, c) standing tree, d) water.

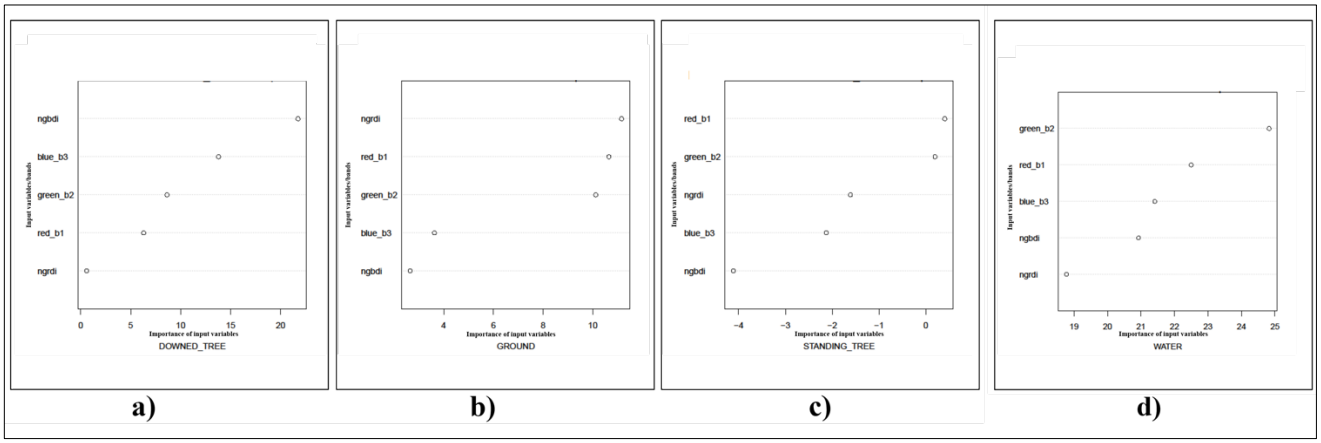

Figure 31. Variable importance plots generated using the ModelMap package in R, displaying the relative importance of each input variable for classifying windstorm damage (Site 4) using dataset without lidar-CHM: a) downed tree, b) ground, c) standing tree, d) water.

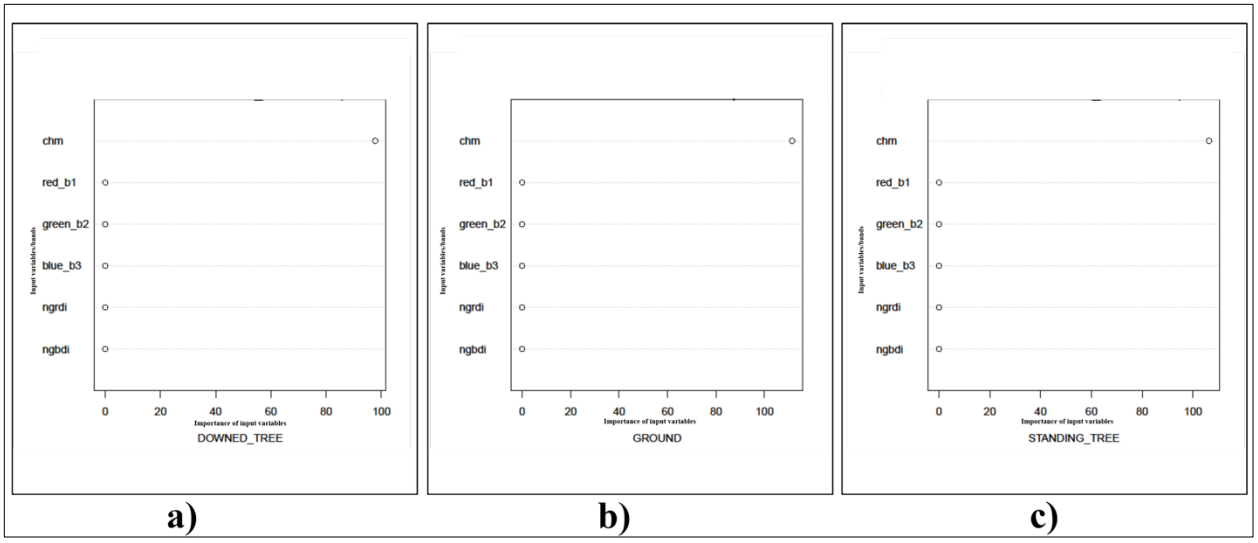

Figure 32. Variable importance plots generated using the ModelMap package in R, displaying the relative importance of each input variable for classifying windstorm damage (Site 5) using lidar-CHM integrated dataset: a) downed tree, b) ground, c) standing tree.

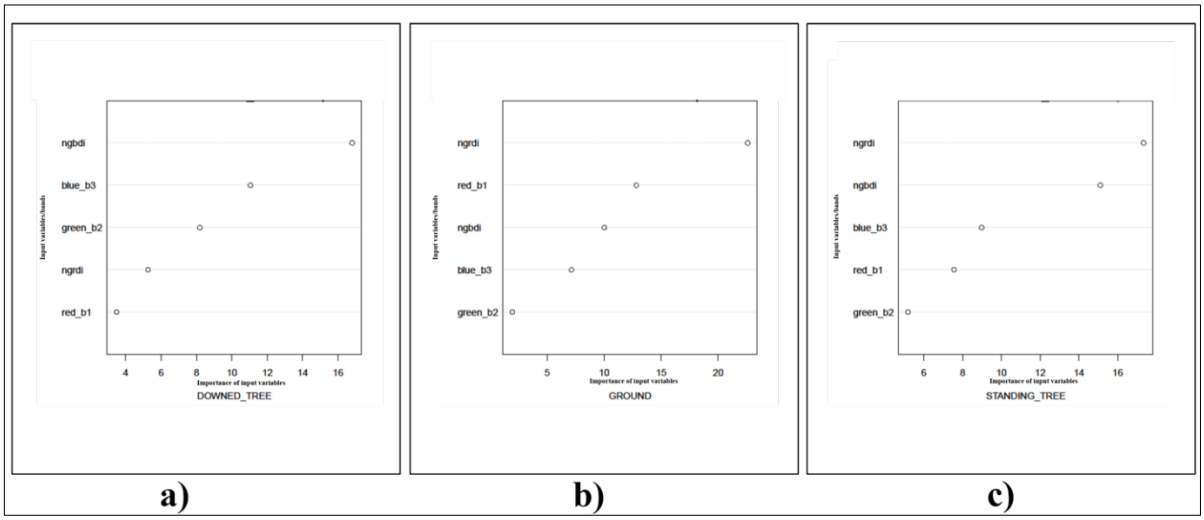

Figure 33. Variable importance plots generated using the ModelMap package in R, displaying the relative importance of each input variable for classifying windstorm damage (Site 5) using dataset without lidar-CHM: a) downed tree, b) ground, c) standing tree.

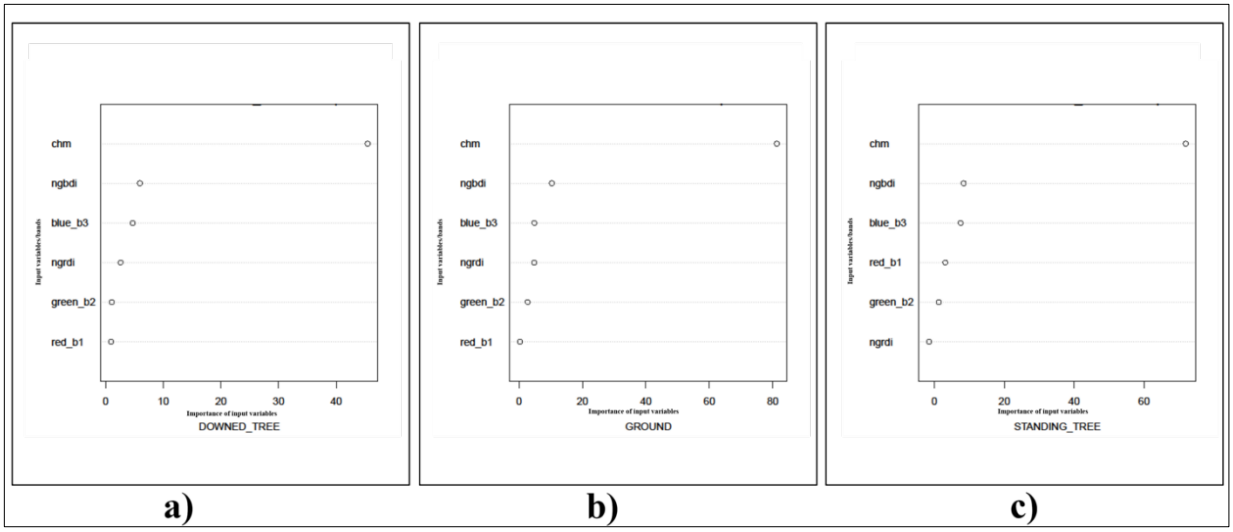

Figure 34. Variable importance plots generated using the ModelMap package in R, displaying the relative importance of each input variable for classifying windstorm damage (Site 6) using lidar-CHM integrated dataset: a) downed tree, b) ground, c) standing tree.

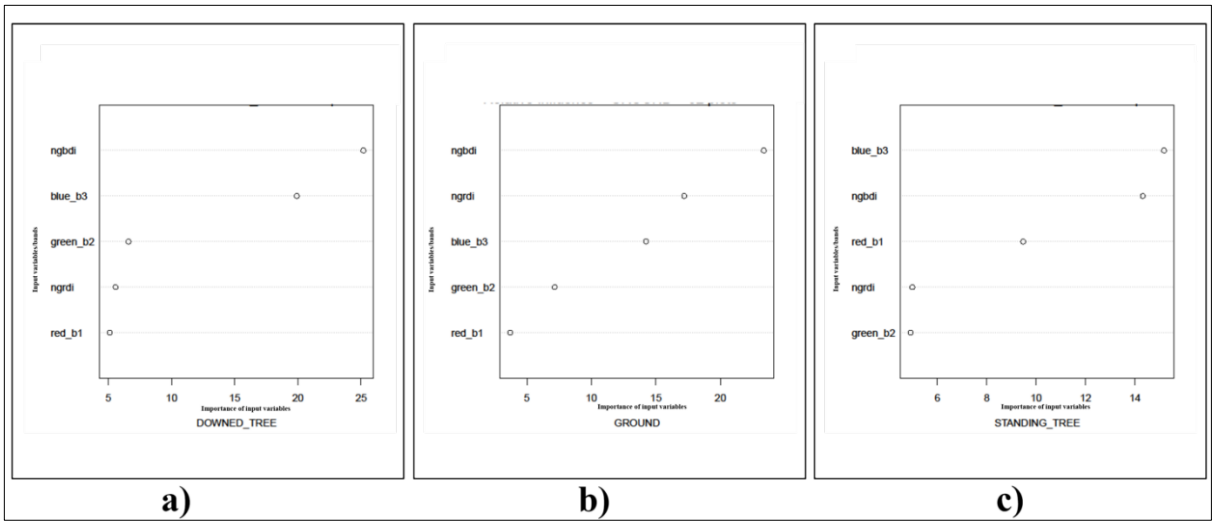

Figure 35. Variable importance plots generated using the ModelMap package in R, displaying the relative importance of each input variable for classifying windstorm damage (Site 6) using dataset without lidar-CHM: a) downed tree, b) ground, c) standing tree.

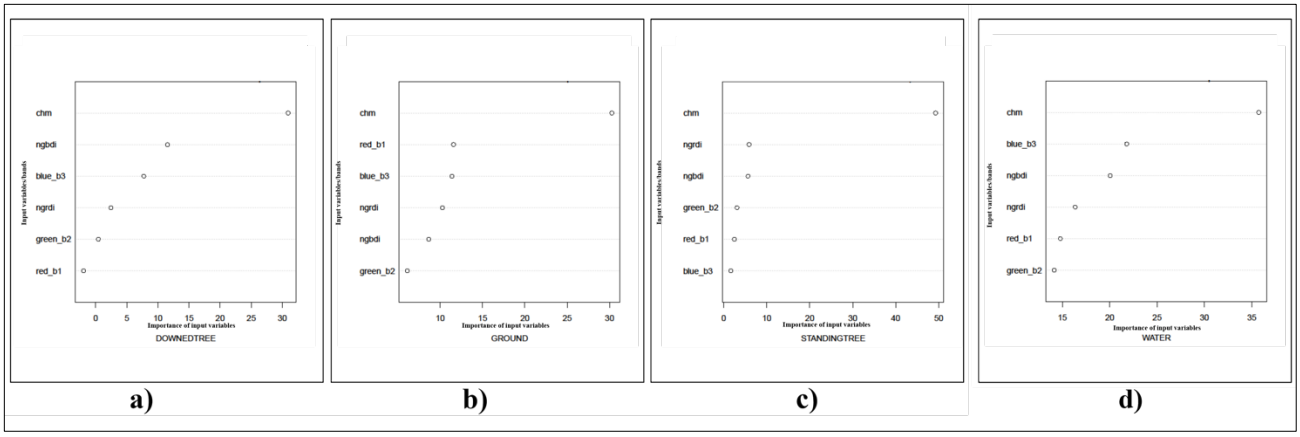

Figure 36. Variable importance plots generated using the ModelMap package in R, displaying the relative importance of each input variable for classifying windstorm damage (Site 7) using lidar-CHM integrated dataset: a) downed tree, b) ground, c) standing tree, d) water.

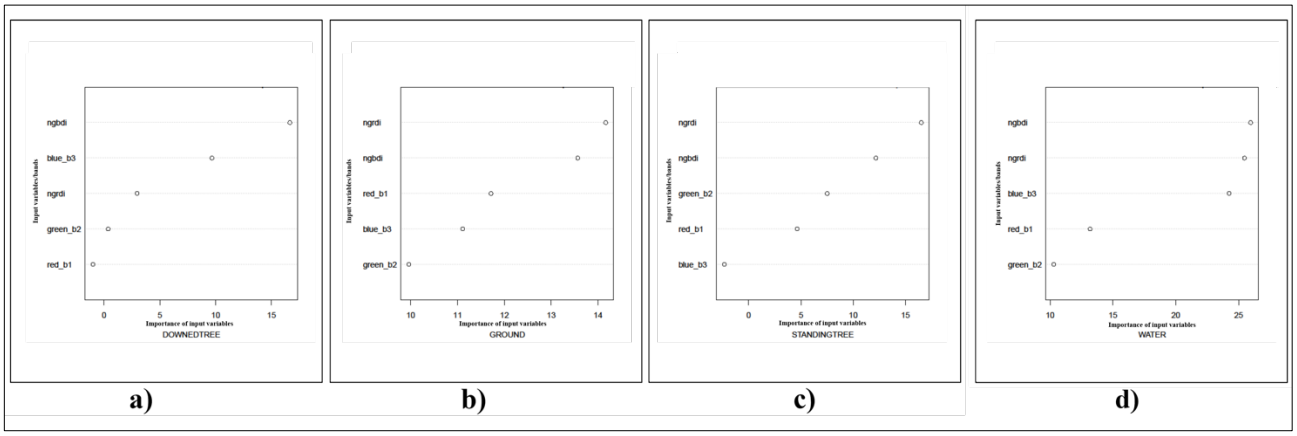

Figure 37. Variable importance plots generated using the ModelMap package in R, displaying the relative importance of each input variable for classifying windstorm damage (Site 7) using dataset without lidar-CHM: a) downed tree, b) ground, c) standing tree, d) water.

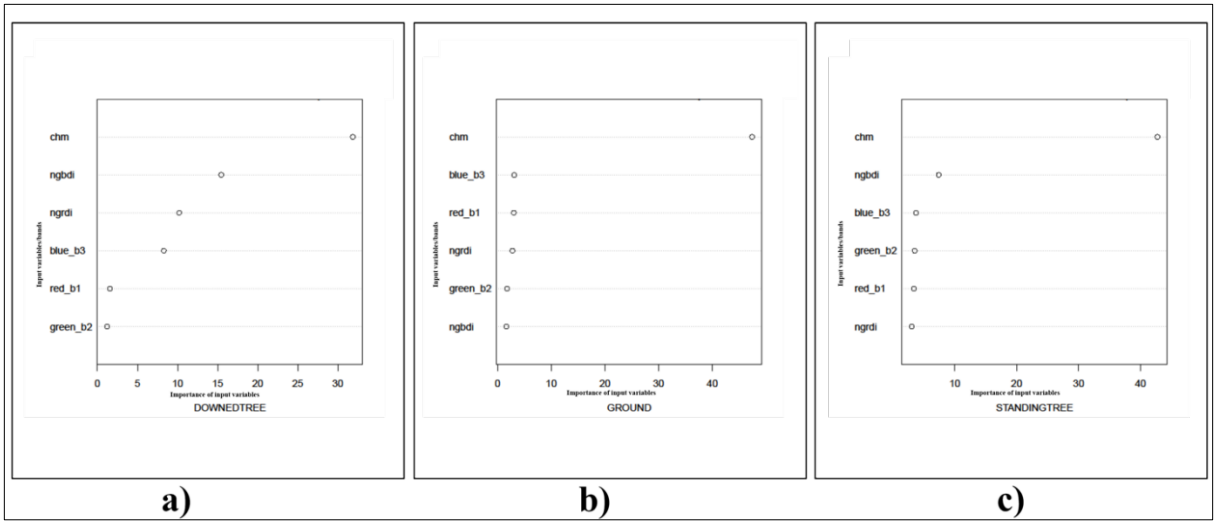

Figure 38. Variable importance plots generated using the ModelMap package in R, displaying the relative importance of each input variable for classifying windstorm damage (Site 8) using lidar-CHM integrated dataset: a) downed tree, b) ground, c) standing tree.

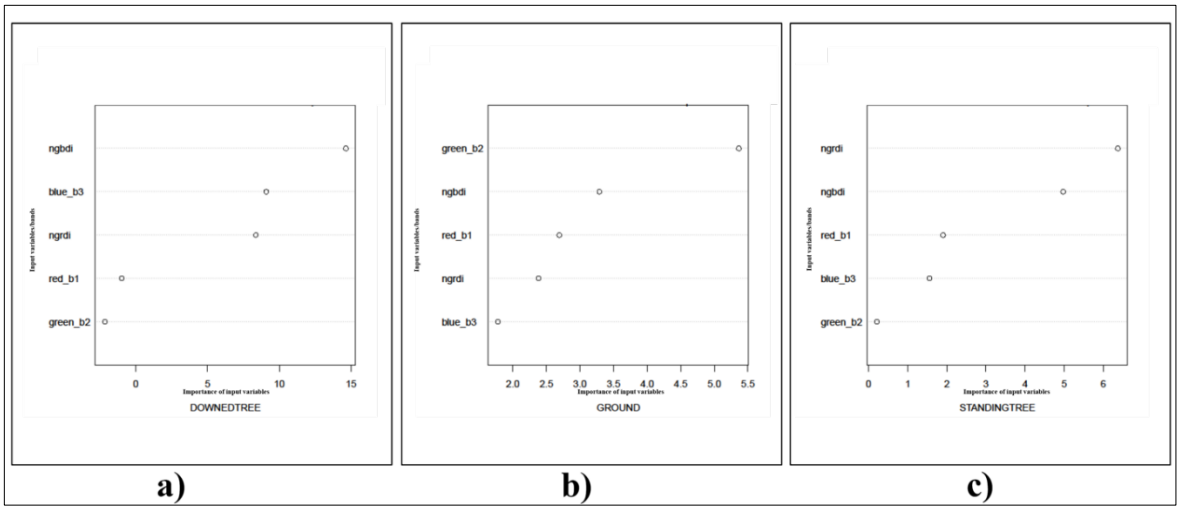

Figure 39. Variable importance plots generated using the ModelMap package in R, displaying the relative importance of each input variable for classifying windstorm damage (Site 8) using dataset without lidar-CHM: a) downed tree, b) ground, c) standing tree.

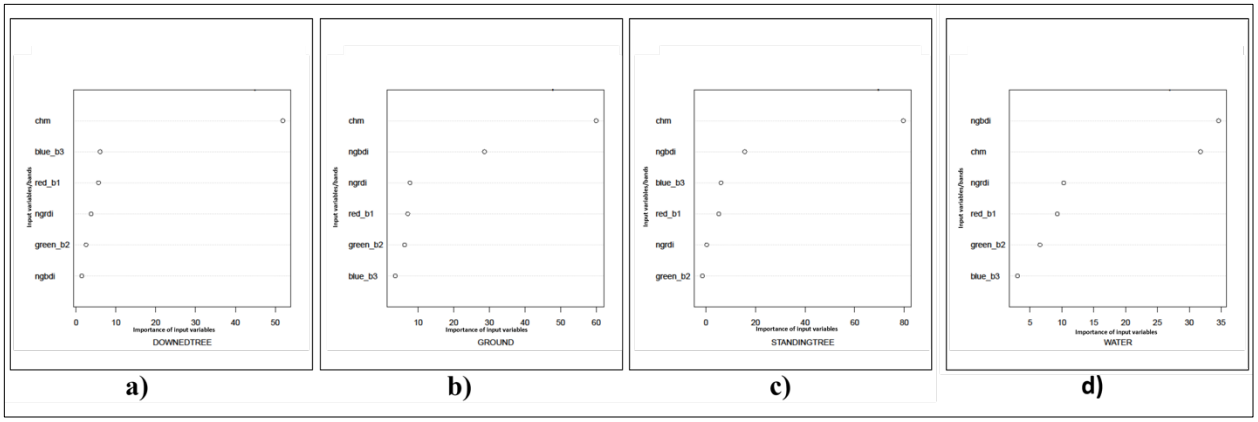

Figure 40. Variable importance plots generated using the ModelMap package in R, displaying the relative importance of each input variable for classifying windstorm damage (Site 9) using lidar-CHM integrated dataset: a) downed tree, b) ground, c) standing tree, d) water.

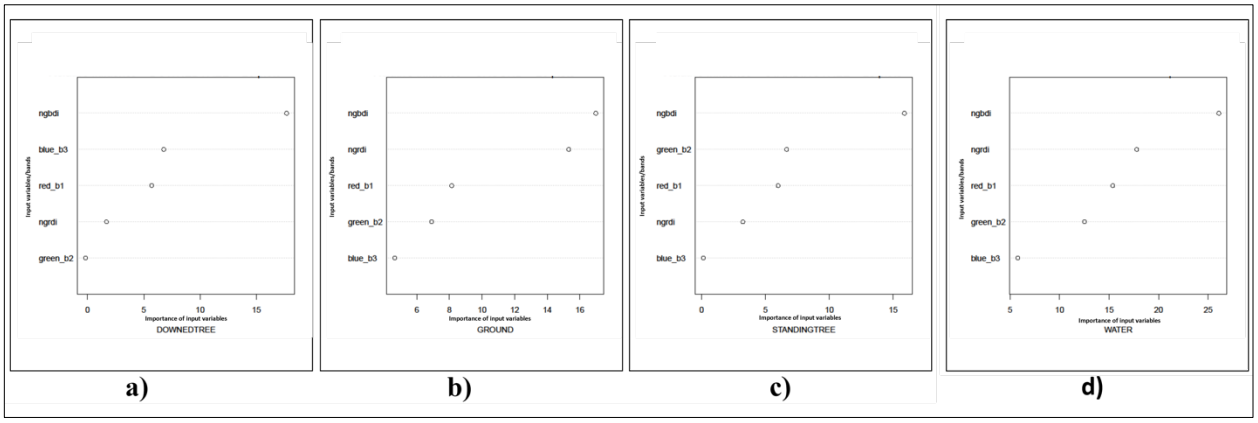

Figure 41. Variable importance plots generated using the ModelMap package in R, displaying the relative importance of each input variable for classifying windstorm damage (Site 9) using dataset without lidar-CHM: a) downed tree, b) ground, c) standing tree, d) water.

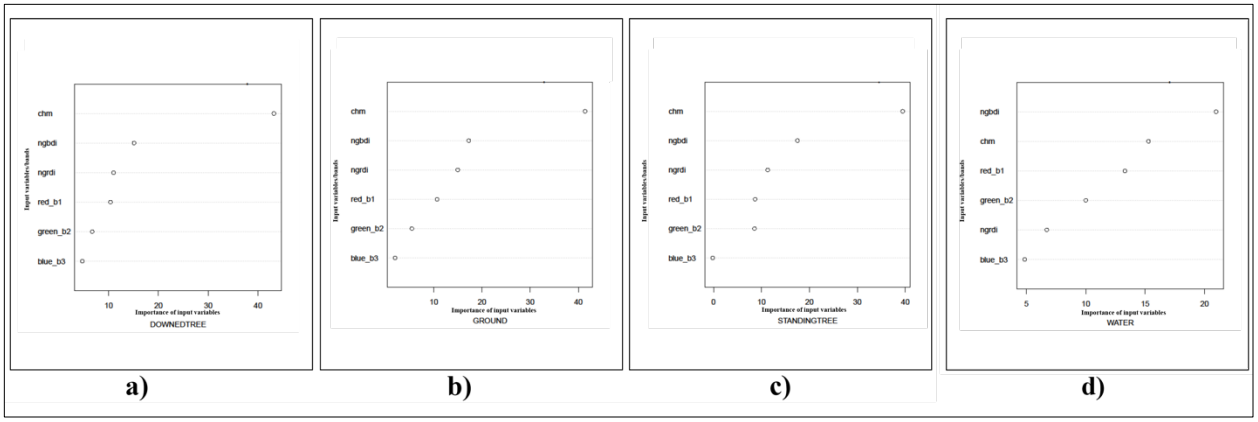

Figure 42. Variable importance plots generated using the ModelMap package in R, displaying the relative importance of each input variable for classifying windstorm damage (Site 10) using lidar-CHM integrated dataset: a) downed tree, b) ground, c) standing tree, d) water.

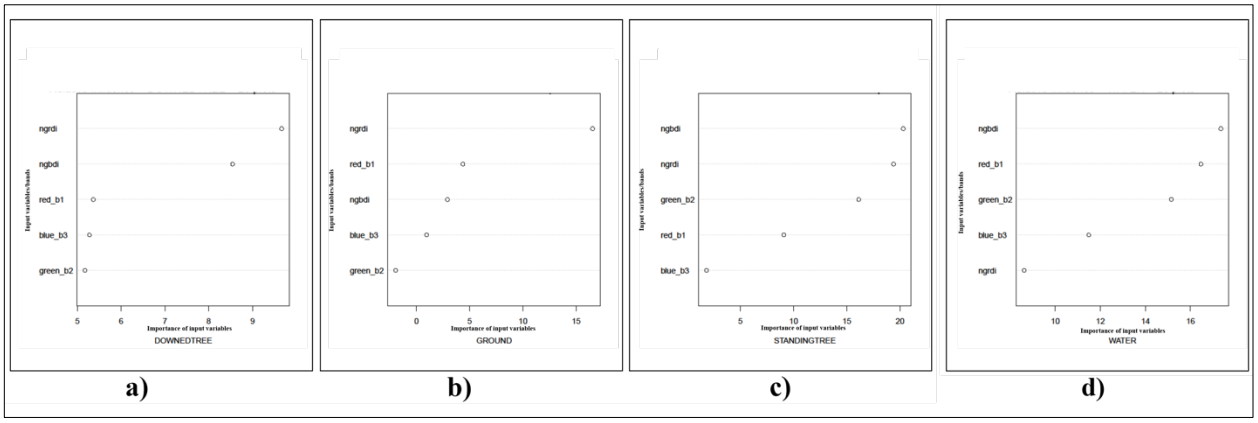

Figure 43. Variable importance plots generated using the ModelMap package in R, displaying the relative importance of each input variable for classifying windstorm damage (Site 10) using dataset without lidar-CHM: a) downed tree, b) ground, c) standing tree, d) water.